UNIVERSITY OF PADUA
—
DEPT. OF MANAGEMENT AND ENGINEERING
—
DOCTORAL SCHOOL OF MECHATRONICS AND
PRODUCT INNOVATION ENGINEERING
CYCLE XXVIII

TRAJECTORY PLANNING AND CONTROL OF CABLE-DRIVEN PARALLEL ROBOTS

A dissertation submitted in partial fulfillment
of the requirements for the degree of
Doctor of Philosophy in Mechatronics and Product Innovation Engineering

Prof. ALESSANDRO PERSONA, Chair of the School
Prof. GIULIO ROSATI, Candidate Supervisor

Ph.D. Candidate: SAEED ABDOLSHAH

Acknowledgment

The research presented in this thesis has been carried out at the Department of Management and Engineering (DTG), University of Padua (Italy), and partially, at the The Robotics And Rehabilitation Lab, Columbia University in the City of New York, USA.

The author acknowledges his debt to those who have helped to develop the results presented in this thesis. In particular, I wish to express my gratitude to my supervisor, Professor Giulio. Rosati, for his fundamental suggestions and valuable contributions to this work, and to Professor Aldo Rossi for his continued encouragement.

I would also like to include my gratitude to Professor Sunil Agrawal for his hospitality at the The Robotics And Rehabilitation Lab.Furthermore, I would like to thank all the Ph.D. candidates at the DTG-Robotics Research Group for the assistance they provided during these three years. Finally, I want to thank my family for the encouragement and the support.

Contents

Abstract

The aim of this work is to investigate on trajectory planning and control of cable-driven parallel robots to improve the system performance. Stiffness and dexterity are the performance indices widely used in design and control of robotic systems.

No previous work on adaptive cable-driven systems has discussed how to control the position of the pulley blocks to achieve optimal dexterity and stiffness. Considering a quasi-static motion of the end-effector, we neglected the active stiffness of the system and proposed pulley blocks trajectory planning strategies that maximize dexterity and elastic stiffness indices simultaneously for some cases of adaptive cable-driven designs by taking advantage of the increased redundancy.

For non-adaptive design of cable-driven parallel robots, it is impossible to change the dexterity and elastic stiffness indices for a certain position of end-effector due to fixed orientation and length of cables; however, active stiffness can be modified by changing the tension in cables. Tension increment can be desirable due to stiffness augmentation, higher trajectory tracking performance, more precise motion and disturbance rejection; however, it can increase power consumption, and saturation in actuators may occur. Usually, cable tension distribution methods work based on a fixed minimum tension in cables. Such values are chosen through experiments to gain the desired trajectory tracking performance of the system, considering capability of actuators at the same time.

To improve the system performance we proposed Dynamic Minimum Tension Control (DMTC) method. In this approach, the minimum tension is changing on-the-fly according to stiffness, dynamics of the system, and error values as feedback. We used a simple test bed to compare traditional fixed minimum tension utilization, and the proposed approach. Experimental results showed that the DMTC is more efficient than traditional approaches in terms of accuracy and energy consumption.

Also an appropriate control algorithm can improve the system performance. The linear quadratic optimal control can play an important role in controlling cable-driven parallel robots by providing all the states of the system for the feedback, including velocity and position, in addition to optimal results. A linear quadratic optimal controller was designed and tested. The significant experimental results are presented and discussed.

Keywords:
adaptive cable-driven robots, performance indices, transverse vibration, dynamic minimum tension control(DMTC), linear quadratic optimal control

Riassunto

L'obiettivo di questo progetto è di investigare la pianificazione di traiettoria ed il controllo di robot paralleli a cavi al fine di migliorare le prestazioni del sistema. Rigidezza e destrezza sono indici di prestazione ampiamente utilizzati del progetto e controllo di sistemi robotici.

Allo stato dell'arte, non esistono lavori relativi a sistemi a cavi adattativi riguardanti il controllo della posizione delle pulegge per ottenere indici di rigidezza e destrezza ottimali. Considerando un moto quasi-statico dell'organo terminale e trascurando la rigidezza attiva del sistema, è stato possibile proporre strategie di pianificazione di moto delle pulegge che massimizzino gli indici di destrezza e rigidezza elastica. E' stato possibile massimizzare simultaneamente tali indici per alcuni casi di robot a cavi adattativi sfruttando la ridondanza dei sistemi analizzati.

Per il progetto di robot a cavi paralleli non adattativi, è impossibile cambiare gli indici di destrezza e di rigidezza elastica per una certa posizione dell'organo terminale a causa dell'orientazione e della lunghezza dei cavi fissata; comunque, la rigidezza attiva può essere modificata cambiando la tensione dei cavi. L'incremento della tensione dei cavi può essere desiderabile a causa dell'aumento di rigidezza, del miglioramento delle prestazioni di inseguimento di traiettoria, più precisamente movimento e risposta ai disturbi; tuttavia, può aumentare il consumo energetico e portare a saturazione gli attuatori. Tipicamente i metodi di distribuzione delle tensioni operano mantenendo costante il valore di tensione minimo da applicare ai cavi. Tali valori sono scelti attraverso esperimenti per raggiungere le prestazioni di inseguimento della traiettoria desiderata, considerando anche le capacità degli attuatori.

Per migliorare le prestazioni del sistema, viene proposto un metodo dinamico di controllo delle tensioni minime (DMTC). In questo approccio è possibile variare la tensione minima in tempo reale sulla base della rigidezza, della dinamica del sistema e del valore dell'errore ottenuto come feedback. Attraverso un semplice apparato sperimentale, è stato possibile confrontare il metodo tradizionale di distribuzione delle tensioni basato sulla tensione minima fissa ed il metodo proposto. I risultati sperimentali hanno mostrato che il metodo Dinamico di Controllo delle Tensioni Minime risulta più efficiente rispetto all'approccio tradizionale in termini di accuratezza e consumo energetico.

Inoltre, un appropriato algoritmo di controllo può migliorare le prestazioni del sistema. Il controllo ottimo lineare quadratico riveste un ruolo fondamentale nel controllo di un robot a cavi parallelo fornendo tutti gli stati del sistema per la retroazione, incluse velocità e posizione, in aggiunta ai risultati ottimali. Un controllo ottimo lineare quadratico è stato progettato e testato. I risultati significativi sono quindi stati presentati e discussi.

Parole chiave: robot adattativi a cavi, indici di prestazione, vibrazioni trasversali, metodo dinamico di controllo delle tensioni minime, controllo ottimo lineare quadratico.

Chapter 1

Introduction

In the recent past, many research works have been published on cable-based systems, reflecting the considerable interest of the researchers in this area. Cable-Driven Parallel Robots (CDPRs) use cables to control the end-effector (EE) pose, strengthening classic advantages characterizing closed-chain architectures, like large payloads, high dynamic performances, better efficiency, etc., while providing peculiar advantages, such as very light weight, large workspace, reduced manufacturing and maintenance costs, superior modularity and reconfigurability [1]. Moreover, CDPRs can be easily shaped and adapted to fit certain application or performance requirements, showing greater flexibility with respect to traditional robot designs [2]. In this section, a brief introduction to cable-based systems is presented.

1.1 Application

The application of cable-driven systems has risen significantly. One of the first application of cable systems is RoboCrane [3]. It uses the basic idea of the Stewart platform parallel link manipulator and cables. The NIST RoboCrane has the capacity to lift and precisely manipulate heavy loads over large volumes with fine control in all six degrees of freedom. Also, NIST developed an advanced RoboCrane controller. The graphic off-line control capability of this controller made programming of numerous controllers easy and fast [4]. Recently, a new cable-driven system for transportation of loads in industrial area has been developed which

Figure 1.1: a. The NIST RoboCrane [4], b. Cogiro (The Europe biggest cable-driven parallel robot) [5]

is called CoGiRo [5]. It is the Europe biggest cable-driven parallel robot with a crane-like configuration. It can be controlled with a manual operation mode via joystick. The RoboCrane and Cogiro are shown in Fig. 1.1.

Kawamura et al. [6] presented a new ultrahigh speed robot design, FALCON-7 which is a cable- driven parallel system. They showed that the use of wires with nonlinear spring characteristics improved the system transient response, but it also complicated the study of stability. Their experimental results showed stable manipulator performance. In their new study [7], an effective method based on using internal force of cables was proposed to reduce vibration.

Yangwen et al. [8] made a new wire-driven parallel suspension system for airplane model in low-speed wind tunnel, and studied the methods to measure and calculate the aerodynamic parameters of the airplane model. The research results validated the feasibility of using a wire-driven parallel manipulator as the suspension system for low-speed wind tunnel tests.

Gosselin et al. [9] presented a 3-DOF cable-driven planar parallel haptic interface. The control of the prototype developed in this work was based on the use of the force/torque sensor to infer the intentions of the user and to calculate corresponding prescribed poses. To limit the forces involved, the platform of the prototype of haptic interface was manipulated with the hands. Gallina et al. [10] developed a 4-wire driven 3-DOF planar haptic device

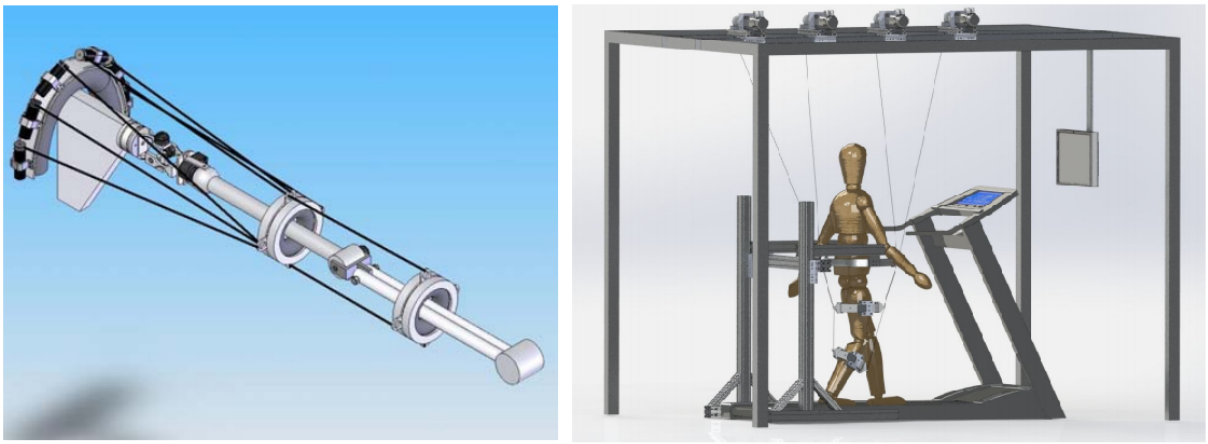

Figure 1.2: a. A wearable upper arm exoskeleton for human users [13], b. A design of a cable-driven active leg exoskeleton (C-ALEX) for human gait training [14]

called Feriba-3.The device demonstrated to be a well-performing haptic device, ensuring a good manipulability in a large workspace.

Many researchers have used cable-driven systems to design more efficient medical devices. Rosati et al. [11], [12] developed a three degrees-of-freedom (DoF), wire-driven robot for poststroke upper-limb rehabilitation (NeReBot). Basically, the robot consists of a set of three wires independently driven by three electric motors. The wires are connected to the patient's upper limb by means of a splint and are supported by a transportable frame, located above the patient. By controlling wire length, rehabilitation treatment (based on the passive or active-assistive spatial motion of the limb) can be delivered over a wide working space.

Brackbill et al. [13] proposed a cable-driven exoskeleton. The dynamics, control, and preliminary experiments on a wearable upper arm exoskeleton intended for human users with four degrees-of-freedom, driven by six cables was presented. Cable-driven systems are used in rehabilitation devices, which yield some benefits (Fig. 1.2.a). A design of a cable-driven active leg exoskeleton (C-ALEX) for human gait training was proposed in [14]. The advantages of cable-driven designs are that they have a simpler structure, add minimal inertia to the human limbs, and do not require precise joint alignment. The results of their experiments showed that the proposed sysmtem is capable of helping the subjects better track a prescribed ankle path (Fig. 1.2.b).

In another study [15], the possibility of using a cable-driven system to train subjects oper-

ating a laparoscopic tool was investigated. A cable-driven system was developed to help the tip of the laparo-tool to stay on a desired trajectory. An experiment was conducted with the system to test training subjects with a simple trajectory following task with the laparoscopic tool. The result of the experiment showed that the subjects were able to better perform the task after training with the robot .

A rapidly deployable cable robot to augment search and rescue mobile robots was proposed in [16]. This system can greatly increase the range of mobile robots as well as provide overhead views of the disaster site, allowing rescue workers to reach survivors as quickly as possible while minimizing the danger posed to rescue workers. In addition to the system concept, they presented a novel kinematic structure for the cable robot. Merlet et al. [17] proposed an innovative fully autonomous parallel wire crane. Their design had the flexibility for managing the location of the anchor points of the cables on the ground and on the platform. The possibility of partial platform location control through the management of the kinematics with less than 6 cables was considered in this robot. This device can play an important role in rescue operations by providing quickly a heavy lift ability in environment.

Five hundred meter aperture spherical radio telescope (FAST) was built consisting a light focus cabin (end-effector) driven by cables and servomechanism plus a parallel robot as secondary adjustable system to carry the most precise parts of the receivers for astronomical observation [18] (Fig. 1.3.a). Pott et al. [19] introduced a family of cable-driven parallel robot called IPAnema that are designed for industrial processes. They addressed the system architecture, key components such as winches and controller, as well as design tools. Furthermore, some experimental data from the evaluation were presented to illustrate the performance of cable robots.

Recently, a new cable robot simulator was developed at the Max Planck Institute for Biological Cybernetics. CableRobot Simulator [20] is an advanced virtual reality simulator. In the cable-driven simulator, the motion of the simulator cabin is controlled by eight unsupported steel cables attached to winches. In contrast to conventional motion simulators, the use of cables makes it possible to reduce the moving mass and to scale the workspace to any required size (Fig. 1.3.b).

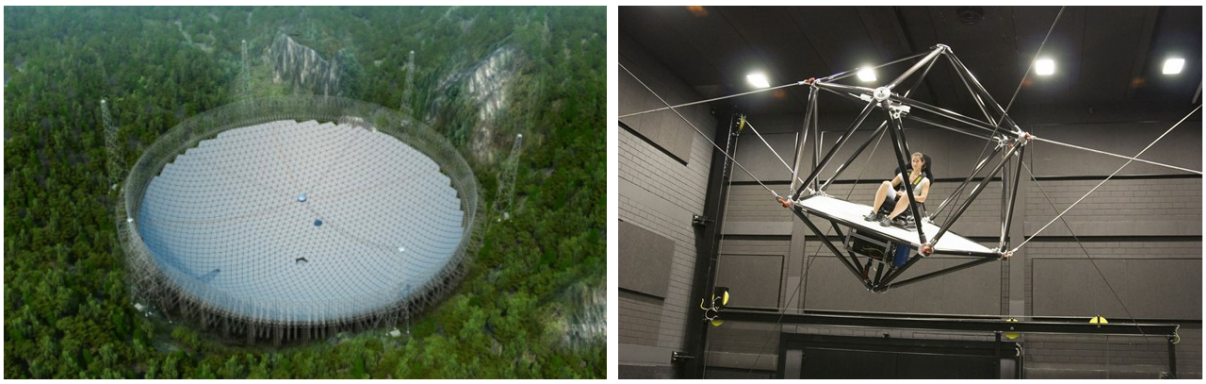

Figure 1.3: a. Five hundred meter aperture spherical radio telescope (FAST) [18] , b. CableRobot Simulator developed at the Max Planck Institute for Biological Cybernetics [20]

Figure 1.4: A cable-suspended camera system [23]

Cable-suspended camera systems are widely used in stadiums and arenas. They usually feature four motorized winches, each connected to the end-effector (i.e., the camera) with a cable passing through a fixed idle pulley [21]. Such systems consist of three major components: the reel—the motor drive and cables, the spar—the counterbalanced pan and tilt video camera, and central control, the computer software used by the operator to fly the camera [22]. (Fig. 1.4)

1.2 Design

A complete review of cable-driven systems design can be found in [24] which is presented in this section. In the past years, the employment of cables in robotics gave rise to a variety of design solutions. Basically, cables may work in conjunction with a rigid-link structure by actuating the kinematic chain, or may substitute traditional rigid-link structures, by directly acting on a rigid body (i.e., the moving platform or end-effector). In both cases, the motors may be mounted at the base of the manipulator, thus reducing the inertial load.

Cable-driven serial link structures (Fig. 1.5) are often used in planar devices (e.g. [25], [26]). Even though hybrid solutions have been developed where a parallel chain made by cables is employed to actuate the serial structure [27], [28], the commonly adopted layout is the one having each cable passing through the previous joints before reaching the corresponding rigid link (e.g. [29]). Thus, it may be an issue to guide cables around the joints in 3D applications. The problem can be tackled by using bowden cables [30], [31], however, this solution increases friction, which must be compensated by control. Prototypes of this class of manipulators have been recently presented in the field of rehabilitative robotics [32]. Determining the controllable workspace of generic cable-driven open chains still remains an open question, even though a novel study has recently been published, which deals with this topic [33]. Parallel rigid-link chains that are driven by cables have been designed as well (Fig. 1.6). These designs present a further advantage, as the load can be distributed among the actuators [34], [35].

This work focuses on cable-based parallel robots, i.e., those devices where a single rigid body, called the end-effector, is directly supported by cables. Traditionally, each cable is actuated by an independent motor, which controls the cable length and tension. Besides the actuated cables, a set of passive, fixed-length wires may also be installed to constrain the movements of the platform [34].

A main difference between cable-based parallel systems and common parallel robots is that cables can only carry tension forces. This characteristic is usually referred to as unilateral actuation. The use of elements capable of exerting unilateral forces has many implications. First of all, having the number of actuators greater than the number of DOFs forces the de-

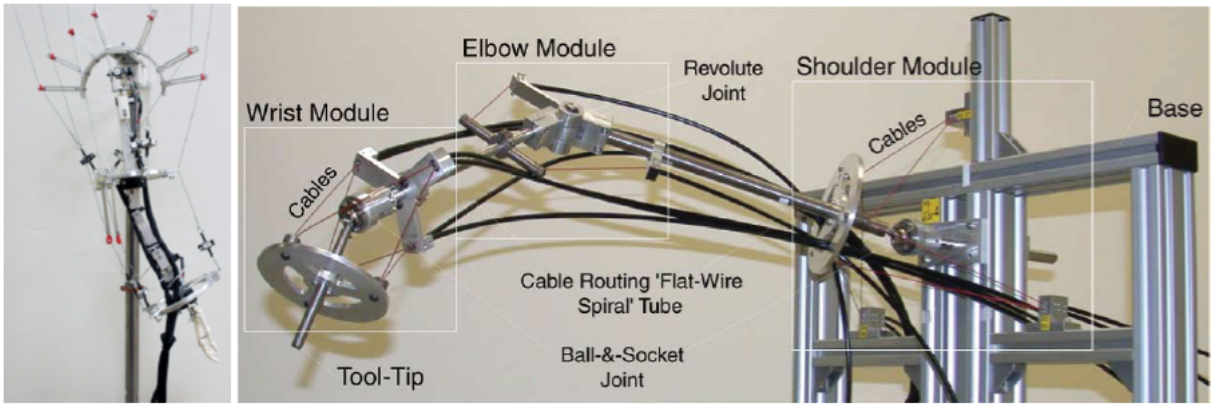

Figure 1.5: Two examples of cable-driven serial link structures: a. the Wearable cable-driven upper arm exoskeleton [29]; b. the Biologically Inspired Cable-Driven Robotic Arm [30].

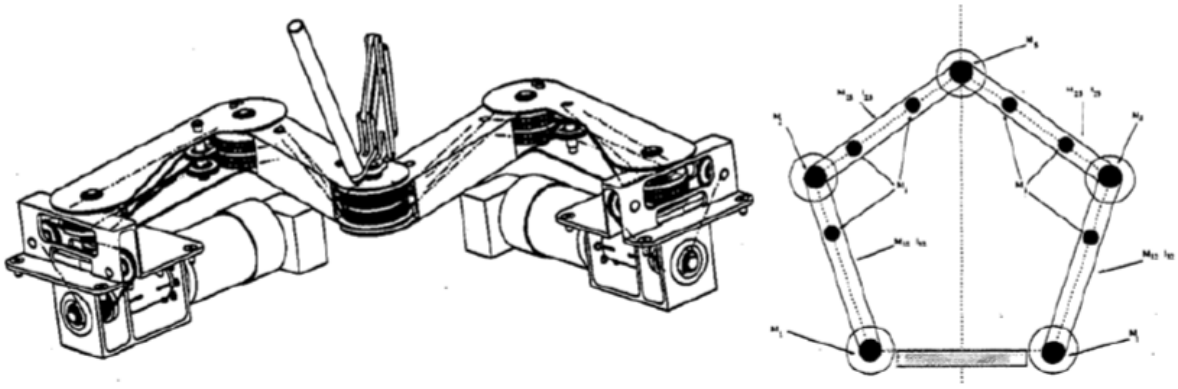

Figure 1.6: Haptic display consisting of a parallel rigid-link structure driven by cables [35].

signer to employ algorithms that seek a feasible tension distribution for any given wrench. Secondly, unlike traditional rigid-link devices, the workspace does not depend on geometric constraints solely. Indeed, the workspace wherein the mobile platform is controllable is a function of both the cables configuration and of the allowable range for the cable tensions.

As it will be discussed in the following section, the analysis and optimization of the workspace is a major topic in the related Literature [34]. The broadest definitions of workspace (e.g. "theoretical" [35], "force-closure" [36], "statics" [35], "controllable" [37] or "useful" [34] workspace) are purely geometrical. These depend on cable disposition only and are related to the capability of exerting arbitrary wrenches at end-effector. Other workspaces may be depened as subsets of the previous ones, by introducing additional requirements (e.g. cable tension constraints, required set of wrenches or accelerations, etc.).

Definitnition We define the workspace of a cable-based system as the set of end-effector poses in which the system is manipulable [38]. A cable-based system is manipulable at a given configuration if any wrench can be exerted with only positive tensions on cables [1].

A necessary and sufficient condition for a cable-based robot to be manipulable was first investigated by Y. Shen e H. Osumi [41], who stated that a rigid body with m DOFs can be manipulated by at least n = m+ 1 cables if and only if the structure matrix **S**.[2], that maps the vector of cable tensions to that of the exerted wrenches is full rank, and there exists a vector $\alpha \in ker(S) s.t. (\alpha > 0) \vee (\alpha < 0)$.

Cable-driven parallel robots can be classified into Incompletely Restrained Positioning Mechanisms (IRPMs, $n \leq m+1$), Completely Restrained Positioning Mechanisms (CRPMs, $n = m+1$), and Redundantly Restrained Positioning Mechanisms (RRPMs, $n > m+1$). This classification derived from a previous notation by Ming and Higuchi [42]. IRPM are not manipulable by means of the forces exerted by the cables. Indeed, they relies on an external force to keep the cables stretched, which can be provided by dynamics, gravity, or an extra actuator/spring. The definition of tensionability was introduced to address the aptitude of an IRPM to remain in tension under any loading, with a large enough ballast force [39].

[1] Other authors used different, equivalent terms to denote the condition of manipulability (e.g., tensionability [39] and controllability[40])

[2] The transposed Jacobian matrix of a cable-based parallel manipulator is usually denoted as the structure matrix in the Literature.

Clearly, knowing the workspace of the system and its force exertion capabilities is crucial for planning even basic tasks. Unfortunately, close-form definitions of the workspace boundaries are available for specific classes of devices only [43]. The common tools to investigate general designs are numerical algorithms. In [44], a distinction is pointed out between discrete and continuous numerical algorithms.

In the former approach, the feasible range of values for each design parameter is discretized into a set of values. A superset of the target workspace (usually a spatial box) is also discretized into a grid of equally spaced points. Then, for each combination of the design parameters, a certain performance index is computed in each point of the grid. The resulting optimal design is the one yielding the maximum average value of the performance index [45]. Sometimes the number of points belonging to the controllable workspace is employed instead of a specific performance index.

Discrete algorithms are generally unable to detect singularities and require higher computational times as the resolution of the grid is incremented. To overcome these issues, continuous algorithms based on the interval analysis have been recently proposed. A detailed review on these approaches is presented in [44].

Roughly speaking, motors number and locations must be chosen carefully, in order to achieve the desired controllable workspace: otherwise forces exertion will be strongly reduced both in magnitude and allowable directions, despite of the sizes of the motors and the number of cables. Besides workspace optimization and positioning accuracy, the control system may be another major issue, since cables must always be kept in tension. Cable interference and disturbances due to friction in pulley-block [3] rollers increase the complexity of the control architecture as well.

1.3 Adaptive Cable-Driven Parallel Robots

Adaptive cable-driven parallel robots are defined as those cable-driven systems wherein the locations of one or more pulley blocks are controlled as a function of the end-effector pose

[3] The term is used throughout this thesis to indicate a pulley and the set of devices required to control its position and the exerted torque (e.g., motor, gearboxes, idle pulleys, feedback sensors, etc.).

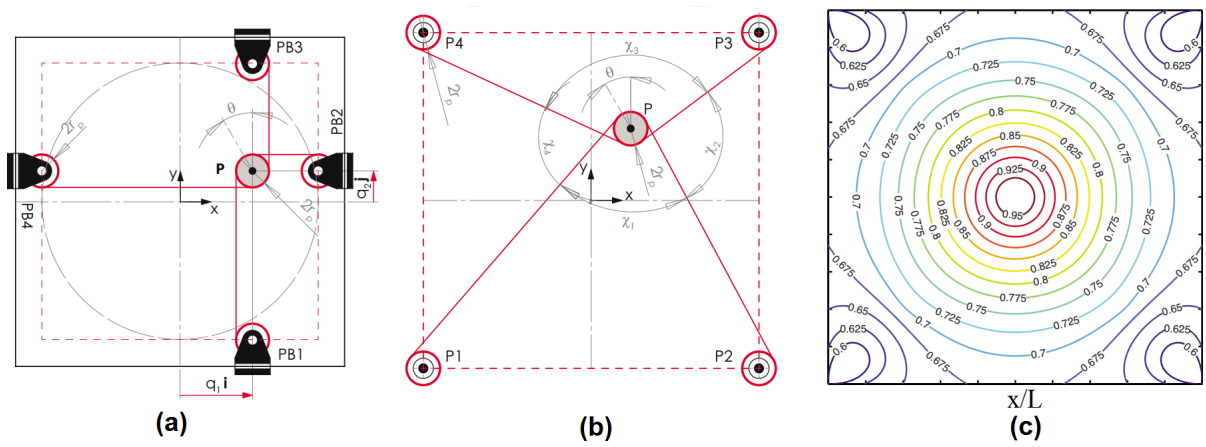

Figure 1.7: a. Adaptive and b. Traditional design of four-cable, 3-DOF cable-driven parallel robot, c. Dexterity index for the traditional design [2]

to optimize given performance indices within a target workspace [2]. Fig. 1.7.d depicts an adaptive design of 3-DOF planar cable-driven system and a traditional 3-DOF cable-driven parallel robot is shown in Fig. 1.7.b.

Due to the augmented kinematic redundancy, such systems enable higher performance compared to traditional designs with fixed cable entry points and equal number of cables. This feature can be quite beneficial in several applications. For example, cable-suspended camera systems are widely used in stadiums and arenas. They usually feature four motorized winches, each connected to the end-effector (i.e., the camera) with a cable passing through a fixed idle pulley. The use of adaptive cable-driven system in this scenario would increase dexterity and stiffness throughout the workspace volume, thus making the device more robust to adverse weather effects (e.g., wind gusts) and to collisions with external objects (e.g., a ball), which may cause failures in these systems [22].

Rosati and co-workers proposed the use of movable pulley-blocks to increase the workspace area and the maximum isotropic force in 2-degree-of-freedom (DOF) cable-driven parallel systems [46]. They presented a method to keep the end-effector in the best part of the working space by properly moving the pulley-blocks. They applied their novel design concept to different planar point-mass cable-driven robots, with one or more translating pulley-blocks. The maximum feasible isotropic force, and dexterity were employed to compare the performances of different configurations. Fig. 1.7.c shows the contour lines of reciprocal dexterity

index for the traditional design of Fig. 1.7.b. The reciprocal dexterity index is changing between 0 and 1 for this design; however they showed that the adaptive design is capable of keeping ideal dexterity (dexterity index is alwys 1) in all the workspace.

The same authors later formalized a new design method for such systems, which enables to determine the optimal trajectory planning of the moving pulley blocks given a target level of performance and a workspace area [2]. They also validated this method experimentally through the first prototype of adaptive cable-driven robot, named Sophia-3. Their results from the first experiment conducted on a group of healthy subjects confirmed the feasibility of the semiadaptive design; the implemented force field was capable of significantly improving users' performance in terms of movement accuracy and execution time [47].

Zhou et al. [48], [49] introduced the cooperating mobile cable robots, a type of payload cable-driven manipulators. They proposed a generalized modeling framework for systematic design and analysis of cooperative mobile cable robots, building upon knowledge base of multi-fingered grasping, and illustrated it with a case study of four cooperating gantry mounted cable robots transporting a planar payload. They showed its wrench closure workspace and reconfiguration to extend the workspace, as well as redundancy resolution by optimally repositioning the bases to maximize tension factor along a given trajectory. They used mobile pulley blocks to increase flexibility and to maximize the ratio between the minimum and the maximum cable tension (i.e., the tension factor) along a desired trajectory. Based on this concept, they designed a planar system with three cables routed to the end-effector [50]: the extremities of each cable were fixed on a double-slider moving along the side of an equilateral triangle.

The same authors later proposed the design of a compliant mobile robot with springs connected in series to cables to achieve optimal stiffness [51]. They presented a elastic mobile cable robot and explored the modulation of its task space stiffness via both internal tension as well as utilizing the configuration redundancy. It was shown the kinematic redundancy allows for wider range of control over the Cartesian stiffness matrix than utilizing only internal tensions. They have shown that the stiffness can be actively modulated along a desired trajectory for better positioning accuracy. In this prototype, the vibration induced by the springs,

coupled with parametric uncertainties could not be controlled efficiently.

Several groups studied spatial reconfigurable cable-driven systems. Rosati et al. [52], [53] presented a 5-DOF spatial cable robot for post-stroke rehabilitation. This system features wires connected to moveable links to enhance the workspace. The study revealed statistically significant benefits of robotic therapy in persons with stroke-related paralyzed or paretic upper limb.

Nguyen et al. [54], [55] introduced a spatial reconfigurable cable suspended robot for lifting and transferring heavy loads. They proposed a 6-DOF mobile platform of the CDPR, which was driven by 8 cables and two overhead bridge cranes. Their algorithm for reconfiguration solves an optimization problem, using power consumption and the displacement of the moving pulley-blocks as cost functions. By minimizing the sum of the cable tensions, the cable exit points were moved to the positions, where the cables were as vertical as possible while balancing the mobile platform weight.

Gagliardini et al. presented a spatial reconfigurable cable robot for sandblasting and painting of large structures [56]. To reconfigure the CDPR from one side of the structure to another one, they proposed one or several cables to be disconnected from their current anchor points and moving to new ones. They minimized the robot size as well. Later, they proposed an optimization method to minimize the number of reconfigurations as well as the reconfiguration set-up time [57].

1.4 Cable-Based Devices at DTG

In this Section, the robotic devices developed at the Robotics, Mechatronics and Rehabrobotics Labs of DTG (The Department of Management and Engineering, University of Padua, Padua, Italy) are introduced using [24].

1.4.1 General-Purpose Haptic Displays

The Feriba3 [10], [38], depicted in Fig. 1.8.a, is a 4-wire planar CRPM with a circular end-effector and a square-shaped workspace. It was designed to be used as a general-purpose

(a) (b)

Figure 1.8: The desktop-like, general-purpose haptic displays designed at DTG: Feriba3 [10], [38] (a) and Piroga5 [58], [59], [60] (b).

haptic display, i.e., a device capable of reproducing real and virtual environments by exerting a variable mechanical impedance to the user's hand. It exploits 4 driven cables to generate 3 generalized forces on a round-shaped end-effector. The end-effector position is imposed by the operator, who perceives the force-feedback from the device. The direction and amount of force reflected depends on end-effector position and on the specific remote or virtual environment represented.

Each wire is fixed to the lateral side of the circular end-effector (named spool) and can wind around the end-effector. The other end of the wire is wound around a pulley, that is directly keyed on the shaft of a DC motor. Each pulley-block provides tension in the corresponding cable up to $f_{max} = 10N$. The motors are mounted on a steel base at the vertices of a square ($l = 450mm$).

The spool consists of a lower disc-shaped base and an upper circular handle that are connected by means of a universal joint, so as to avoid transmission of dumping moments. To minimize the spool friction, a sheet of glass is fixed on the base and a flux of compressed air is blown towards the glass through a series of little holes drilled in the lower side of the spool.

This solution, together with the selection of low rolling-friction motors, aims to reduce the mechanical impedance perceived at the end-effector, thus improving the haptic transparency

obtained at the end-effector. The base of the end-effector and the pulleys have the same winding radius $r = r_p = 30mm$: this feature ensures a simple, closed-form forward kinematic algorithm, avoids cable/end-effector interferences and has favorable consequences on the performances of the device, since two force components and one moment can be generated independently on the end-effector, regardless its position in the working space.

PiRoGa5 is a cable-driven 5-DOF haptic display, with a pen-like shaped end-effector [58], [59], [60]. Six wires are attached to the end-effector, three to each end-point of the pen(Fig. 1.8.b). Each wire is tensioned by a motor-pulley direct drive system. Pulley radius is 15mm: this value represents a trade off between the maximum force each wire can exert and the transparency of the haptic display.

The operator is able to move the end-effector along six DOFs; nevertheless, the control system is able to apply only five generalized forces to the pen (three forces and two torques), since wire configuration prevents the system from generating any torque along the pen axis. Each wire is forced to pass trough a PTFE eye-bolt: odd and even eye-bolts belong to two different parallel planes. On each plane, the three corresponding connections to the ground represent the vertexes of an equilateral triangle.

The force generated by the three wires connected to the each extremity of the pen belongs to the pseudo-pyramid formed by the same wires: hence, the total wrench acting on the end-effector is given by the composition of two such forces. Accurate machining leads one to consider the three wires meeting on the pyramid vertex, so that forward kinematics and wire tension computation can be carried out in closed form.

The wire-driven architecture leads to a very simple and light mechanical structure, low costs and high transparency. The main drawback is that with six actuators, only five generalized forces can be generated on the end-effector. Correspondingly, the control system is not able to detect end-effector orientation along its main axis.

1.4.2 Robots for the Rehabilitation of the Upper-Limb

Both the Feriba3 and the Piroga5 were not specifically conceived for rehabilitation purposes, and were used for laboratory tests, both in the field of haptic teleoperation and in the simu-

lation of virtual environments. In the following, three cable-based devices specifically conceived for the treatment of post-stroke patients will be discussed: the NeReBot, the MariBot and the Sophia-4.

The NeReBot (NEuro REhabilitation roBOT) employs 3 cables to sustain and move the forearm of the patient during the rehabilitation treatment. The device is easily transportable, and represents a good compromise between robot simplicity and range of motion.

The NeReBot is shown in Fig. 1.9.a. The robot is composed of a wheeled base and a manually adjustable overhead structure, from which the wires originate. Three driven wires are used to sustain a splint on which the forearm of the patient is fastened [61], [11]. The exercise can be recorded by using a very simple teaching-by-showing procedure: the therapist moves the patient's arm through a set of via-points, which are recorded by the machine learning phase); after this, the control system generates joint-interpolated trajectories for the three motors which control the wires. As a result, a very smooth and comfortable motion of the upper arm is obtained (therapy phase. During NeReBot-assisted therapy, the upper limb of the patient is a 5-DOF kinematic chain constrained by three unidirectional actuators only. Hence, the whole system still have 2 DOF [12]. This gives a very good sensation to the patient, who never feels to be restrained by the machine.

The arm trajectories obtained with the NeReBot have been evaluated by developing a simulation tool addressing the static interaction between the human arm and the robot. By extensively using this simulation tool, a set of optimal configurations of the adjustable overhead structure has been identified. In this way, machine set-up can be optimized according to the specific rehabilitation exercise [11], [12].

This device was tested in two randomized controlled trials (RCT) that gave encouraging clinical results [62], [11], [53]. These results also demonstrated that even a simple, low-cost transportable machine can be very effective in the rehabilitation of post stroke patients.

Some limitations of the NeReBot came up during first clinical trials. Mainly, since the wires originate from a fixed overhead structure, the NeReBot has a good vertical range of motion, but less control of movements in the horizontal plane. To overcome this and other limitations of the first prototype, a new machine was developed, named MariBot [63], [52].

(a) (b)

Figure 1.9: The desktop-like, general-purpose haptic displays designed at DTG: Feriba3 [10], [38] (a) and Piroga5 [58], [59], [60] (b).

The MariBot (MARIsa roBOT) is shown in Fig. 1.9.b. The basic principles from which the NeReBot was designed were maintained. However, the manually adjustable overhead structure was replaced with a controlled 2-DOF serial robotic arm. In this way, wire configuration can be changed during therapy, according to the horizontal motion of the upper limb of the patient. As a result, the working space was improved, encompassing nearly the whole range of motion of the human arm. Moreover, the MariBot does not need to be set-up before the beginning of therapy. Also, the weight of the robot has been reduced significantly, by using a commercial li.ing device as base structure to build the robot. The MaRiBot is currently undergoing lab tests and clinical trials will start in the next future.

Sophia-4 (String Operated Planar Haptic Interface for the Arm-rehabilitation) was conceived for the rehabilitation of chronic patients, and came up as an evolution of the general purpose haptic display FeRiBa3.

The prototype is depicted in Fig. 1.10. Two major aspects were considered in the early design of the device: workspace shape and force capabilities. The dimensions of the workspace were calculated considering the dimensions of the patient's body [64] and his/her sitting pos-

Figure 1.10: The desktop-like, general-purpose haptic displays designed at DTG: Feriba3 [10], [38] (a) and Piroga5 [58], [59], [60] (b).

ture. The length of the lower base of the trapezoidal layout was determined based on the average shoulder distance of adult males, thus allowing the patient to lean his/her elbows outside the lower pulley-blocks during robot therapy. The manipulability index was employed to adjust the force capabilities of the machine to the requirements [65], [66].

A commercial office table constitutes the mechanical structure of Sophia-4. The patient, while sitting on a wheelchair, holds a handlebar-grip that can be moved over a flat horizontal surface, sliding on low-friction PTFE discs. Four nylon cables are used to exert forces at the end-effector, each having one end fixed to a point on the axis of the grip, and the other directly keyed to a direct-drive pulley.

Pulley-blocks which can spin around a vertical axis are used to pass cables underneath the table surface, where the DC motors are mounted. The cables are all attached to a single point of the end-effector, so the device is capable of exerting only horizontal pure forces on the patient's hand. The handlebar-grip itself is mounted on the base of the end-effector by means of a ball bearing, in such a way that no moment can be transmitted to the patient's hand along the vertical axis.

A real-time high-level controller manages the type of assistance to be given to the patient, while a low-level controller is responsible for kinematics, force distribution algorithms and

surveillance routines [67], [66]. The therapy consists of point-to-point reaching tasks.

Chapter 2

Problem Statement

The aim of this research is to investigate on trajectory planning and control of cable-driven parallel robots to increase the performance. Stiffness and dexterity are the most important performance indices used in design and control of robotic systems. Also employing an appropriate high-level control algorithm can increase the system performance. In this chapter, the main research studies related to stiffness, vibration, cable tension distribution and control algorithms are reviewed and the contribution of this work to increase the performance of cable-driven parallel robots is presented in the last section.

2.1 Stiffness and Vibration

Poor stiffness may result in vibrations, which can lead to some problems, specially in applications requiring high bandwidth or stiffness [68]. A large number of studies have been performed to assess the stiffness and vibration of cable-driven parallel robots. The main focus of many studies was dedicated to gain a stiffness matrix under different assumptions, such as neglecting the cable mass while discussing on stability of cable-based manipulators. Behzadipour et al. [69] introduced a new approach to derive the total stiffness of parallel cable-driven robots. They categorized the total stiffness of a cable-based parallel manipulator to two different stiffness matrices. The first one is representing the cable stiffness and a part of the cable forces effects. The second one is a rotational stiffness and caused only by internal

forces which may be unstable even if the manipulator is rigid.

However, it has been pointed out that when the cable mass is considered, the effect of tension in cables on the stiffness of the robot is high. Arsenault [70] considered the cable mass and showed that the sagging of the cables under their own weight influences the stiffness heavily and proposed to keep a minimum level of cable tension to minimize the effect of cable sagging. Moreover, no special idea about cable vibration wave can be gained by neglecting the cable mass.

On the other hand, the stiffness of cable-driven robots is mostly studied in terms of longitudinal vibration of the cables; however a cable with large longitudinal tension expresses an increased transversal stiffness [71]. In many real applications of parallel cable-driven robots, such as cable-suspended camera systems [21] and rehabilitation [11], transversal stiffness can be a major issue which is directly linked to the average of the tension in cables, Izard et al. proposed to increase the tension in cables to generate higher transverse stiffness [72].

Another group of research studies was focused on transverse vibration of an axially accelerating cable in different environments. Initially, the transverse vibration equation of a cable in motion was derived by Miranker [73]. Later, equations were solved for the case of a special velocity profile as a prescribed function of time, by means of converting the formulation to the Mathieu equation [74].

Later, different conditions and equations were considered mostly solved by Galerkin method. Zen et al. [75] derived the equations of motion with the extended Hamilton's principle and discretized in the space domain with the finite element method. The stability of the system was analyzed with the Floquet theory for cases where the transport velocity is a periodic function of time. Direct time integration using an adaptive step Runge-Kutta algorithm was used to verify the results of the Floquet theory. The presence of friction adversely affects stability, but using non-zero spring stiffness on the guiding force has a stabilizing effect. They showed the use of the finite element method and Floquet theory is an effective combination to analyze stability in gyroscopic systems with stationary friction loads.

Chen et al. [76] explored the steady-state periodic transverse responses with their stabilities of axially accelerating viscoelastic strings. Unlike previous studies, they assumed that

longitudinally varying tension due to the axial acceleration was recognized in the modeling. A governing equation of transverse nonlinear vibration was derived from the generalized Hamilton principle and the Kelvin viscoelastic model on the assumption that the string deformation is not infinitesimal, but still small. They applied the method of multiple scales to solve the governing equation in the parametric resonances when the axial speed fluctuation frequency approached the first three natural frequencies of the linear generating system based on 1–3 term truncations.

Korayem et al. [77] studied dynamic analysis of an axially moving cable with time dependent tension and velocity. They assumed that tension force and the moving speed are harmonic. It is found that there exists a specific value of speed in which natural frequency of the system approaches zero. This specific speed for such a critical condition is called critical speed. They carried out the stability analysis for different sets of excitation frequency. In this research, a comprehensive parametric study was carried out and effects of different parameters like the moving speed and tension force on the responses were studied both in frequency and time domain.

Zhang et al. [78] set up the nonlinrear equation of transverse vibration of an axially accelerating string under the consideration of harmonic fluctuations of initial tension and axially velocity. They used the Kelvin model to describe viscoelastic behaviors of the material. Their results showed that the convergence velocity of the complex-mode Galerkin method is higher than that of the real-mode Galerkin method for a variable coefficient gyroscopic system.

No analytical solutions were proposed, and all studies implemented by numerical methods; however, there was no experimental data to validate the numerical results. One reason for further investigation on cable stiffness in cable-driven robots is that recent studies introduced novel approaches in cable robots design [2], [47] and control [79] which may take advantages of novel results on cable stiffness. In such studies, dynamical adaptation of robot geometry and control parameters is proposed, as means of increasing cable robot performance and optimization.

2.2 Cable Tension Distribution

In the case of over-constrained cable robots, where multiple sets of cable tensions can be used to gain the same wrench at the end-effector, many researchers proposed different methods to find optimal tension distributions [80]. The most common approach consists in fixing a constant value as the minimum tension needed in each cable, then finding a set of tensions among those ensuring the desired end-effector wrench with at least one cable at minimum tension [38]. The choice of the set of tension is usually made in according with an optimization method.

Some researchers proposed linear programming to minimize sum of all tensions without cable slack and violating the controllable workspace condition. Normally, the standard form of linear program deals with a non-negative variables. So an algorithm can be introduced to convert bound torque variables into non-negative variables. Optimal torque solutions can be obtained using this method [81], [82], [83].

Moreover, quadratic programming methods for estimation of two-norm optimal tension distributions were applied [84], [85], while Lim et al. [86] proposed a gradient projection method and compared it with linear and quadratic programming. Also, a factor was introduced to adjust the tension solution towards the upper or lower tension limits. Simulation results showed that the algorithm produces tension solutions that are continuous and smooth.

Furthermore, some other methods such as convex optimization for minimization of actuator forces [87], minimization of p-norm [88], L1-norm optimization [89], and using pattern of fingers grasp were proposed [90]. Pott compared different methods and defined weakness of these algorithms, while suggested a modified closed form solution [80]. He showed that no method is known that is real-time capable, covers the full workspace, delivers continuous solution for control, and works for robot with arbitrary degree-of-redundancy.

These methods are based on a *fixed* minimum of cable tension value. Such value was chosen through experiments to gain the desired path tracking accuracy of the system, considering capability of actuators at the same time. Higher minimum tension results in greater stiffness, less vibration, and superior accuracy of motion [81], [91]. Recent studies proposed a lower bound for stiffness to achieve a proper trajectory tracking [92], [51]; however, a feasible

solution may not always exist. More recently, we introduced a method to dynamically change the minimum tension in cables based on total wrench [79].

2.3 Control Algorithms

Applying a proper high-level control algorithm can result in higher performance of a system. Several control schemes such as PID controller were proposed [79] for cable-driven parallel robots. The PID control scheme is the most common control algorithm used in many applications, particularly in the industry, because of its simplicity. However, difficulties in tuning the PID controller gains in the Cartesian cable robot were reported in [93]. They tuned the PID specifically for each of the three Cartesian axis both for translations and rotations which makes this operation more complex than for a PID in joint space. Furthermore, in case of multiple challenges, the PID controller demonstrates low robust ability even if the gains are well-tuned.

Other similar methods have been employed, such as the Robust PID for a translational system with the minimum number of wires under a zero-gravity condition, and the robustness of the control scheme against wire length error was demonstrated [94]. They proposed a robust point-to-point (PTP) position control method in the task-oriented coordinates for completely restrained parallel wire-driven robots, which are translational systems using the minimum number of wires under zero-gravity conditions. In the cases where parallel-wire driven robots are disassembled/assembled and used outdoors (also applied in space), actuator positions would be uncertain or contain some errors. The error of internal force among wires that results from such uncertainty of actuator positions deteriorates positioning performance. To overcome such a difficulty, adaptive compensation was employed for robust PD control against the error of internal force. They showed, not only does this robust PD control method ensure precise positioning using external sensors; it enhances the robustness for uncertainty of the Jacobian matrix, which results from the error of actuator installation.

An adaptive PD [95] was proposed for controlling the suspended parallel robot, and the task-space PD controller was found to exhibit better performance than the joint-space PD controller. They presented a novel model independent task-space PD controller that ensures

end-effector position and attitude tracking based on the quaternion algebra.

In another study, a Robust PD was used to control a cable robot with uncertain dynamic equations. They have outlined the robust PD control using an uncertain Jacobian matrix (called a wire matrix in this research study) for the CR translational system that uses the minimum number of wires under zero-gravity conditions. The results showed that directly measuring not only the position of the controlled object, but also the wire length, ensures linearization of the internal force term. They showed the motion convergence to the desired points, and discussed its robustness based on Lyapunov stability analysis. Results of their experiments and simulations showed that the robust PD control with adaptive compensation is very useful for the case using the uncertain wire matrix. Furthermore, its robustness against wire length error was demonstrated. Suitable tracking performance was shown in experiments of a three degree-of-freedom (DOF) planar cable robot [96].

To control the wind-induced vibration of the end-effector in a suspended cable-driven system, the new fuzzy plus proportional–integral control (FPPIC) method was proposed, and the results that the tracking error of the new algorithm was smaller than that of the PID controller. They provided the examples of simulation and experiment to justify the dynamic modeling for control and to test the proposed method. The simulation and experimental results showed the effectiveness of the proposed control framework. This design was carried on directly in discrete-time and the structure chosen for the realization permits fast computation [97]. Two controllers based on Lyapunov methods and feedback linearization techniques were applied to control a 6-DOF cable-suspended robot; consequently, both controllers showed satisfactory results with a small error [98].

Alikhani et al. [99] addressed the issue of modeling and robust control for a new large scale suspended cable-driven robot. The effectiveness of the sliding mode control was also tested on a large-scale suspended cable-driven robot with unknown disturbances. The asymptotic stability and robustness of the proposed control law was proven by using the second method of Lyapunov. The proposed robust controller ensures positive cable tensions while acquired inequalities hold. Numerical simulation results illustrated the effectiveness of the proposed scheme.

Recently, several methods based on optimization techniques, such as the H∞ Control, were applied. Such a controller can manage both the position of the end-effector and the cable tension. Flexible effects of the cables can be considered and the improvement in bandwidth can be achieved; however, the proposed method was not adaptable to all the behaviors of the system [100].

By comparing the inaccuracy of cable robots with the rigid linked robots, the LQ optimal control can play an important role in controlling these robots by providing all the states of the system for the feedback, including velocity and position, in addition to optimal results. To the best knowledge of the authors, the LQ optimal controller has been rarely used in cable-driven parallel robots. Habibnejad et al. [101] applied the LQ optimal controller, mainly concentrating on improving the bandwidth and maximizing the Dynamic Load Carrying Capacity (DLCC). They used the LQ optimal controller to optimize controlling gains and experimentally tested the method on a 2-DOF constrained planar cable robot and a 6-DOF under-constrained cable robot. They achieved satisfactory results in terms of motor torques and tracking errors.

2.4 Contributions and Thesis Outline

Dexterity and stiffness are widely employed in design and control of robots. The purpose of this work is to investigate on trajectory planning and control of cable-driven parallel robots considering these two performance indices. Dexterity is an index, which only depends on the orientation of the cables [102]. Stiffness can be categorized to active and passive(elastic) parts. The elastic stiffness depends on the orientation and the lengths of cables, whereas the active stiffness depends on orientation and the tension in cables [69].

Adaptive cable-driven parallel robots have augmented kinematic redundancy and the inverse kinematics problem of such robots may have more solutions compared to the traditional cable-driven parallel robots. The solution with the best dexterity and stiffness can be considered as an optimum solution.

Active stiffness is related to the tension in cables, which is associated to the end-effector motion trajectory. Also changing the cable orientations to achieve optimum elastic stiffness

and dexterity can affect the active stiffness. In this research study, a quasi-static trajectory is considered for end-effector of adaptive cable-driven robots and the active stiffness index is neglected. Moreover, typical settling time of a mechanical system is much higher than that of motor torques; so, cable orientation adaptation is a proper approach to improve the stiffness index in wider regions of the workspace and to avoid interference of cables. This adaptability cannot provide fast changes in stiffness, which may be necessary to face external disturbances.

No previous work on adaptive cable-driven systems has discussed how to control the position of the pulley blocks to achieve optimal dexterity and elastic stiffness. We investigate on the optimum trajectory of pulley blocks. The motivation behind the third chapter is to propose pulley blocks trajectory planning strategies that maximize dexterity and elastic stiffness indices simultaneously for some examples of adaptive cable-driven designs previously introduced in [11] by taking advantage of the increased redundancy.

In non-adaptive design of cable-driven parallel robots, orientation and length of the cables are fixed for a specified position of end-effector, so it is impossible to improve performance considering dexterity and elastic stiffness indices. The performance improvement can be implemented by changing the tension in cables and adjusting the active stiffness. It is the only way of rapidly adapting stiffness specially in case of large tracking errors.

Cable tension increment can be desirable due to stiffness augmentation, higher trajectory tracking performance, more precise motion and disturbance rejection; however, it can increase power consumption, and saturation in actuators may occur. Cable tension distribution methods work based on a fixed minimum tension in cables. Such values are chosen through experiments to gain the desired path tracking accuracy of the system, considering capability of actuators at the same time.

The fourth chapter investigates on proposing an algorithm to change the minimum tension in cables to improve the robot performance. We introduced a method that allows running the system efficiently by dynamically controlling the minimum tension in cables considering accuracy and power consumption. The main idea behind this algorithm consists in dynamically calculating a suitable minimum value for cable tensions, while applying a stan-

dard tension distribution algorithm.

In addition, applying a proper high-level control algorithm is important to increase the system performance. The fifth chapter is dedicated to linear quadratic(LQ) optimal control of cable-driven parallel robots. By comparing the inaccuracy of cable robots with the rigid linked robots, the LQ optimal control can play an important role in controlling cable robots by providing all the states of the system for the feedback, including velocity and position, in addition to optimal results. This algorithm has been rarely used in cable-driven parallel robots. In the fifth chapter, the results of testing a LQ optimal controller on a planar cable-driven parallel robot are presented.

Chapter 3

Optimizing Stiffness and Dexterity of Planar Adaptive Cable-Driven Parallel Robots

This chapter is dedicated to investigate on increasing adaptive cable-driven parallel robots performance by controlling the position of pulley blocks to achieve optimal dexterity and elastic stiffness. Adaptive cable-driven parallel robots are a special subclass of cable-driven systems in which the locations of the pulley blocks are modified as a function of the end-effector pose to obtain optimal values of given performance indices within a target workspace. A sample design of 2-DOF planar apativecable-driven robot is shown in Fig. 3.1. The pulley blocks are capable of moving along the sides of an equilateral triangle.

Due to their augmented kinematic redundancy, such systems enable larger workspace volume and higher performance compared to traditional designs featuring the same number of cables. Previous studies have introduced a systematic method to optimize design and trajectory planning of the moving pulley-blocks for a given performance index. We study the motions of the pulley blocks that optimize two performance indices simultaneously: elastic stiffness and dexterity. Specifically, we present a method to determine the pulley blocks motions that guarantee ideal dexterity with the best feasible elastic stiffness, as well as those that guarantee isotropic elastic stiffness with the best feasible dexterity. We demonstrate the

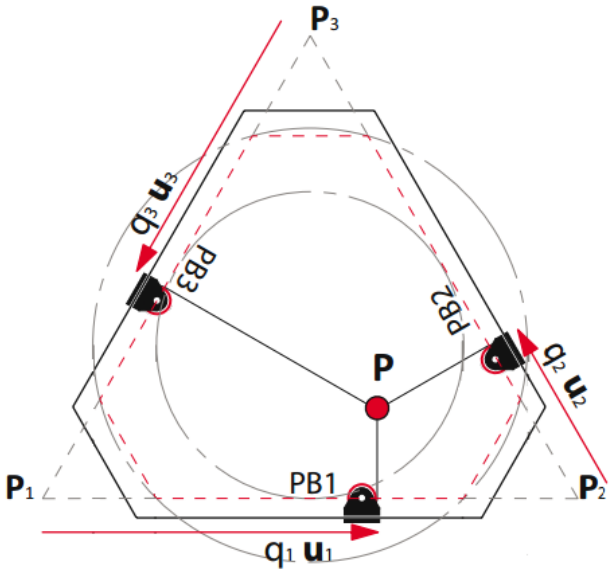

Figure 3.1: Planar 2-DOF adaptive design of a cable-driven parallel robot with linear guides

proposed approach on some practical cases of planar adaptive cable-driven parallel robots.

3.1 Planning Strategy

Elastic stiffness and dexterity are widely employed as performance indices in the design and control of robotic manipulators. The elastic stiffness index depends on the relative orientation of the cables and on their lengths (in the following, we use the term cable configuration to address this pair of variables), whereas dexterity depends on the relative orientation of the cables only. The following methods are proposed to obtain the conditions that guarantee: (i) ideal dexterity with the best feasible elastic stiffness and (ii) isotropic elastic stiffness (or the best feasible stiffness, if isotropy cannot be achieved) with the best feasible dexterity.

3.1.1 Elastic stiffness with ideal dexterity

Step 1: Choose a specific design of fully adaptive cable-driven device.

Step 2: Set the design goal: to achieve ideal dexterity with the best feasible stiffness in a target

region of the workspace.

Step 3: Derive a set of acceptable cable orientations, which yield ideal dexterity.

Step 4: For each location in the target workspace, derive the stiffness and magnitude indices for the set of acceptable cable orientations identified in step 3. Choose the cable orientation yielding the best stiffness and magnitude indices.

Step 5: Define the movements of the pulley blocks as a function of the trajectory of the end-effector, which allow the system to achieve the cable configurations identified in step 4.

Step 6: Calculate design parameters for a workspace capable of maintaining ideal dexterity and $\kappa(K) \leq \kappa(K)_{\mathrm{REQ}}$.

3.1.2 Best feasible dexterity with isotropic elastic stiffness

Step 1: Choose a specific design of fully adaptive cable-driven device.

Step 2: Set the design goal: to achieve isotropic stiffness with the best feasible dexterity in a target region of the workspace.

Step 3: For each location in the target workspace, derive a set of acceptable cable configurations, which yield isotropic stiffness. If isotropic stiffness cannot be achieved, choose the set of cable configurations, which yield the highest stiffness indices.

Step 4: For each location in the target workspace, derive the dexterity index for all the acceptable cable configurations identified in step 3. Choose the cable configuration yielding the best dexterity.

Step 5: Define the movements of the pulley blocks as a function of the trajectory of the end-effector, which allow the system to achieve the cable configurations identified in step 4.

Step 6: Calculate design parameters for a workspace capable of maintaining isotropic stiffness and $\kappa(J) \leq \kappa(J)_{\text{REQ}}$.

3.2 Performance Indices

3.2.1 Dexterity index

The dexterity index, which describes the local kinematic behavior of a system, is defined as [102]

$$\kappa(J) = \frac{\sigma_{\max}}{\sigma_{\min}}, \tag{3.1}$$

where $\sigma_{\max}$ and $\sigma_{\min}$ are the largest and the smallest singular value of the Jacobian matrix J, respectively. $\kappa(J)$ may vary from 1 to infinity: when it approaches 1, the Jacobian matrix is well-conditioned and the pose of the end-effector is far from singularity. Therefore, from the design and control standpoints, configurations yielding $\kappa(J)$=1 are desirable.

3.2.2 Elastic stiffness index and Magnitude

The total stiffness of a cable-driven device is the sum of elastic and active stiffness. The former depends on the stiffness of the cables; the latter is related to the tension in the cables. Since the elastic stiffness has generally a much higher effect on the overall stiffness of the system [103], in this thesis we focus on elastic stiffness only. The elastic stiffness matrix is defined as

$$K = J^{t}\Omega J, \qquad \begin{pmatrix} k_1 & 0 & 0 & \cdots & 0 \\ 0 & k_2 & 0 & \cdots & 0 \\ 0 & 0 & k_3 & \cdots & 0 \\ \vdots & \vdots & \vdots & \ddots & \vdots \\ 0 & 0 & 0 & \cdots & k_n \end{pmatrix}, \qquad k_i = \frac{E_i A_i}{L_i}, \qquad i = 1,2,..,n, \tag{3.2}$$

where Ω is a diagonal matrix having spring constants k_i in the main diagonal. E_i and A_i are the Young's modulus and the cross section area of the ith cable (both considered fixed and equal for all cables), and L_i is the length of the ith cable. Because it is desirable to have a uniform stiffness distribution along all the DOFs, the condition number of the elastic stiffness matrix can be taken as a performance index. This is defined by the following ratio

$$\kappa(K) = \frac{\lambda_{\max}}{\lambda_{\min}}, \tag{3.3}$$

where $\lambda_{\max}$,$\lambda_{\min}$ are the largest and the smallest eigenvalue of the elastic stiffness matrix, respectively. When $\kappa(K)$ is equal to 1, isotropic stiffness is achieved. However, stiff systems and compliant ones might share the same $\kappa(K)$. To capture the stiffness magnitude with a scalar metric, we use the following metric, first suggested by Yeo et al. [104]:

$$\kappa(K) = \frac{{\lambda_{\max}}^2.{\lambda_{\min}}^2}{{\lambda_{\max}}^2 + {\lambda_{\min}}^2}, \tag{3.4}$$

This function has higher values when $\lambda_{\max}$,$\lambda_{\min}$ are equal and large.

3.3 2-DOF planar cable-driven parallel robot with triangular workspace

3.3.1 Traditional design

The traditional design of 2-DOF planar cable robot with triangular workspace consists of a single end-effector supported in parallel by three cables and tensioning actuators. The pulley blocks are fixed in the vertices of a triangle (Fig. 3.2.a). Theoretically, the end-effector can

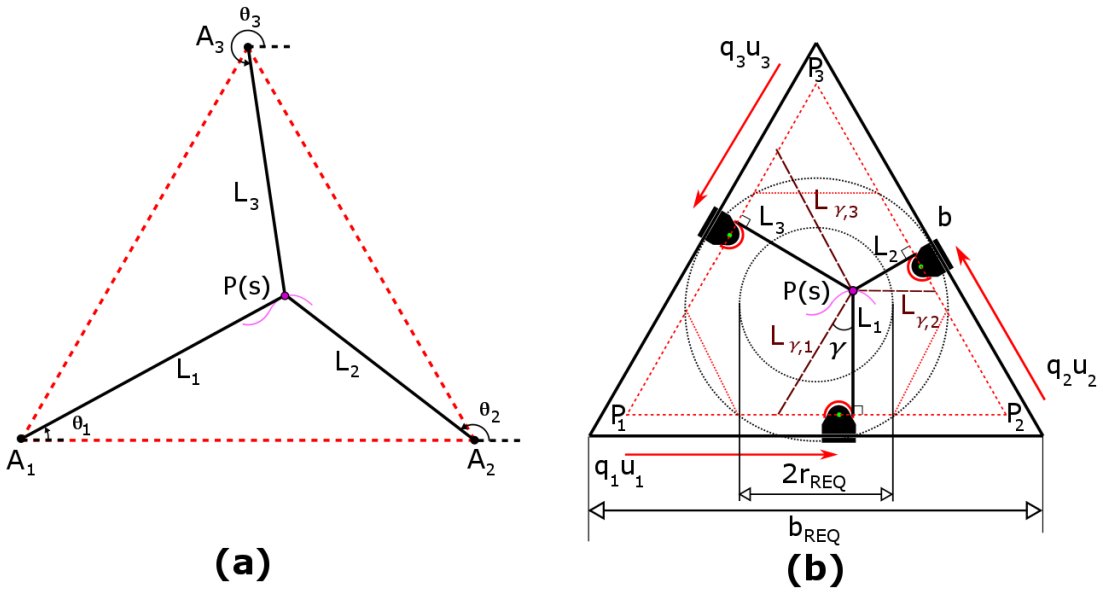

Figure 3.2: a. Traditional design of 2-DOF planar cable-robot with triangular workspace, b. Adaptive 2-DOF planar cable-driven robot with pulley blocks that move along the sides of an equilateral triangle

reach any point within the base polygon and the position of moving point is determined only by length of the cables.

Fig. 3.3 shows the dexterity, elastic stiffness and the normalized magnitude of 2-DOF traditional design. The ideal dexterity and the isotropic elastic stiffness occurs only at the centroid of the workspace and increases while moving the end-effector from the centroid. We will show that similar adaptive design has much better performance and is capable to keep the ideal dexterity within the whole workspace and isotropic stiffness in some parts of the workspace. On the other hand, the normalized stiffness magnitude of the adaptive system is higher than the traditional design shown in Fig. 3.3.c. To show the priority of the adaptive design we investigate on the cases of keeping the ideal dexterity with the best feasible elastic stiffness, as well as isotropic elastic stiffness with the best feasible dexterity.

3.3.2 Adaptive Design

In an adaptive design, the pulley blocks can move and the position of end-effector is dependent to the cable lengths and the location of the pulley blocks. In Fig. 3.2.b pulleys move along

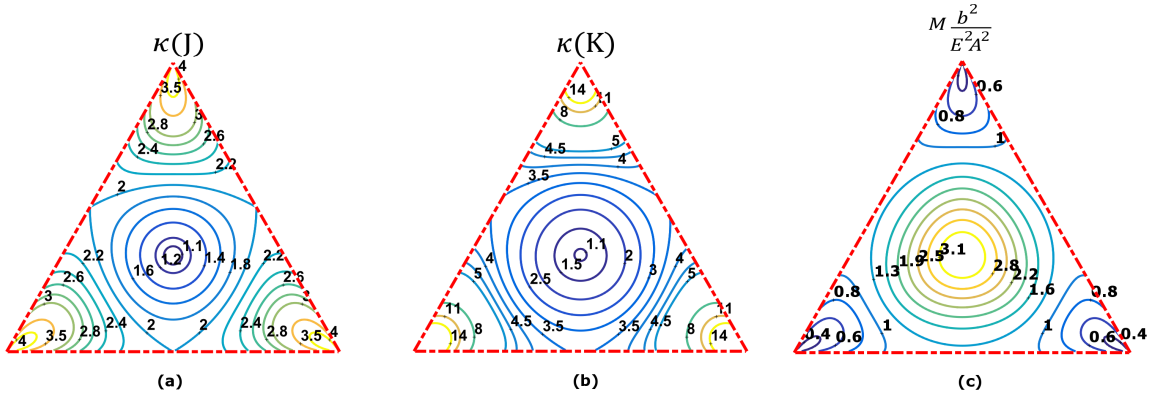

Figure 3.3: a. Dexterity index, b. Elastic stiffness index and c. Normalized magnitude plot for the 2-DOF traditional design with triangular workspace

the sides of an equilateral triangle, which can produce some benefits in terms of performance indices.

2.3.2.1 Elastic stiffness with ideal dexterity for adaptive design

Theorem: Let us consider the 2-DOF adaptive planar cable-driven robot shown in Fig. 3.2.b, with pulley blocks that move along the sides of an equilateral triangle. Under the ideal dexterity condition, the following facts hold: (i) the elastic stiffness index $\kappa(K)$ only depends on the position of the end-effector; (ii) in any given position of the end-effector, the elastic stiffness magnitude is maximum when each cable is orthogonal to the side of the triangle along which its pulley-block can slide.

Proof: Based on the defined strategy, we chose the triangular design (step 1) and we set the goal to achieve the ideal dexterity with the best feasible stiffness (step 2). The condition for ideal dexterity ($\kappa(J) = 1$) imposes equal angles between any pair of adjacent cables [2]. Therefore, for any given position of the end-effector, the set of all cable configurations with ideal dexterity can be obtained by rigidly rotating a reference configuration having all cables orthogonal to the sliding guides by an angle γ (step 3). If L_i and $L_{\gamma,i}$ are the lengths of the ith cable in the reference and in the generic configurations, the stiffness of the ith cable $k_{\gamma,i}$ can

be written as:

$$k_{\gamma,i} = cos(\gamma)k_i, \quad cos(\gamma) = \frac{L_i}{L_{\gamma,i}}, \quad i = 1,2,3. \tag{3.5}$$

Therefore:

$$\Omega_\gamma = cos(\gamma)\begin{pmatrix} k_1 & 0 & 0 \\ 0 & k_2 & 0 \\ 0 & 0 & k_3 \end{pmatrix}, \qquad K_\gamma = J^{\mathrm{t}}\Omega_\gamma J = cos(\gamma)K. \tag{3.6}$$

Since the eigenvalues of K_γ are equal to those of K multiplied by $cos(\gamma)$, the elastic stiffness index does not change with rigid rotations, while the elastic stiffness magnitude (Eq. 5.4) is maximum when $cos(\gamma) = 1$, i.e., when each cable is orthogonal to the side of the triangle it is connected to (step 4). For γ=0 and a triangle with sides equal to b, the elastic stiffness matrix is

$$K = \frac{EA}{4}\begin{pmatrix} 3(\frac{1}{L_2}+\frac{1}{L_3}) & \sqrt{3}(\frac{1}{L_2}-\frac{1}{L_3}) \\ \sqrt{3}(\frac{1}{L_2}-\frac{1}{L_3}) & (\frac{4}{L_1}+\frac{1}{L_2}+\frac{1}{L_3}) \end{pmatrix}, \tag{3.7}$$

where E and A are the Young's modulus and the cross section area of the cables, which are considered the same for all cables. Fig. 3.4.a depicts the contour plot of the elastic stiffness index $\kappa(K)$ under the ideal dexterity condition. The elastic stiffness index is unitary in the centroid of the triangle, the best portion of the workspace is located near the centroid, and the steepest decrease in the index occurs while moving the end-effector from the centroid outwards, along a line that is orthogonal to one of the guides. It can be inferred that under ideal dexterity conditions, the level of stiffness isotropy is dictated by the position of the end-effector, and by moving the end-effector towards the boundaries, the isotropic stiffness index increases. Fig. 3.4.b shows the normalized maximum elastic stiffness magnitude. The highest increase in elastic stiffness magnitude occurs while moving from the centroid to the corners and the smallest stiffness magnitude is nearby the centroid.

Let $P(s)$ be a planar curve inside the workspace

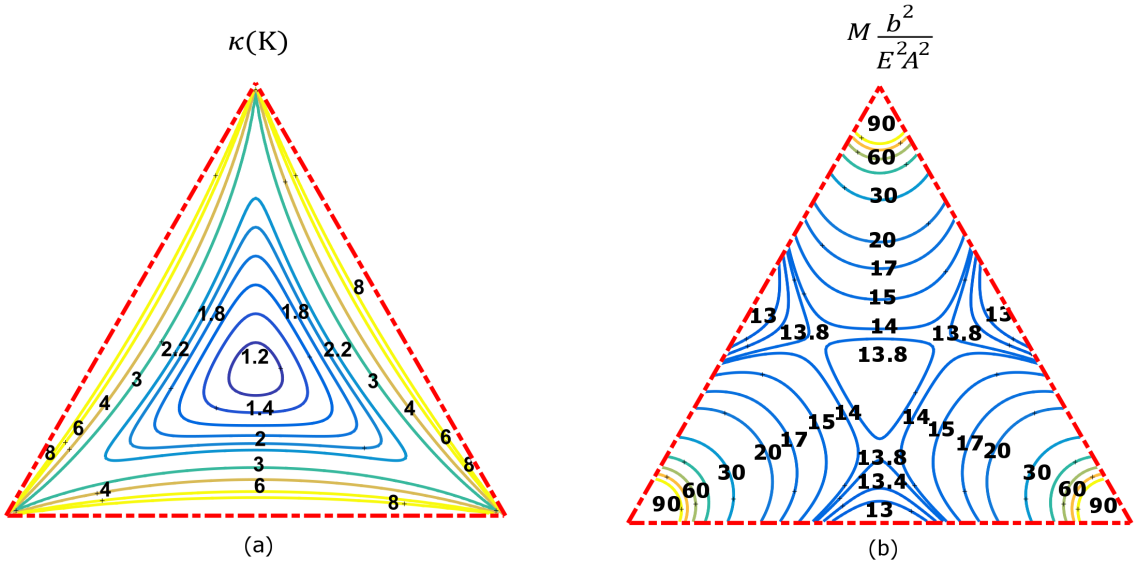

Figure 3.4: a. Elastic stiffness index and b. Normalized maximum magnitude plot for the three-cable, 2-DOF design in ideal dexterity condition

$$P(s) = \{x(s), y(s)\}^{\mathrm{t}}, \qquad s \in [0, L], \tag{3.8}$$

where L is the length of the curve. The positions of the pulley-blocks that yield ideal dexterity are given by (step 5)

$$q_i(s) = u_i.(P(s) - P_i), \tag{3.9}$$

where u_i is the unit vector along the ith linear guide and P_i is the position vector of the ith vertex of the triangle (Fig. 3.2.b).

Suppose that the following design problem is given (step 6):

Design a 2-DOF adaptive cable-driven robot with triangular workspace capable of maintaining ideal dexterity and $\kappa(K) \leq \kappa(K)_{\mathrm{REQ}}$ inside a circular region with radius r_{REQ}.

Let us assume an equilateral triangle with sides equal to b and a circumference that is centered at the triangle's centroid. The radius of the circumference r belongs to the interval $(0; \frac{\sqrt{3}}{6}]$. Fig. 3.5 depicts how the maximum $\kappa(K)$ along a circumference with normalized radius of $\frac{r}{b}$ changes. The design steps can be summarized as follows.

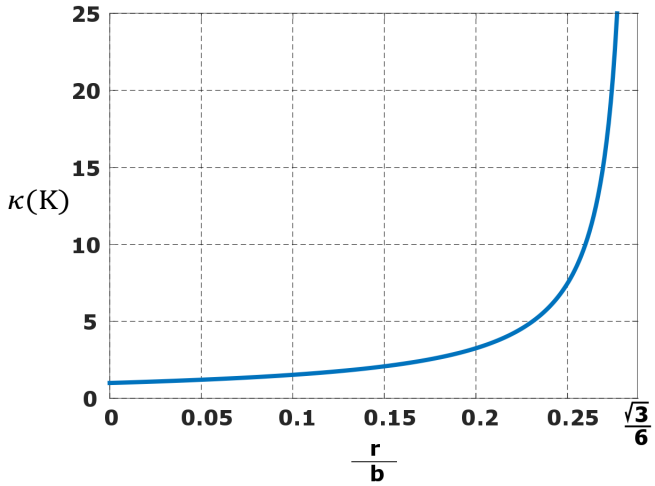

Figure 3.5: Stiffness index as a function of $\frac{r}{b}$

1. Use Fig. 3.5 to choose the value of $\frac{r}{b}$ for which $\kappa(K) = \kappa(K)_{REQ}$. Indicate this value as $(\frac{r}{b})_{REQ}$.

2. Calculate the side of the triangle as $b_{REQ} = r_{REQ}/(\frac{r}{b})_{REQ}$.

2.3.2.2 Dexterity with best achievable elastic stiffness for adaptive design

In this part, interval analysis method is used, so before analysing the next case, interval analysis is described briefly.

The main focus of interval arithmetic is the simplest way to calculate upper and lower endpoints for the range of values of a function in one or more variables. These endpoints are not necessarily the supremum or infimum, since the precise calculation of those values can be difficult or impossible.

$$[a,b] = \{x \in \mathbb{R} | a \leq x \leq b\}, \tag{3.10}$$

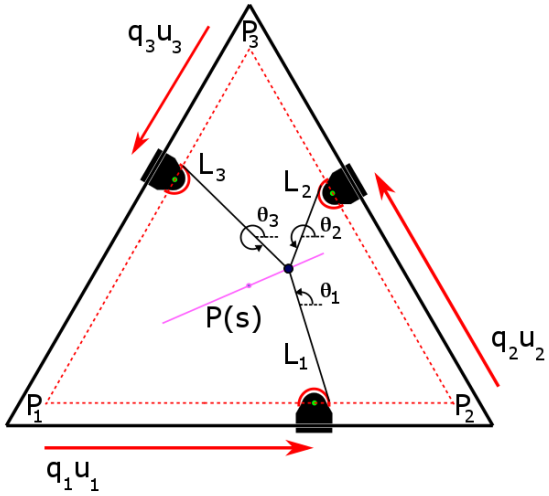

Figure 3.6: Adaptive 2-DOF planar cable robot with pulley blocks moving on linear guides

where $a = -\infty$ and $b = \infty$ are allowed; with one of them infinite we would have an unbounded interval, while with both infinite we would have the extended real number line.

As with traditional calculations with real numbers, simple arithmetic operations and functions on elementary intervals must first be defined. More complicated functions can be calculated from these basic elements [105].

Let us consider again a 2-DOF adaptive cable-driven robot with pulley blocks that move along the sides of an equilateral triangle (step 1, Fig. 3.6). The goal is to achieve the isotropic stiffness (if possible) with the best feasible dexterity within the workspace (step 2).

Using eq. 2, the elastic stiffness matrix of the system can be written as

$$K = EA \begin{pmatrix} \sum_{i=1}^{3} \frac{1}{L_i} cos^2(\theta_i) & \sum_{i=1}^{3} -\frac{1}{L_i} cos(\theta_i) sin(\theta_i) \\ \sum_{i=1}^{3} -\frac{1}{L_i} cos(\theta_i) sin(\theta_i) & \sum_{i=1}^{3} \frac{1}{L_i} sin^2(\theta_i) \end{pmatrix}, \tag{3.11}$$

where θ_i is the angle between the x axis and the ith cable, measured in the counterclockwise direction (Fig. 3.6). By calculating the eigenvalues of K and setting $\kappa(K)$ equal to 1, the conditions for isotropic elastic stiffness can be obtained. A set of angles and related cable lengths must be found, which satisfy the following equations:

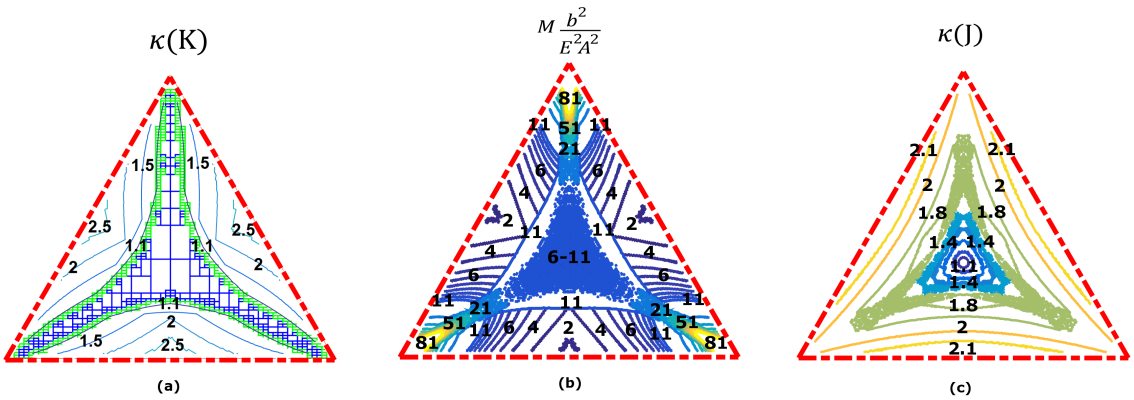

Figure 3.7: a. The best feasible elastic stiffness index for a three-cable, 2-DOF design, b. Magnitude and c. Dexterity index for the condition of the best feasible elastic stiffness in three-cable system

$$\sum_{i=1}^{3} \frac{1}{L_i} cos(2\theta_i) = 0 \quad , \quad \sum_{i=1}^{3} \frac{1}{L_i} sin(2\theta_i) = 0 \tag{3.12}$$

Fig. 3.7.a shows the region of the workspace where isotropic elastic stiffness can be achieved, using interval analysis [106]. The contour lines indicate the value of the best elastic stiffness index outside the isotropic region. It can be noticed that isotropic stiffness is achievable only near the angle bisectors, as the end-effector moves from the centroid to any vertex. Conversely, moving the end-effector from the centroid towards any of the sides results in higher $\kappa(K)$, which is not desirable. Fig. 3.7.b and Fig. 3.7.c depict the contour plots of the stiffness magnitude and dexterity indices for the configurations yielding the best achievable stiffness shown in Fig. 3.7.a. The system has the highest stiffness magnitude near the corners, whereas the minimum magnitude occurs close to the perpendicular bisector of each side. The best dexterity is achieved near the centroid, whereas moving the end-effector towards the sides increases the dexterity index.

For each point of a given end-effector trajectory, the configuration of the cables (i.e., the angles and lengths $(\theta_1, \theta_2, \theta_3, L_1, L_2, L_3)$) that yields the best achievable elastic stiffness index can be computed numerically (step 3). In case of multiple solutions, the one with the best dexterity index is selected (step 4).

Fig. 3.8.a shows a sample trajectory of the end-effector and the corresponding cable con-

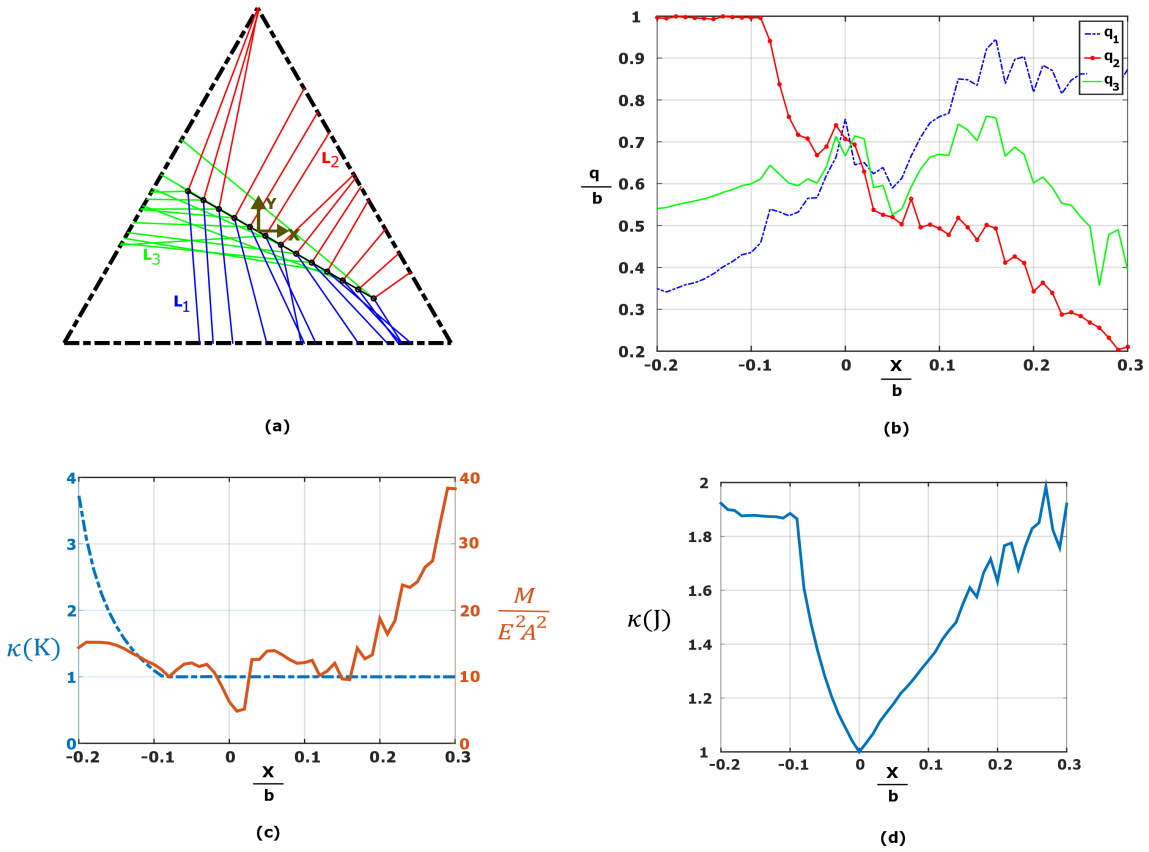

Figure 3.8: a. A sample end-effector trajectory and the corresponding, b. Cable configurations, c. Elastic stiffness, magnitude and d. The dexterity

figurations yielding the best stiffness index. Fig. 3.7.b depicts the locations of the pulley blocks for the same motion. Elastic stiffness, magnitude and the dexterity indices corresponding to the sample trajectory are shown in Fig 3.7.c, d.

Once the configuration of the cables (i.e., the angles and lengths) are determined, the positions of the pulley-blocks for any configuration can be determined using the following expression (step 5)

$$q_i(s) = u_i.(P(s) - P_i) + u_i(L_i sin(\phi_i)), \tag{3.13}$$

where ϕ_i is

$$\phi_1 = \theta_1 - \frac{\pi}{2}, \qquad \phi_2 = \theta_2 - \frac{7\pi}{6}, \qquad \phi_3 = -\theta_3 + \frac{11\pi}{6}. \tag{3.14}$$

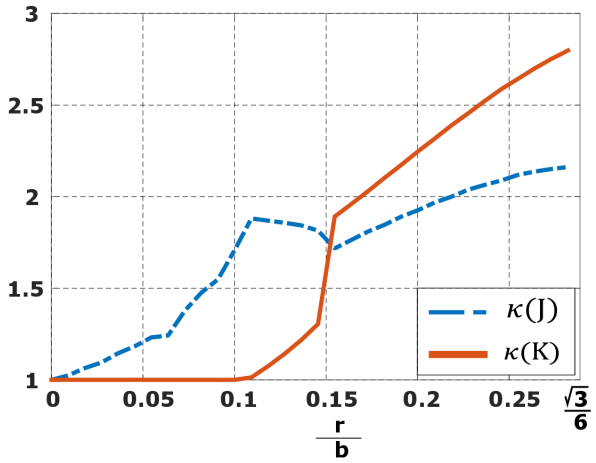

Figure 3.9: Stiffness and dexterity change as a function of the parameter $\frac{r}{b}$

Suppose that the following design problem is given (step 6):

Design a 2-DOF adaptive cable-driven robot with triangular workspace capable of achieving isotropic stiffness and $\kappa(J) \leq \kappa(J)_{\text{REQ}}$ inside a circular region with radius r_{REQ}.

Let us assume again an equilateral triangle with side length b and a circle centered in the triangle's centroid with radius $r \in (0; \frac{\sqrt{3}}{6}]$. Fig. 3.9 depicts how the maximum $\kappa(K)$ and $\kappa(J)$ change while increasing the normalized radius $\frac{r}{b}$. The design method can be summarized as follows.

1. Using Fig. 3.9, choose the value of $\frac{r}{b}$ such that $\kappa(K) = 1$ and $\kappa(J) = \kappa(J)_{\text{REQ}}$. Indicate this value as $(\frac{r}{b})_{REQ}$. If such value does not exist, then the design problem is not solvable with a triangular design, and $kappa(J)_{\text{REQ}}$ should be increased.

2. Calculate the length of the triangle side as $b_{REQ} = r_{REQ}/(\frac{r}{b})_{REQ}$.

3. If the resulting design is too cumbersome, increase $\kappa(J)_{\text{REQ}}$ and return to step 1.

The proposed adaptive system and the motion patterns result in higher performance compared to the traditional design.

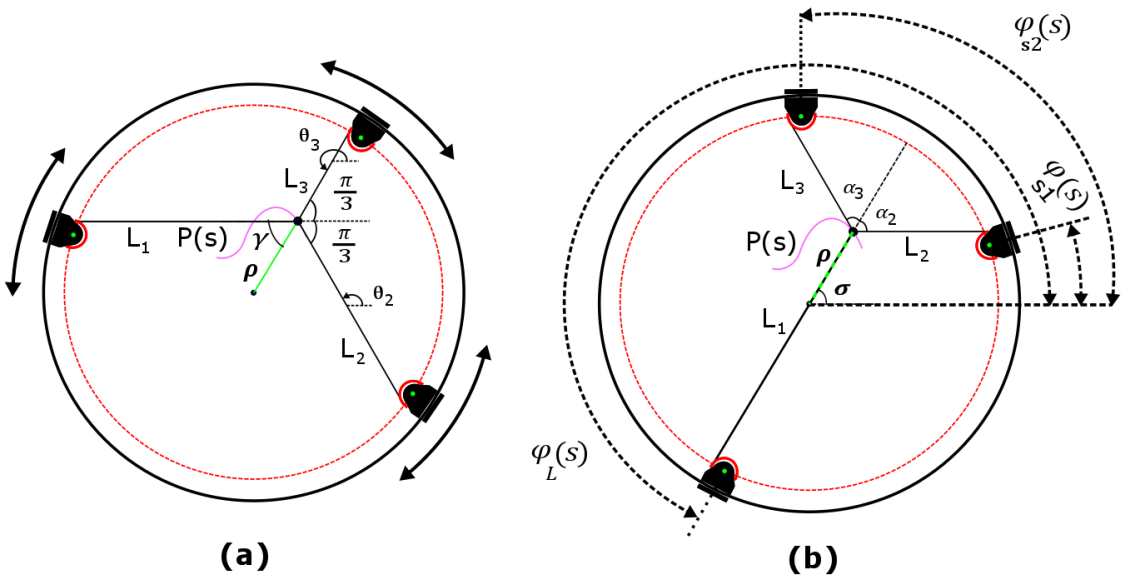

Figure 3.10: Adaptive 2-DOF planar cable robot with pulley blocks moving on a circle

3.4 2-DOF planar adaptive cable-driven parallel robot with circular workspace

3.4.1 Elastic stiffness with ideal dexterity

Let us consider a 2-DOF adaptive cable-driven parallel robot with pulley blocks moving on a circumference (step 1). We set the goal to achieve the ideal dexterity with the best feasible stiffness as mentioned in step 2 of the proposed algorithm. Under the ideal dexterity hypothesis, the cables arrangement must be symmetric [2] (step 3). Because the design is axially symmetric, we can assume without loss of generality that cable L_1 is horizontal (Fig. 3.10.a). The length of the ith cable and the corresponding stiffness coefficient can be written as

$$L_i = \rho cos(\beta_i) + \sqrt{1-\rho^2 sin^2(\beta_i)}, \quad k_i = \frac{EA}{L_i}, \tag{3.15}$$
$$\beta_1 = \gamma, \quad \beta_2 = \frac{2\pi}{3} - \gamma, \quad \beta_2 = \frac{2\pi}{3} + \gamma,$$

where ρ, L_i, β_i are the normalized distance of the end-effector from the center ($\rho \in [0,1]$), the

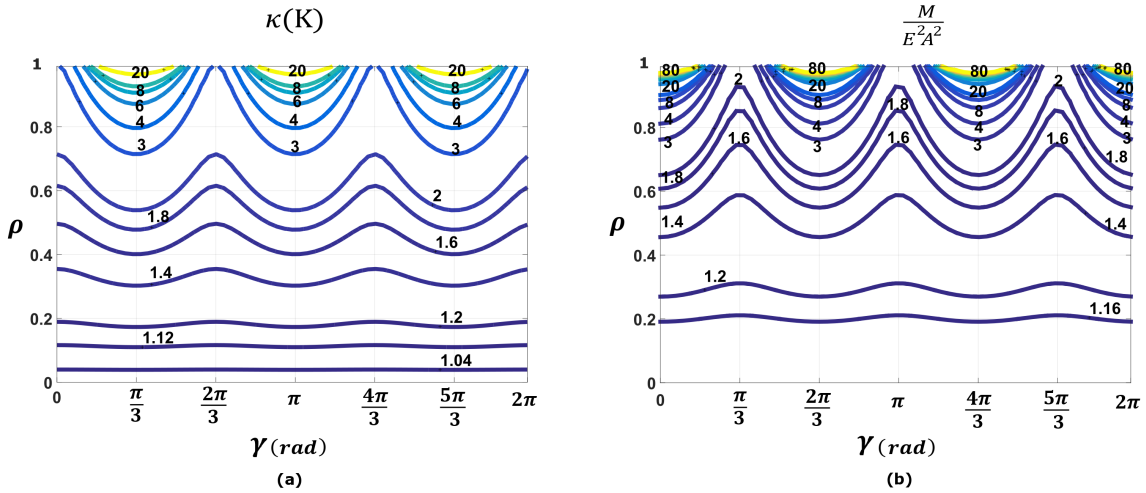

Figure 3.11: a. Elastic Stiffness index, b. Normalized stiffness magnitude for a 2-DOF circular cable-driven parallel robot under ideal dexterity condition

length of the ith cable, and the angle between ρ and L_i, respectively. γ is a rigid rotation.

By substituting the expressions of L_i from Eq. 3.15 into Eq. 3.2, and setting $\theta_1 = 0, \theta_2 = \frac{2\pi}{3}, \theta_3 = \frac{4\pi}{3}$ (symmetric configuration), the eigenvalues of K can be computed as a function of γ and ρ only, yielding the expressions of the elastic stiffness index and magnitude:

$$\kappa(K) = \frac{\lambda_{\max}(\rho,\gamma)}{\lambda_{\min}(\rho,\gamma)} \quad , \quad M = \frac{{\lambda_{\max}}^2(\rho,\gamma).{\lambda_{\min}}^2(\rho,\gamma)}{{\lambda_{\max}}^2(\rho,\gamma) + {\lambda_{\min}}^2(\rho,\gamma)} \tag{3.16}$$

Fig. 3.11.a shows the elastic stiffness index of the system. The minimum value of $\kappa(K)$ for any ρ occurs in $\gamma = 0, \frac{2\pi}{3}, \frac{4\pi}{3}$. These angles correspond to the same configuration, i.e., one with the longest cable (L_1, L_2 or L_3 for the three cases, respectively) crossing the center of the circle, and the other two cables having the same length. Therefore, this is the only configuration where the lowest feasible value of the isotropic stiffness index can be obtained while the system has ideal dexterity. Fig. 3.11.b shows the contour plot of the normalized stiffness magnitude. Again, for any ρ the maximum magnitude is achieved in $\gamma = 0, \frac{2\pi}{3}, \frac{4\pi}{3}$. Hence, it can be concluded that the configurations having the best elastic stiffness also show the highest stiffness magnitude (step 4).

The best elastic stiffness index and the best normalized magnitude under ideal dexterity are functions of ρ only. They can be computed as:

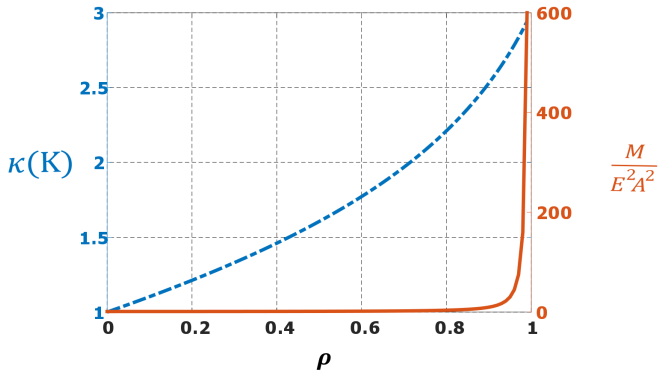

Figure 3.12: The best feasible elastic stiffness and magnitude of the adaptive 2-DOF planar cable robot with pulleys moving on a circle under the ideal dexterity condition

$$\kappa(K) = \frac{3(1+\rho)}{1+\sqrt{4-3\rho^2}}, \tag{3.17}$$

$$\frac{M}{E^2A^2} = \frac{9(1+\sqrt{4-3\rho^2})^2}{2(\rho-\sqrt{4-3\rho^2})^2(7+3\rho(3+\rho)+\sqrt{4-3\rho^2})}, \tag{3.18}$$

Fig. 3.12 shows the best feasible elastic stiffness index and the best feasible normalized elastic stiffness magnitude under the ideal dexterity condition for the adaptive 2-DOF planar cable robot with pulley blocks moving on a unitary circumference. $\kappa(K)$ reaches the ideal condition in the center (i.e., $\rho = 0$), while moving away from the center towards the circumference (in any direction) increases $\kappa(K)$. The elastic stiffness magnitude also increases while moving away from the centroid towards the circumference. Hence, the constraint of ideal dexterity imposes that stiffness isotropy degrades towards the boundary of the workspace, whereas stiffness magnitude increases towards the boundary, similarly to the triangular design. Unlike the triangular design, however, in the circular design the indices $\kappa(K)$ and M only depends on the distance from the center ρ.

Suppose the trajectory of the end-effector is defined in polar coordinates (ρ, σ), with $\rho \in (0;1], \sigma \in [0;2\pi)$. The corresponding pulley block trajectories can be defined as (step 5)

$$\phi(s) = \begin{pmatrix} \phi_{\mathrm{L}}(s) \\ \phi_{\mathrm{s1}}(s) \\ \phi_{\mathrm{s2}}(s) \end{pmatrix} = \begin{pmatrix} \sigma + \pi \\ \sigma - \frac{\pi}{3} + arcsin(\frac{\sqrt{3}\rho}{2}) \\ \sigma + \frac{\pi}{3} - arcsin(\frac{\sqrt{3}\rho}{2}) \end{pmatrix}, \tag{3.19}$$

where $\phi(s)$ is the vector of the polar angles yielding the positions of the pulley blocks (Fig. 3.10.b). In particular, $\phi_{\mathrm{L}}(s)$ indicates the pulley block attached to the longest cable, while $\phi_{\mathrm{s1}}(s)$ and $\phi_{\mathrm{s2}}(s)$ are related to the other two cables.

Let us consider again the design problem again. The goal is to design a 2-DOF adaptive cable-driven robot that achieves ideal dexterity and $\kappa(K) \leq \kappa(K)_{\mathrm{REQ}}$ inside a circular region with radius r_{REQ} (step 6).

Given a circular adaptive design, Fig. 3.12 depicts how $\kappa(K)$ changes while moving from the centroid (normalized radius $\rho = 0$) to the circumference ($\rho = 1$). The design method can be summarized as follows.

1. Using Fig. 3.12, choose the value of ρ such that $\kappa(K) \leq \kappa(K)_{\mathrm{REQ}}$. Indicate this value as ρ_{REQ}.
2. Calculate the radius of the smaller adaptive circular design which satisfies the specifications as $R_{REQ,C} = \frac{r_{REQ}}{\rho_{REQ}}$.

3.4.2 Dexterity with isotropic elastic stiffness

The design of 2-DOF adaptive cable-driven robot with pulley blocks with pulley blocks moving on a circumference is considered again (step 1). The goal is to achieve the isotropic stiffness with the best feasible dexterity within the workspace (step 2). The conditions for isotropic elastic stiffness are similar to Eq. 3.12. To simplify the problem, we consider the special case where one cable passes through the center of the circumference, as shown in Fig. 3.10.b. By using the following transformation

$$\theta_2 = \pi - \alpha_2, \quad \theta_3 = \pi + \alpha_3, \tag{3.20}$$

the isotropic stiffness conditions (11) are rewritten as (step 3)

$$\begin{aligned} &\frac{1}{\rho+1} + f(\rho,\alpha_2)cos(2\alpha_2) + f(\rho,\alpha_3)cos(2\alpha_3) = 0, \quad (a) \\ &f(\rho,\alpha_2)sin(2\alpha_2) = f(\rho,\alpha_3)sin(2\alpha_3), \quad (b) \end{aligned} \tag{3.21}$$

where:

$$f(\rho,\alpha) = \frac{1}{-\rho cos(\alpha) + \sqrt{1-\rho^2 sin^2(\alpha)}}, \tag{3.22}$$

It can be easily seen that a solution to Eqns. 3.21 and 3.22 always exists in the form $\alpha_2 = \alpha_3 = \alpha$. In this case, α and ρ are dependent on each other (step 3, 4):

$$\rho = \frac{-1-2cos(4\alpha)}{3-2cos(\alpha)-2cos(3\alpha)+2cos(4\alpha)}, \tag{3.23}$$

The dexterity index under the isotropic stiffness condition ($\theta_1 = 0,\ \alpha = \alpha_2 = \alpha_3$) is given by

$$\kappa(J) = \frac{1+2cos^2(\alpha)}{2sin^2(\alpha)}, \tag{3.24}$$

Fig. 3.13.a illustrates how α, the angle between the two cables not passing through the center, decreases as the end-effector moves from the center towards the circumference. Fig. 3.13.b depicts the corresponding dexterity index and the normalized stiffness magnitude under isotropic elastic stiffness. The dexterity index - which is ideal in the center ($\rho = 0$) - degrades to higher values as the end-effector moves towards the circumference. The plot also shows that the normalized magnitude increases towards the circumference.

If the position of the end-effector is (ρ,γ) with $\rho \in (0;1]$, $\sigma \in [0;2\pi)$, the corresponding positions of the pulley-blocks for ideal stiffness are (step 5)

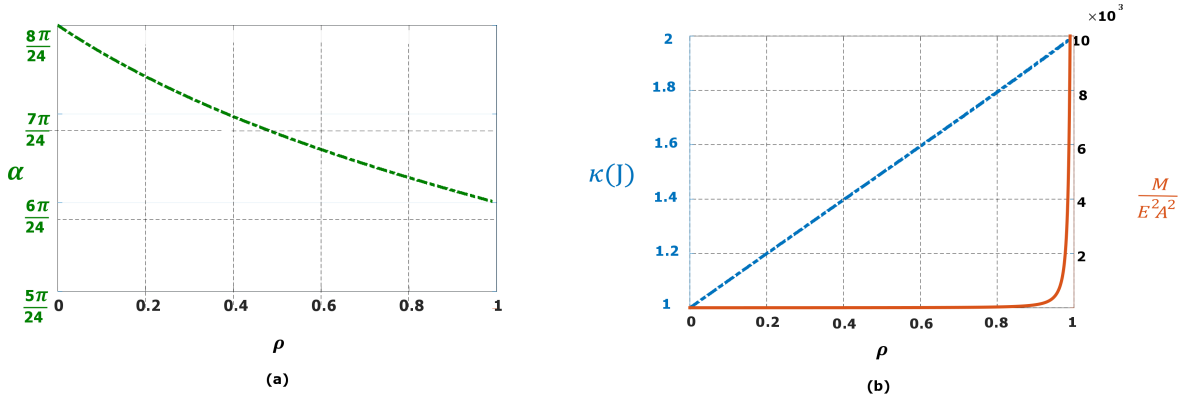

Figure 3.13: a. Changing in value of α and b. The dexterity index and the normalized stiffness magnitude from the center to the circumference under the isotropic elastic stiffness

$$\phi(s) = \begin{pmatrix} \phi_{\mathrm{L}}(s) \\ \phi_{\mathrm{s1}}(s) \\ \phi_{\mathrm{s2}}(s) \end{pmatrix} = \begin{pmatrix} \sigma + \pi \\ \sigma - \alpha + arcsin(sin(\alpha)\rho) \\ \sigma + \alpha - arcsin(sin(\alpha)\rho) \end{pmatrix}, \tag{3.25}$$

where $\phi(s)$ is the vector of the angular position of the pulley blocks, and α can be determined by solving (Eq. 3.23).

Consider the following design problem (step 6):

Design a 2-DOF adaptive cable-driven robot with circular workspace capable of achieving isotropic stiffness and $\kappa(J) \leq \kappa(J)_{\mathrm{REQ}}$ inside a circular region with radius r_{REQ}.

Let us assume again an adaptive circular design. Fig. 3.13.b illustrates how $\kappa(J)$ changes when moving from the centroid ($\rho = 0$) to the circumference ($\rho = 1$). The design method can be summarized as follows.

1. Using Fig. 3.13.b, choose the value of ρ such that $\kappa(J) \leq \kappa(J)_{\mathrm{REQ}}$. Indicate this value as ρ_{REQ}.

2. Calculate the radius of the smaller adaptive circular design which satisfies the specifica-

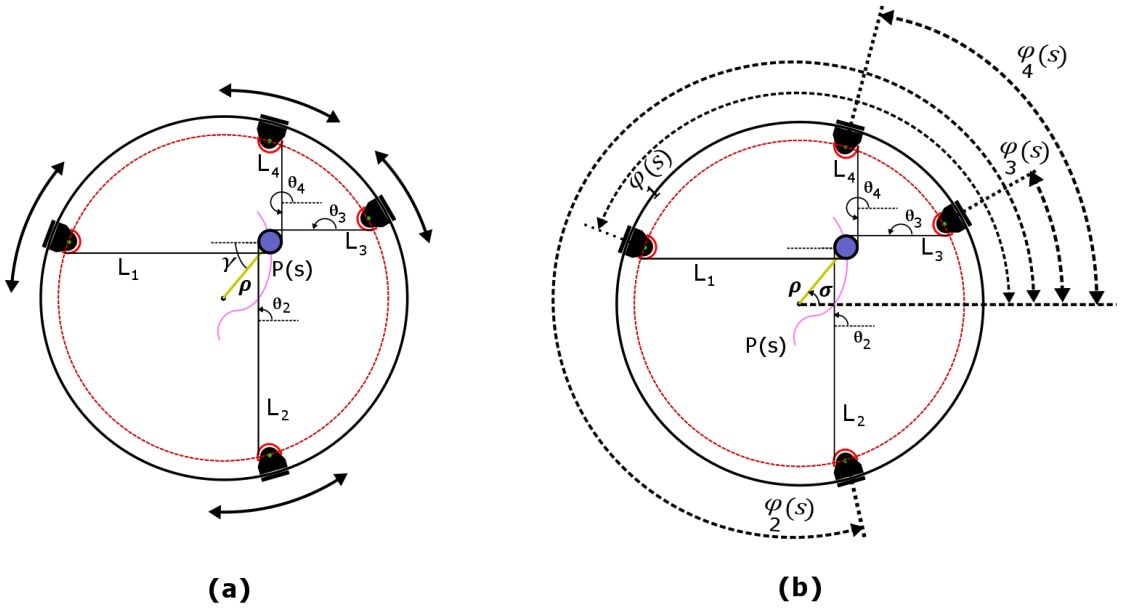

Figure 3.14: Adaptive 3-DOF planar cable robot with pulleys moving on a circumference

tions as $R_{REQ,C} = \frac{r_{REQ}}{\rho_{REQ}}$.

3.5 3-DOF circular planar adaptive cable-driven parallel robot

3.5.1 Elastic translational stiffness and dexterity

Let us analyze the elastic translational stiffness under the ideal dexterity condition for the 3-DOF adaptive cable-driven robot shown in Fig. 3.14.a, which features 4 pulley blocks moving on a circumference (step 1). For a 3-DOF cable robot, the configuration of the cables yielding ideal dexterity (step 2) is the one wherein all the angles between adjacent cables are equal (step 3) (i.e., all the pairs of adjacent cables should be orthogonal, [2]). We will show that under the ideal dexterity condition, the system has the best elastic translational stiffness when the configuration of the cables is symmetric with respect to the line crossing the center of the circumference and the end-effector position (i.e., $\gamma = \frac{\pi}{4}$ in Fig. 3.14.a).

Without loss of generality, let us assume that $\theta_1 = 0$, $\theta_2 = \frac{\pi}{2}$, $\theta_3 = \pi$, $\theta_4 = \frac{3\pi}{2}$, where θ_i is the angle between a given x axis and the ith cable. The stiffness matrix can be written as:

$$\begin{pmatrix} F \\ M \end{pmatrix} = \begin{pmatrix} K_{11}(N/m) & K_{12}(N) \\ {K_{12}}^{\mathrm{T}}(N) & K_{22}(N.m) \end{pmatrix} \begin{pmatrix} S \\ \phi \end{pmatrix}, \tag{3.26}$$

$$K_{11} = EA \begin{pmatrix} \frac{1}{L_1} + \frac{1}{L_3} & 0 \\ 0 & \frac{1}{L_4} + \frac{1}{L_2} \end{pmatrix}, \quad K_{12} = EA \begin{pmatrix} r(\frac{1}{L_3} - \frac{1}{L_1}) \\ r(\frac{1}{L_2} - \frac{1}{L_4}) \end{pmatrix}, \quad K_{22} = EA \sum_{i=1}^{4} r^2 \, (\frac{1}{L_i}), \tag{3.27}$$

where F and M define the force and the moment, S and ϕ indicate a small displacement in x, y directions and a small rotation, r is the radius of the moving platform (which equals to the radii of the pulley blocks). The elastic stiffness matrix is inhomogeneous and has three eigenvalues. Two of them are related to the translational stiffness and one corresponds to the rotational part. In this study, we focus on the translational stiffness index, which can be calculated as the ratio of the eigenvalues corresponding to the translational DOFs. Eq. 3.26 can be re-written as:

$$F = K_{11}S + K_{12}\phi, \qquad M = {K_{12}}^{\mathrm{T}}S + K_{22}\phi \tag{3.28}$$

To homogenize the stiffness matrix, Taghvaeipour et al. [107] proposed an approach based on dimensionless parameter vectors. For the force vector (F), they transferred the translational and rotational motion to a dimensionless vector using eigenvectors of ${K_{11}}^{\mathrm{T}}K_{11}$ and ${K_{12}}^{\mathrm{T}}K_{12}$, respectively. As a result, $K_{11}S$ and $K_{12}\phi$ change to $K_{11}H_S\psi_S$ and $K_{12}H_\phi\psi_\phi$, where H_s and H_ϕ are the orthogonal matrices whose columns are the eigenvectors of ${K_{11}}^{\mathrm{T}}K_{11}$ and ${K_{12}}^{\mathrm{T}}K_{12}$, and $\psi = \{\psi_S, \psi_\phi\}^{\mathrm{T}}$ is a dimensionless vector. Hence, the first equation in (27) can be written as:

$$F = G_F\psi, \qquad G_F = [K_{11}H_S \quad K_{12}H_\phi]. \tag{3.29}$$

The square root of the eigenvalues of $G_F{G_F}^{\mathrm{T}}$ can be used to calculate the translational stiffness index:

$$G_F {G_F}^{\mathrm{T}} = (EA)^2 \begin{pmatrix} (\frac{1}{L_1}+\frac{1}{L_3})^2 + r^2(\frac{1}{L_1}-\frac{1}{L_3})^2 & r^2(\frac{1}{L_1}-\frac{1}{L_3})(\frac{1}{L_4}-\frac{1}{L_2}) \\ r^2(\frac{1}{L_1}-\frac{1}{L_3})(\frac{1}{L_4}-\frac{1}{L_2}) & (\frac{1}{L_2}+\frac{1}{L_4})^2 + r^2(\frac{1}{L_2}-\frac{1}{L_4})^2 \end{pmatrix}, \tag{3.30}$$

The elements on the secondary diagonal of the matrix $G_F {G_F}^{\mathrm{T}}$ are a multiple of r^2. Considering the small radius of the end-effector compared to the workspace, the elements of the secondary diagonal are much smaller than the primary diagonal elements. So the matrix $G_F {G_F}^{\mathrm{T}}$ can be very similar to a diagonal matrix (isotropic elastic stiffness) depending on the radius of the end-effector and the cable lengths. Let us assume an adaptive 3-DOF planar cable robot with pulley blocks moving on a unitary circumference with r=0.04.

Fig. 3.15.a shows the elastic translational stiffness index. The minimum of $\kappa(K)$ for any ρ occurs in $\gamma = \frac{\pi}{4}, \frac{3\pi}{4}, \frac{5\pi}{4}, \frac{7\pi}{4}$. All these angles correspond to the same configuration, where the cables are symmetric with respect to the line crossing the center of circumference and the end-effector position ($\gamma = \frac{\pi}{4}$). Under this condition, the lowest value of the elastic translational stiffness index can be obtained, which is approximately unitary. It can be concluded that in this configuration, the system can achieve both ideal dexterity and isotropic translational stiffness with a negligible tolerance. Fig. 3.15.b shows the normalized stiffness magnitude. The maximum of the stiffness magnitude occurs in $\gamma = \frac{\pi}{4}, \frac{3\pi}{4}, \frac{5\pi}{4}, \frac{7\pi}{4}$. Therefore, it can be inferred that the best elastic stiffness condition and the highest stiffness magnitude are achieved in the same configuration. The minimum normalized stiffness magnitude occurs in the center of the workspace, while moving the end effector towards the circumference increases the normalized stiffness (step 4).

If the trajectory of the end-effector is (ρ, σ), with $\rho \in (0;1], \sigma \in [0;2\pi)$, the corresponding pulley block trajectories can be written as (step 5)

$$\phi(s) = \begin{pmatrix} \phi_1(s) \\ \phi_2(s) \\ \phi_3(s) \\ \phi_4(s) \end{pmatrix} = \begin{pmatrix} \sigma + \frac{3\pi}{4} - arcsin(\frac{\sqrt{2}\rho}{2}) \\ \sigma - \frac{3\pi}{4} + arcsin(\frac{\sqrt{2}\rho}{2}) \\ \sigma - \frac{3\pi}{4} + arcsin(\frac{\sqrt{2}\rho}{2}) \\ \sigma + \frac{3\pi}{4} - arcsin(\frac{\sqrt{2}\rho}{2}) \end{pmatrix}, \tag{3.31}$$

where $\phi(s)$ is the vector of the pulley blocks angular positions in polar coordinates (Fig. 3.14.b). As the system is capable of achieving approximately isotropic translational stiffness,

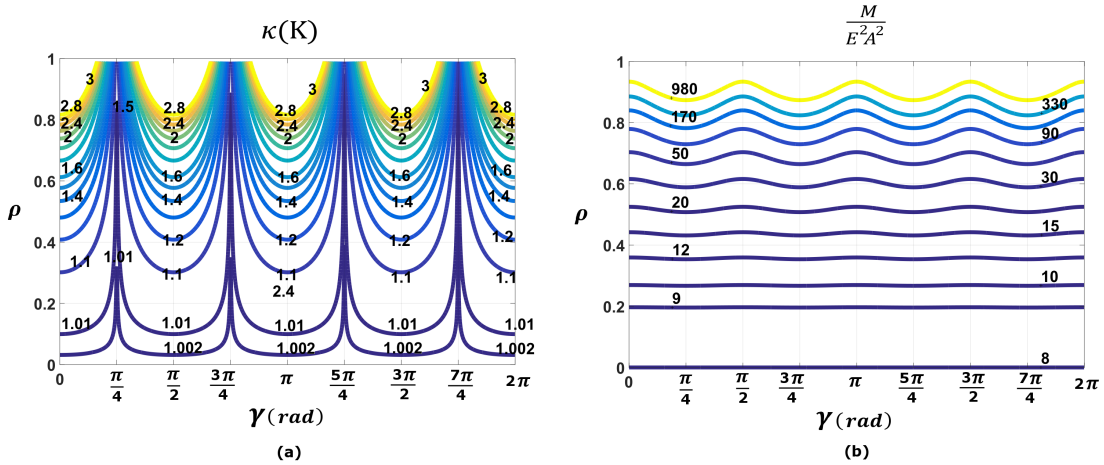

Figure 3.15: a. Elastic Stiffness index, b. Stiffness magnitude for a 3-DOF circular cable-driven robot under ideal dexterity condition

and ideal dexterity, we change the design problem compared to other cases. Suppose that the following design problem is given (step 6):

Design a 3-DOF adaptive cable-driven robot with circular workspace capable of achieving approximately isotropic translational stiffness, and ideal dexterity and $M \leq M_{REQ}$ inside a circular region with radius r_{REQ}.

Let us consider the 3-DOF design shown in Fig. 3.14.b. Fig. 3.16 illustrates how M changes while moving from the centroid ($\rho = 0$) to the circumference ($\rho = 1$). The design method can be summarized as follows.

1. Use Fig. 3.16 to choose the value of ρ for which $M = M_{REQ}$. Indicate this value as ρ_{REQ}.
2. Calculate the radius of the smaller 3-DOF adaptive circular design which satisfies the specifications as $R_{REQ,C} = \frac{r_{REQ}}{\rho_{REQ}}$.

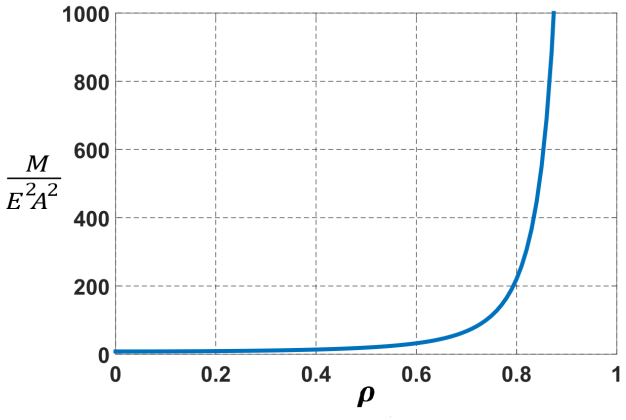

Figure 3.16: Stiffness magnitude change as a function of the parameter $\frac{r}{b}$ for a 3-DOF planar adaptive system

3.6 Application in Cable-Suspended Camera Systems

Cable-Suspended Camera Systems are widely used in the fields of sports and entertainment. Usually four motorized winches are located at the corners of the workspace, and each one is connected to the end-effector (i.e., the camera) with a cable passing by an idle pulley. Despite the widespread use of those systems, some incidents have been reported. In 2011, a camera crashed onto the playing field. Likewise, some ball shots hit the camera in different matches [Wikipedia]. Collisions between the camera and small objects (e.g., a ball) and weather effects (e.g., wind gusts) can be considered as disturbances to the system. On the other hand, increasing the system stiffness can result in disturbance rejection, less vibrations and improved accuracy of trajectory tracking [81], [71]. Because disturbances are generally unpredictable, keeping an isotropic stiffness condition can be desirable to satisfy the desired robot tracking accuracy. On the other hand, dexterity is an important index with respect to the kinematic behavior and force performance of the system. As the camera motion in the plane parallel to the ground is much higher than altitudinal displacement, let us consider the system as a planar cable-driven robot. Fig. 13. a. shows a traditional cable-suspended camera system with four reels anchored at fixed points. The size of the workspace is considered by a ratio of 1.1 to 0.73 (e.g., the size of a standard soccer field is $110m \times 73m$). Suppose the reels were anchored on the corners of a rectangle formed by increasing 30% to the sides of

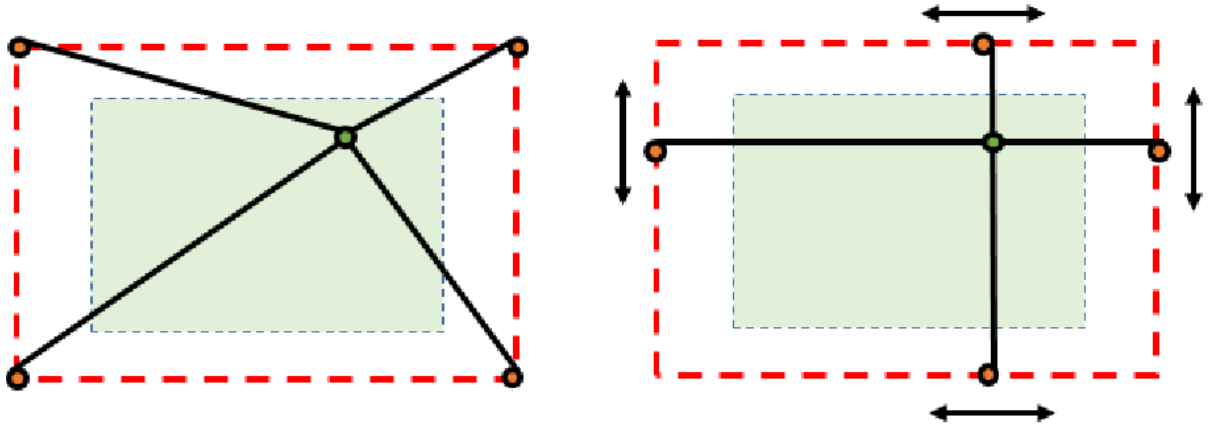

Figure 3.17: a. A sample cable-suspended camera system, b. New design of adaptive cable-suspended camera system

the rectangular workspace. 3.17.b. illustrates an adaptive design for a cable-suspended camera system with four linear guides which are used to form a rectangular workspace. Pulleys can be moved along each guide by means of auxiliary actuators. Pulley blocks are position-controlled such that each cable direction is orthogonal to the corresponding guide. Since $\theta_1 = 0, theta_2 = \frac{\pi}{2}, \theta_3 = \pi, \theta_4 = \frac{3\pi}{2}$, the condition for ideal dexterity is always satisfied. 3.18 depicts the dexterity index for the traditional design of cable-suspended camera system. In all workspace area, no set of angles can comply with the ideal dexterity condition while moving from the centroid to the left and right sides results in approaching the ideal dexterity condition.

Fig. 3.19 shows the elastic stiffness index for the traditional and adaptive design. The elastic stiffness index in new design is smaller which shows the priority of the proposed system in term of stiffness index. Fig. 3.20 depicts the elastic stiffness magnitude (assumed unitary of EA) which shows higher values in case of adaptive system comparing with the traditional one. Let us consider another example. A sample cycling velodrome with a 250 m track and a traditional cable-suspended camera system is shown in Fig. 3.21.a. The new adaptive design with four moveable pulley blocks and orthogonal adjacent cables is illustrated in Fig. 3.21.b. In this configuration, the system can achieve both ideal dexterity and isotropic elastic stiffness. Fig. 3.22.a, b show the dexterity and elastic stiffness index related to the traditional design. Unlike the adaptive design, the traditional system cannot keep the ideal dexterity and isotropic elas-

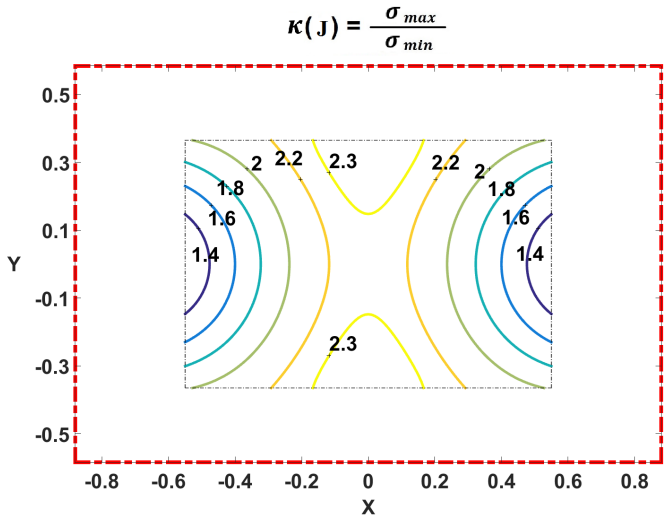

Figure 3.18: Dexterity index for the traditional design of the cable-suspended camera system

tic stiffness in the given workspace. Obviously the stiffness magnitude is much higher in the proposed system due to shorter cables comparing with the traditional design.

3.7 Summary

Adaptive cable-driven parallel robots have augmented kinematic redundancy compared to traditional cable-driven systems with equal number of cables. As a result, the inverse kinematics problem of such robots may have more solutions compared to the traditional cable-driven parallel robots. The motivation of this study was to introduce a systematic methodology to use the augmented kinematic redundancy to increase robot performance. Depending on the application, the most efficient solution can be determined based on one or more performance indices. In this study, two important performance indices, dexterity and elastic stiffness, were considered simultaneously. Dexterity and elastic stiffness are performance indices widely employed in design and control of robots. The dexterity index defines the kinematic behavior of a robot. The elastic stiffness can affect trajectory tracking, disturbance rejection and vibrations of a system.

The best feasible elastic stiffness while keeping ideal dexterity was investigated for two different designs of 2-DOF adaptive-cable driven parallel robots and as a result, the related

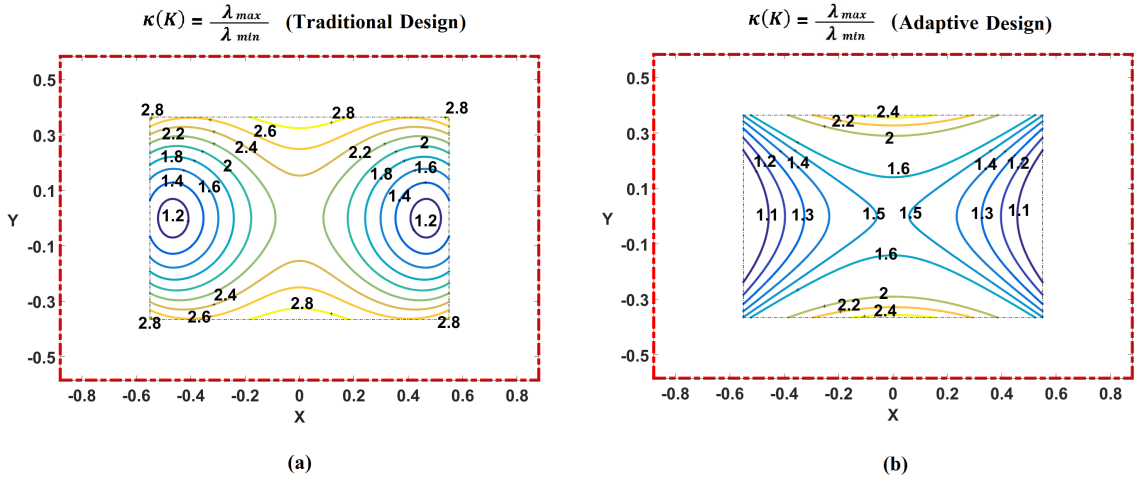

Figure 3.19: a. Elastic stiffness index for the traditional and b. Adaptive design of the cable-suspended camera

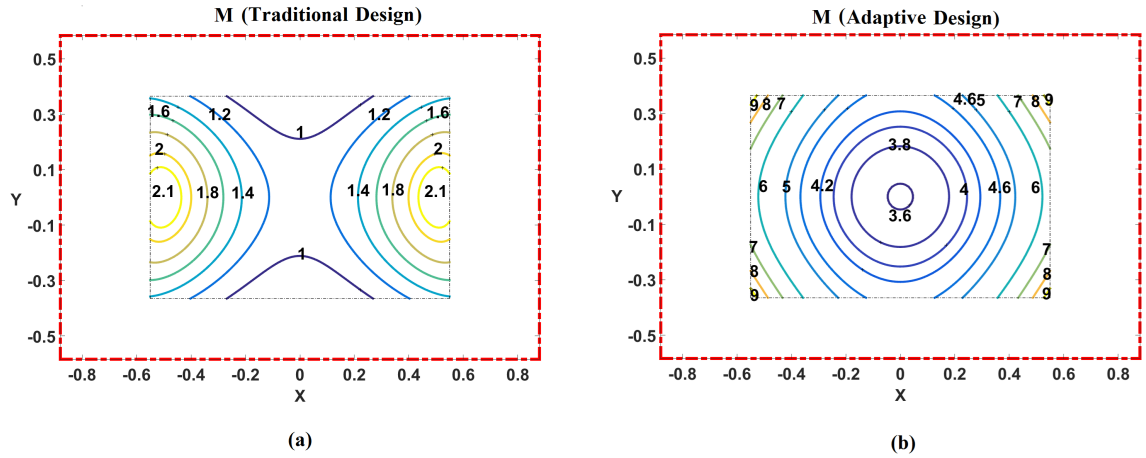

Figure 3.20: a. Elastic stiffness magnitude for the traditional and b. Adaptive design of the cable-suspended camera system

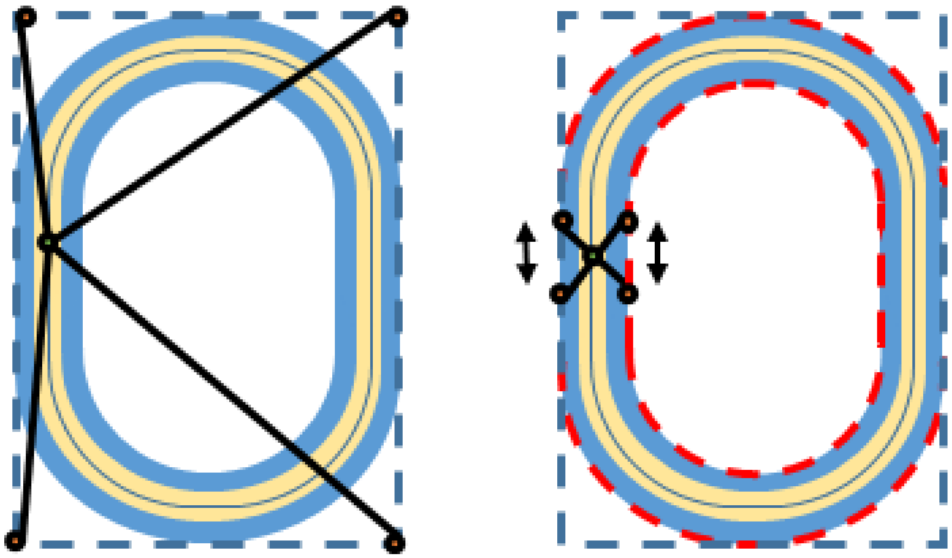

Figure 3.21: a. Traditional and b. Adaptive cable-suspended camera system for a velodrome

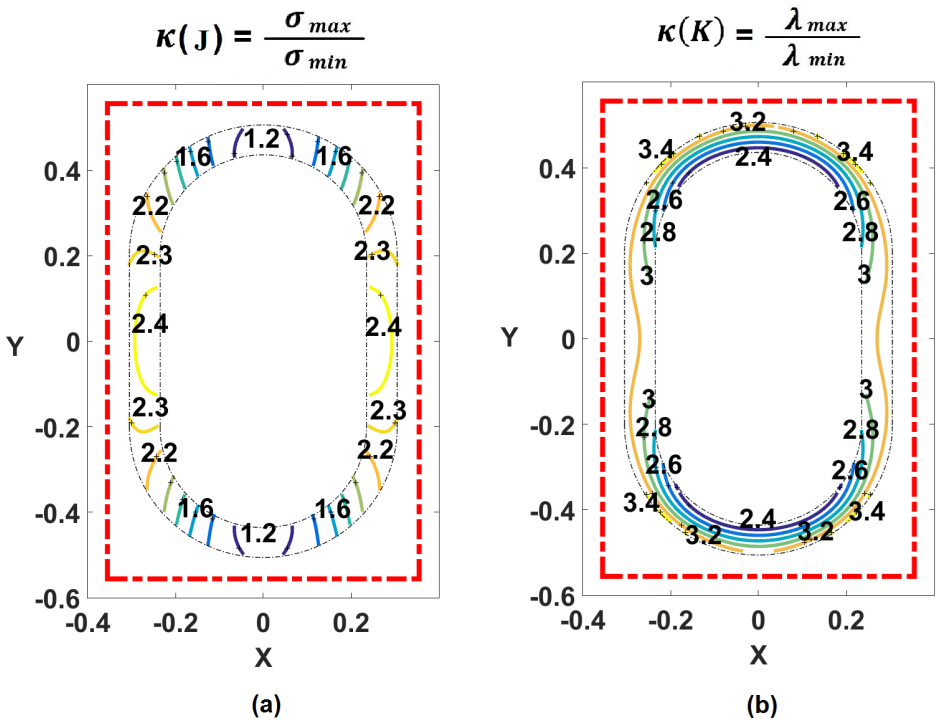

Figure 3.22: a. Dexterity and b. Stiffness index for the traditional cable-suspended camera system of a velodrome

configuration of cables and pulley blocks were determined. The same method was applied to the case of a 3-DOF adaptive cable-driven robot with pulley blocks moving on a circular guide. For this device, we identified the cable configuration, which result in ideal dexterity and approximately isotropic elastic translational stiffness.

The best possible dexterity while maintaining the system in ideal isotropic elastic stiffness was also studied for these three designs. The proposed method uses the augmented kinematic redundancy of the systems and presents a unique solution in each case. In 2-DOF adaptive designs, the both ideal dexterity and isotropic elastic stiffness occur at the centroid and moving outwards the centroid increases the indices. On the other hand, the minimum normalized elastic stiffness magnitude occurs at the center of the workspace in both patterns while moving outwards increases the magnitude. For all cases, the corresponding pulley block trajectories were determined and the related design problem to keep a minimum dexterity or stiffness is solved.

In the next chapter, we investigate on increasing non-adaptive cable-driven parallel robots performance by changing the minimum tension in cables and adjusting the active stiffness.

Chapter 4

Dynamic Minimum Tension Control (DMTC) for cable driven parallel robots

This chapter is devoted to investigate on increasing the performance of non-adaptive cable-driven parallel robots by controlling the minimum tension in cables. As it mentioned before, it is impossible to change the dexterity and elastic stiffness indices for a certain position of end-effector due to fixed orientation and length of cables; however, adjusting the active stiffness by chnging the minimum tension in cables is the only way of adapting system stiffness fast.

Higher tension in cables of a cable-driven parallel robot is preferable due to increased stiffness, higher disturbance rejection, better trajectory tracking performance and a more precise motion; however, cable tension augmentation can result in saturation of actuators and high energy consumption. This chapter is devoted to investigate if dynamically changing the minimum tension in cables can allow achieving an efficient motion in term of power consumption, while preserving good trajectory tracking performance. The proposed method is called Dynamic Minimum Tension Control (DMTC). In this approach, the minimum tension is changing on-the-fly according to stiffness, dynamics of the system, and error values as feedback. A 2-cable, 1-DOF test bed with different settings of the controller has been used to compare traditional fixed minimum tension utilization, and the proposed approach. Experimental results show that the DMTC can be more efficient than traditional approaches in terms of accuracy and energy consumption.

4.1 Dynamic Minimum Tension Control (DMTC) Concept

It is well known that the static equilibrium of an n-DOF cable driven robot, controlled by m cables, can be expressed by the following linear equation system:

$$ST = W \qquad T_{min} \leq T_i \leq T_{max}, \qquad i = 1,2,..,m, \tag{4.1}$$

where T_{min}, T_{max} are the minimum allowable and maximum feasible tension in cables, S $\in \mathbb{R}^{n\times m}$ is the structure matrix of the robot, W is the wrench applied to the end-effector, and T is the vector of cable tensions, which can be written as:

$$W = \begin{bmatrix} F \\ M \end{bmatrix} \in \mathbb{R}^n, \qquad T = \begin{bmatrix} T_1 \\ . \\ . \\ . \\ T_m \end{bmatrix} \in \mathbb{R}^m. \tag{4.2}$$

To determine the tension in cables, an optimization method can be used to find the best solution within the feasible tension range. Tension distribution of an over-constrained cable-driven parallel robot can be converted to an optimization problem as follow [108] :

$$\begin{aligned} &Minimize \quad f, \\ &f = \frac{1}{2}(T - T_{min})^{\mathrm{t}}(T - T_{min}), \\ s.t. \quad &ST = W \quad and \quad T_{min} \leq T_i \leq T_{max} \quad i = 1,2,..,m \end{aligned} \tag{4.3}$$

Selecting a proper value for T_{min} is a challenging subject.

Generally, the resonant frequencies of the transmission system between the sensor and actuator limits the control bandwidth, which results in the fact that many designers consider as 'Stiffer is better' [109, 110] and some researchers presented stiffness adjustable structures [111]. In different studies of cable-driven robots, higher stiffness is considered completely desirable for motion accuracy and stabilization. Inevitable elasticity of cables reduces

the accuracy and bandwidth of the robot, and the stiffness of the system has a direct relation with position accuracy [112, 113, 71].

So, higher values of T_{min} are preferable, as they prevent cable slacking, usually generate higher stiffness, and accuracy. In addition, less vibration, and even better controller tuning are obtained due to higher natural frequency of the cables; however, increasing T_{min} raises norm of tension in cables bringing higher energy consumption. Moreover, increasing T_{min} can lead to saturation of actuators, not only when the total wrench W is large, but also when the end-effector falls close to singular configurations.

The main idea behind the DMTC consists in dynamically calculating a suitable minimum value for cable tensions (T_{min}), while applying a standard tension distribution algorithm. The significant difference with already existing approaches lies in that the value of T_{min} is not fixed. On the contrary, it is changed on-the-fly within a certain range, to gain a good compromise between performance, energy consumption, and the risk of saturating the actuators. Different aspects must be considered before choosing a proper law for T_{min}.

4.1.1 Stiffness and Resonance

Let us consider a cable-driven parallel robot with n degrees of freedom and m cables. The stiffness matrix of the system can be found by using the following equation [69][1]

$$K = S\Omega S^{\mathrm{t}} + \frac{d}{dp}(S)\,T, \tag{4.4}$$

$$\Omega = \begin{pmatrix} k_1 & 0 & 0 & \cdots & 0 \\ 0 & k_2 & 0 & \cdots & 0 \\ 0 & 0 & k_3 & \cdots & 0 \\ \vdots & \vdots & \vdots & \ddots & \vdots \\ 0 & 0 & 0 & \cdots & k_m \end{pmatrix}, \qquad k_i = \frac{E_i A_i}{L_i}, \qquad i = 1,2,..,m, \tag{4.5}$$

where $p = (x, y, z, \theta_x, \theta_y, \theta_z)^{\mathrm{t}}$ are the coordinates of the end-effector in the Cartesian space

[1] Similar formulation was used in the third chapter using Jacobian matrix(J). Structure matrix(S) is denoted as transposed Jacobian matrix of a parallel cable-driven robot which is used in this chapter.

and Ω is a diagonal matrix having spring constants k_i in the main diagonal. E_i, A_i and L_i are the Young's modulus, cross section, and the length of the ith cable. The stiffness matrix is a combination of two parts. The first one is related to the elastic stiffness of the cables, the second part is linked to the tension in cables.

Behzadipour et al. [103] showed that, usually, the elastic stiffness is much higher than the stiffness related to the tension in the cables, but for some positions and directions, the stiffness corresponding to the tension in cables can be dominant.

It should be noticed that the elastic stiffness depends on the orientation and the lengths of cables which is unchangeable for a certain position of end-effector. High stiffness is desirable at the end-effector for proper position accuracy and load capacity [104]. On the other hand, low stiffness can negatively affect trajectory tracking performance, disturbance rejection and vibrations in the system [114, 81], so the stiffness should be considered as a key parameter in cable-driven systems. Some studies set a minimum value for the eigenvalue of the stiffness matrix (σ_{min}) to guarantee a minimum stiffness within the workspace [92].

In applications of cable-driven parallel robots with long cables, not only the longitudal vibration but also the transverse vibration can affect trajectory tracking and a very small excitation can produce high transversal vibrations [115]. To this regard, the minimum tension in the cables can play an important role to decrease the vibration and providing motion trajectory tracking with high accuracy.

In fact, the first natural frequency of transversal vibration of a cable [68] can be calculated as

$$\omega_{cable} = \frac{\pi}{L_i}\sqrt{\frac{T_i}{\rho}}, \tag{4.6}$$

where T_i and ρ are tension and the mass per unit length of the cable. A cable with higher tension has greater natural frequencies allowing for greater control gains which are profitable in term of more accurate motion. To refuse the resonance, the natural frequency of the actuator is usually chosen to be equal or less than half of the cable natural frequency [116]:

$$\omega_{actuator} \leq \frac{\omega_{cable}}{2}. \tag{4.7}$$

Using Eq. 4.6, the following constraint for the tension in cables can be defined:

$$T_i \geq \frac{4\,\omega^2{}_{\text{actuator}}\,{L_i}^2\rho}{\pi^2}. \tag{4.8}$$

4.1.2 Transverse vibration

Transverse vibration of cables in motion can be an important factor influencing on the system performance. To investigate on this effect, transverse vibration equation of a cable in motion was solved and tested on a testbed. The detailed description of this procedure is described in Appendix **??**. The equation was solved using Galerkin method, and ode45. The solution was set to estimate the transverse vibration of the cable for different values of constant tension in a point at the middle of the cable. An experimental setup of two DC motors with pulleys and a cable connected to them, equipped by a high frequency vision system were applied to validate the cable vibration numerical data.

Results showed that higher tension in cables can reduce the amplitude of transverse vibration; however, it can slightly increase the frequency of vibration. In application of cable-driven robots, the necessity of high stiffness is important to achieve an acceptable level of trajectory tracking performance, and resisting against noises and vibration of the system.

The concept was tested on a 1-DOF parallel cable-driven robot, and showed that higher minimum tension in cables can result in more accurate motion. Also, it should be noticed that high minimum tension in cables can increase power consumption and has the risk of saturation of actuators. Therefore, there is always a challenge to choose the optimal minimum tension in cables which can be an important subject of the future work.

4.1.3 Wrench

Using the norm of the end-effector $Wrench$ as an index to change the minimum tension in cables was introduced in our last study [79]. We proposed to increase T_{min} when the desired end-effector wrench W is small, and to decrease T_{min} when the absolute value of the wrench rises. The method is useful to avoid cable slacking in case of low wrench and to prevent the saturation of actuators while the wrench is high.

Clearly, by reducing T_{min}, we will get a vector T satisfying the statics equations with reduced norm. For example, in the case of planar point-mass CDPRs, for a given direction of the desired force W, there will be at least one cable whose direction is opposite to that of W (in the sense that the dot product between the desired force W and the direction of the cable is negative), so the reduction of its tension (T_{min}) will help reducing the tension in all other cables.

4.1.4 Trajectory Tracking Error

The method proposed in [79] guarantees smaller tension in all cables when W is high; however, it does not always guarantee the best efficiency. As an example, let us consider a system working with low total wrench, but also with an acceptable trajectory tracking accuracy; in this case, there is no need to increase T_{min}, which in turn brings higher power consumption. On the other hand, if a system is running with poor trajectory tracking, due to trajectory complexity, noise or improper tuning of controller, stiffness enhancement considering actuators capacity can be an effective solution [71]. So, not only the stiffness is an important issue, but also the accuracy of the system can drive a suitable choice of robot stiffness and minimum cable tension. Trajectory tracking error can be used together with total wrench as feedback to change the minimum tension in cables.

4.2 Dynamic Minimum Tension Control (DMTC) Algorithm

Based on the considerations above, the DMTC algorithm is proposed as the following equation:

$$T_{min} = T_0 + \Delta T[\alpha g_1(W) + (1-\alpha) g_2(E)], \tag{4.9}$$

where T_0 and ΔT are the lower bound and the range of variation of T_{min}; $g_1(W)$ and $g_2(E)$ are functions of $Wrench$ and $Error$ respectively and α is a parameter to determine the weight of the two terms. Functions $g_1(W)$ and $g_2(E)$, and parameter α, range between 0 and 1. In this way, the whole term multiplied by ΔT ranges between 0 and 1 itself, so that T_{min} is always

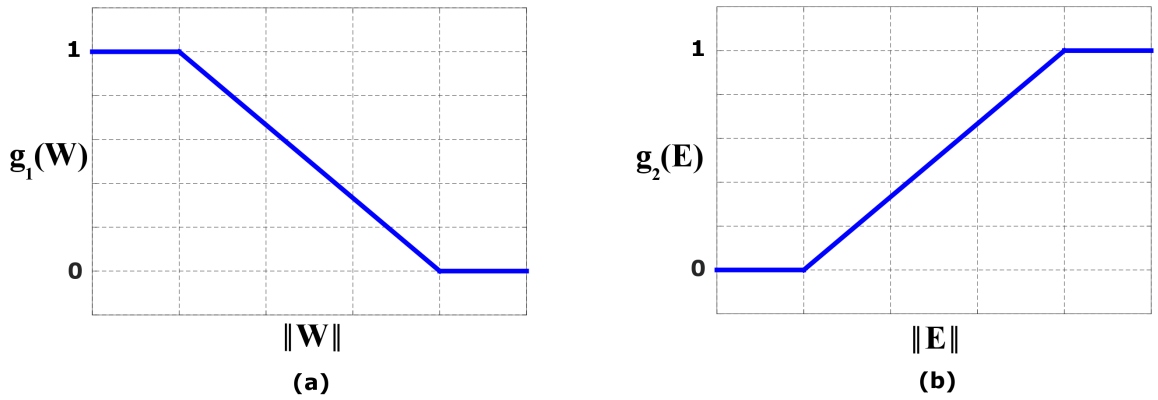

Figure 4.1: a. Mapping function used for changing the minimum cable tension T_{min} according to the absolute desired wrench (W) and b. Absolute position error (E)

between T_0 and $T_0 + \Delta T$.

To express $g_1(W)$ and $g_2(E)$, two look-up tables (LUTs) are proposed (Fig. 4.1). As it is shown, $g_1(W)$ increases in case of $Wrench$ reduction, while $g_2(E)$ raises in case of low accuracy (Large error). The slope of the LUTs, and the α value can be chosen, according to the application, to gain a suitable compromise between accuracy and energy consumption. Such an approach can be applied to any cable-driven parallel robot, regardless to the number of cables , DOFs and to the particular cable tension distribution algorithm adopted.

Fig. 4.2 depicts a flow chart showing how to choose the proper T_{min}. Let us call $T_{0,in}$ as initial value of T_0. First, $g_1(W)$ and $g_2(E)$ are estimated considering the total $Wrench$ and $Error$. In case, the level of motion accuracy is not acceptable ($g_2(E) \geq 1$), we propose to increase T_0 by δT to enhance the tension in cables,[2]. As a result, T_0 and T_{min} increase which results in the motion accuracy increment. On the other hand, if the level of motion error is acceptable ($g_2(E) \leq 1$), we do not need to increase the tension in cables and the system stiffness. So, if T_0 is greater than the initial value $T_{0,in}$, we decrease T_0 and then T_{min} is estimated based on the Eq. 4.9. Knowing T_{min} and $Wrench$ the tension in cables are calculated.

[2] δT can either be constant or be calculated considering the stiffness and resonance requirements

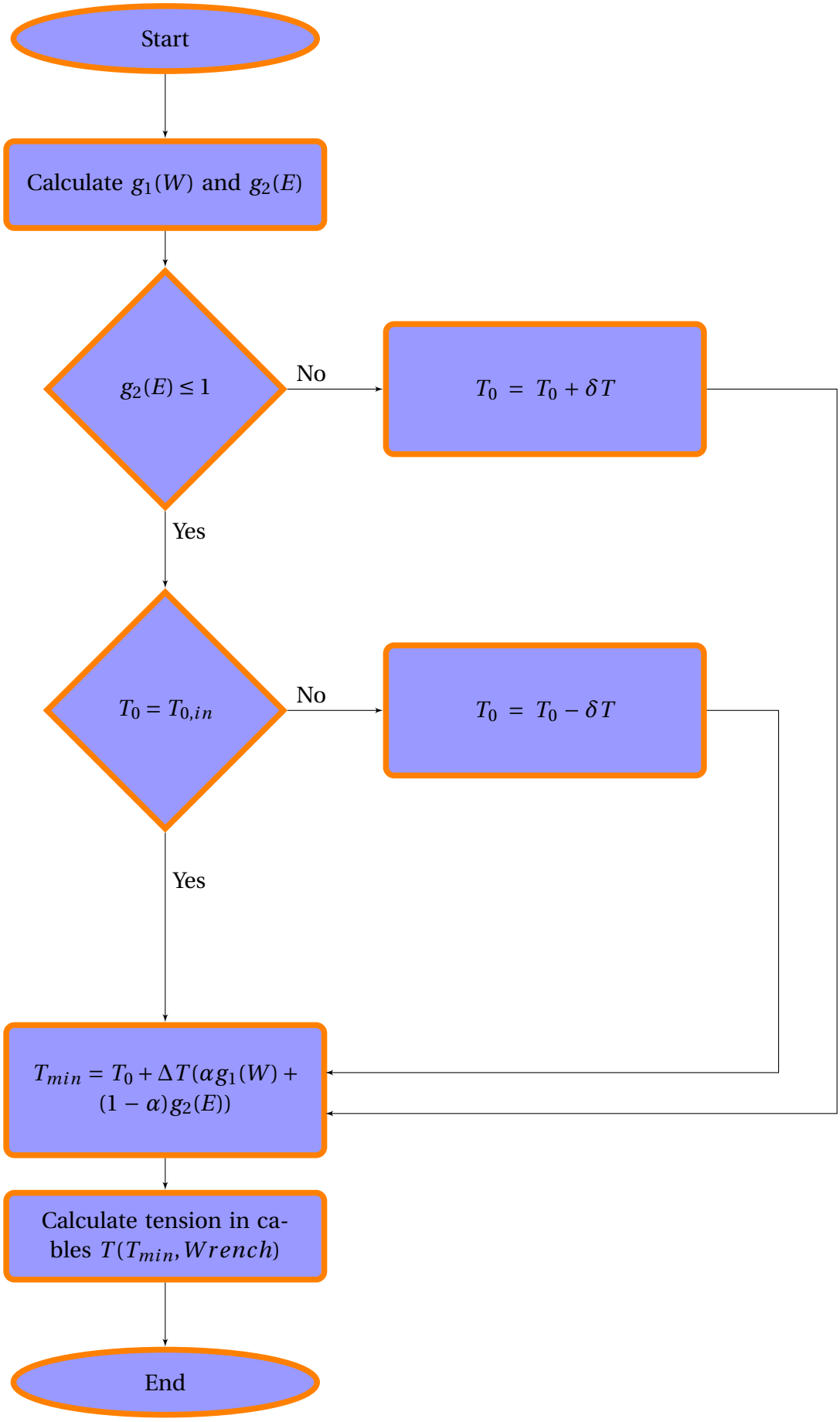

Figure 4.2: The algorithm to estimate T_{min} using Dynamic Minimum Tension Control

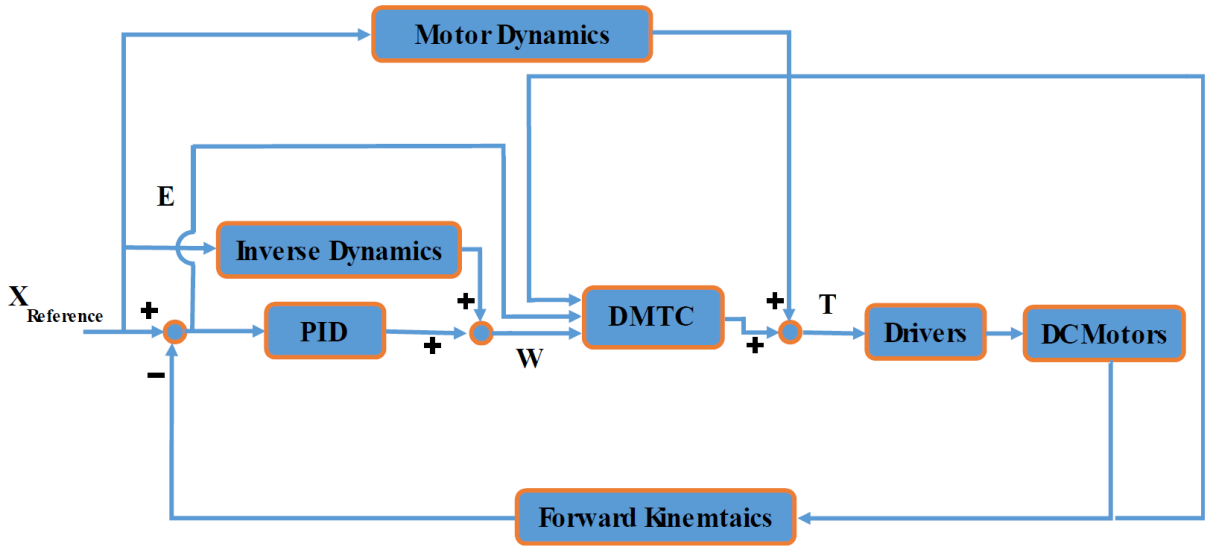

Figure 4.3: Schematic of a position control using the Dynamic Minimum Tension Control (DMTC).

4.3 Experimental Setup and Results

To test the new method, a 1 DOF cable-driven robot with two DC motors and a slider (end-effector) was built (Fig. 4.4). One linear and two rotational encoders were used to measure the position of the slider and the motors. This plant was connected to a PC via a PCI Multifunction I/O Sensoray626 board to control the system by Matlab and Simulink RTWT.

Fig. 4.3 presents a schematic of the position control using the DMTC approach. The output W consists of feedforward which is extracted from system inverse dynamics, and feedback which comes from the controller. In this study, we used PID controller which is widely used and is easily applicable in industrial systems.

The DMTC block calculates T_{min} according to the proposed algorithm and the tension in cables are determined based on $Wrench$ and T_{min}. In this block, different tension distribution methods such as p-norm optimization can be used. After considering motor dynamics, the output is sent to the drivers. Position feedback by encoders closes the feedback loop. A similar approach, except from the DMTC algorithm, is presented by Lamaury et al. in [93].

In the feedforward loop, slider friction was modeled as a function of velocity, based on sum of Stribeck, Coulomb, and viscous components, which were estimated through experiments. In the feedback loop, the position of the end-effector was estimated using rotational

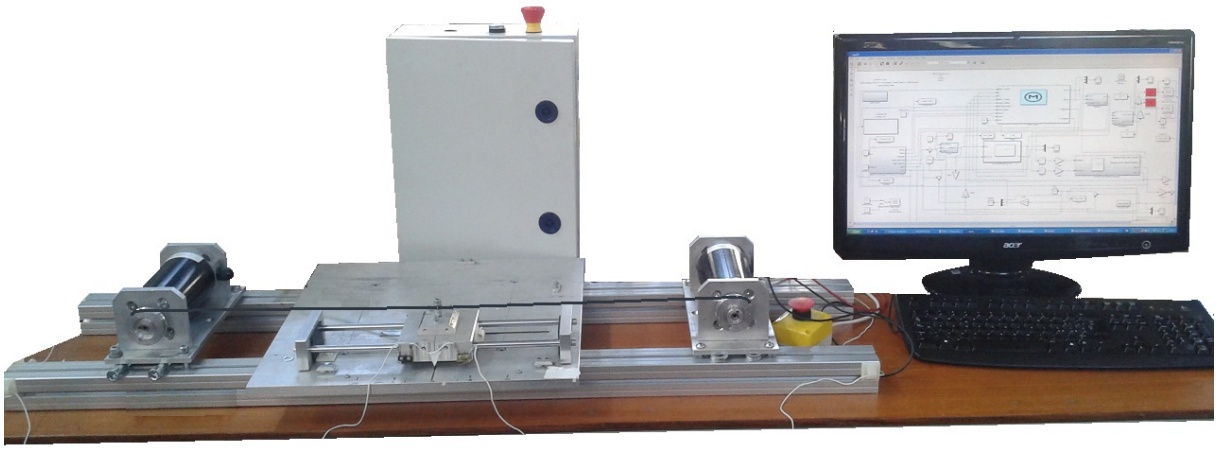

Figure 4.4: Experimental setup for testing optimal force distribution

encoder readings, with additional compensation of cable elongation. The linear encoder was used only to measure the actual position of the end-effector for final assessment of controller performance.

The cable tension calculation algorithm distributed the force in the two cables by simply imposing their tensions to T_{min} and $W + T_{min}$, according to the direction of W. A fifth degree polynomial reference, with frequency of $1Hz$ and $0.5Hz$ was used. The fixed amplitude of the reference was $35mm$ (Total travel 70 mm).

To show the efficiency of the new algorithm, we have used three different methods to run the system. The first one uses fixed minimum tensions of $4N$, $8N$, and $12N$ in cables. The second one uses the DMTC with $\alpha = 1$ (No contribution of tracking error); the third one, uses the DMTC with $\alpha = 0.5$. As it mentioned before, tuning the LUTs is also dependent on the necessities, but we have generated some LUTs to run the system as accurate as usage of fixed tensions to compare the power consumption of new method with formers.

Results are summarized in Table 4.1. To compare the different working conditions, the variance of position error and a power-related index were used. The former was calculated as

the variance of the difference between reference and actual positions. The latter was calculated as the average sum of the squared current references provided to the drivers. Measures were repeated during ten periods (i.e., twenty travels of the slider).

As it is shown, using the proposed formulation with $\alpha = 1$ can reduce power consumption, on the other hand setting $\alpha = 0.5$ results in more power savage due to application of $g_2(E)$, meanwhile accuracy of motion is similar in all conditions. Furthermore, it is clear that in case of higher frequency motions, LUTs have more priority comparing to fixed minimum tension usage.

Table 4.1: Comparison of fixed minimum tension with DMTC algorithm for $\alpha = 1(Wrench\ only)$ and $\alpha = 0.5(Wrench,\ Error)$

F (Hz)	Fixed Minimum Tension			DMTC ($\alpha = 1$)			DMTC ($\alpha = 0.5$)		
	T_{min}(N)	Err Var. (mm)	Pow.(A)	Err Var. (mm)	Pow.(A)	Pow. Savage	Err Var. (mm)	Pow.(A)	Pow. Savage
1	4	0.305	2.27	0.301	2.09	%7.93	0.299	1.97	%13.22
	8	0.261	5.66	0.259	5.20	%8.13	0.259	4.89	%13.60
	12	0.224	11.23	0.223	10.24	%8.82	0.222	9.68	%13.80
0.5	4	0.156	2.98	0.154	2.71	% 9.06	0.152	2.43	%18.46
	8	0.133	6.87	0.132	6.24	%9.17	0.132	5.58	%18.78
	12	0.107	12.68	0.105	11.51	%9.23	0.105	10.19	%19.64

Fig. 4.5.a shows the tension in cables using fixed minimum tension method in motion frequency of 0.5 Hz and T_{min}=4N. One of the cables always has a tension of 4N; however, the second one is changing based on the total wrench. In Fig. 4.5.b the tension in cables for $\alpha = 1$ is illustrated. In this case, the minimum tension is continuously changing based on the total wrench, and part (c) dedicates to the condition of $\alpha = 0.5$, where the minimum tension is in a changing mode in respect to the $Wrench$ and $Error$. The total power which was used for the same reference for the case of $\alpha = 0.5$ was the least one; while the accuracy of all three experiments were similar.

4.4 Summary

In this chapter, we investigated on increasing the performance of cable-driven systems by changing the minimum tension and active stiffness. A dynamic minimum tension control for cable-driven parallel robots was proposed and tested on a simplified scenario. Higher tension in cables results in more stiffness, higher trajectory tracking performance, more precise

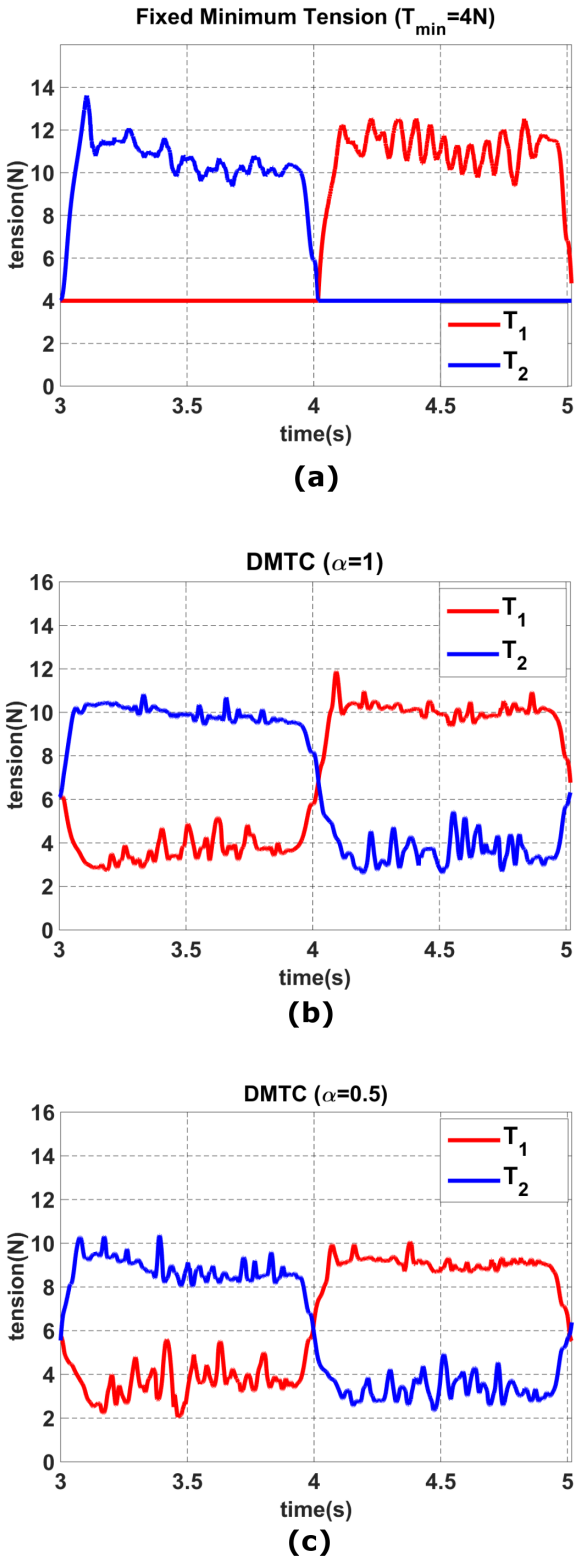

Figure 4.5: Comparision of tension in cables between a. Fixed minimum tension ($T_{min} = 4N$), b. DMTC ($\alpha = 1$) and c. DMTC ($\alpha = 0.5$) method

motion and disturbance rejection. On the other hand, there are always hardware limitations. Therefore, in case of increasing the tension in cables, saturation may occur. Furthermore, energy consumption is an important issue in case of robotic applications. We proposed a method to address this challenge.

This method works based on changing the minimum tension in cables, according to the stiffness, the system dynamics as a feedforward line, and error value of the system as the feedback. The minimum tension is increased in case of low $Wrench$, and reduced when $Wrench$ value is high. Also based on the feedback data, minimum tension reduces in case of high accuracy of motion to save energy consumption; however, minimum tension growth is a good option whenever the error value is high. Using the concept, DMTC algorithm was proposed.

We used the eigenvalues of the stiffness matrix to evaluate and achieve a minimum level of the stiffness intensity and two Look Up Tables (LUTs) in relation with error and total wrench. We offered the ones capable to achieve the same accuracy with less power consumption to show the superiority of the suggested method.

Experimental results showed that this approach yields large benefits in terms of accuracy and power consumption. When compared to fixed minimum tension modes, the DMTC algorithm performs much better to gain the same accuracy with less power consumption. One limitation of this study is that the experimental setup included a single-DOF system, so further testing is needed to verify the DMTC concept in application of complex contexts.

Chapter 5

Linear quadratic optimal controller for cable-driven parallel robots

In the previous chapters, we investigated on performance of cable-driven systems considering stiffness and dexterity indices. A high-level control algorithm can also influence on the system performance. This chapter aims to design a linear quadratic optimal controller for a planar cable-driven parallel robot.

First, optimal control is described. Then, the static modeling of the system is presented and the dynamic equations are obtained in terms of state space equation form. From the control point of view, an optimal controller is designed and applied by defining a performance index that accounts for the position and velocity of the end-effector as well as the applied torques by electric motors during the trajectory tracking. Riccati's equation is implemented to minimize the performance index of the controller. Results demonstrate that the application of the proposed controller leads to high accuracy in the trajectory tracking while the motor-produced torques are always kept below the design limit.

5.1 Linear Quadratic Optimal Control

5.1.1 Introduction

Optimal control emerged as a distinct filed of investigation in the 1950s. Beyond the traditional analytical and computational technique, referring in a unique mode of optimization problem arising in listing and the control of engineering devices and equipment.

The theory of optimal control is concerned with operating a dynamic system at minimum cost. The case where the system dynamics are described by a set of linear differential equations and the cost is described by a quadratic function is called the LQ problem. One of the main results in the theory is that the solution is provided by the linear-quadratic regulator (LQR), a feedback controller whose equations are given below. The LQR is an important part of the solution to the LQG (Linear-Quadratic-Gaussian) problem. Like the LQR problem itself, the LQG problem is one of the most fundamental problems in control theory [117].

5.2 Statics and dynamics of the system

The Feriba-3 is a 3-DOF planar robot with four cables and a circular end-effector. Each cable is fixed to the lateral side of the end-effector, which is able to wind around it. The other end of the cable is wound around a pulley, which is directly connected to a motor shaft. A sheet of glass is fixed onto the base, and a flux of compressed air is blown toward the glass through a series of little holes drilled into the lower side of the end-effector to eliminate friction. The radii of the pulleys are the same as that of the end-effector, which facilitates an easier solution for the kinematics of the robot. The kinematics and stability of the system has been discussed in [38], [10]. Fig. 5.1 illustrates the Feriba-3 cable-driven parallel robot.

The static equilibrium of a n–DOF cable-driven robot, manipulated by cables, can be expressed by the following linear equation system:

$$ST = W, \tag{5.1}$$

where $S \in \mathbb{R}^{n\times m}$ is the structure matrix of the robot that is related to the geometrical con-

figuration of the system, $T \in \mathbb{R}^{m\times 1}$ is the cable tension vector, and $W \in \mathbb{R}^n$ is the wrench acting on the end-effector. In a force-closure workspace, the vector T can be calculated as follows:

$$T = S^{+}W + (I_m - S^{+}S)z, \tag{5.2}$$

where $I_m \in \mathbb{R}^{m\times m}$ is the identity matrix, $z \in \mathbb{R}^{m\times 1}$ is an arbitrary vector, and $S^{+} = S^{T}(SS^{T})^{-1} \in \mathbb{R}^{m\times n}$ is the under-constrained Moore-Penrose pseudo inverse of S. The first term is the particular solution and the second one is the homogeneous solution that maps z to the null space. By choosing z the minimum tension in cables can be changed according to the application or necessity. This equation is considered the Cable Tension Calculation (CTC) algorithm. The tension in cables can be achieved by identifying the structure matrix of the robot and determining the desirable wrench on the end-effector. Once the tension in cables are estimated, the torque of motors can be calculated by the following equation:

$$T_i = \frac{\tau_i - I_i\ddot{\theta}_i}{r_i}, \qquad i = 1,2,..,m \tag{5.3}$$

where T_i, r_i, τ_i are tensions in the ith cable, the pulley radius, and the ith motor torque, respectively. $I_i, \ddot{\theta}_i$ are the moment of inertia and the angular acceleration of the ith pulley. In the case of four cable-driven robot with 3-DOF, the following results can be obtained:

$$S = \begin{pmatrix} cos(\eta_1) & cos(\eta_2) & cos(\eta_3) & cos(\eta_4) \\ sin(\eta_1) & sin(\eta_2) & sin(\eta_3) & sin(\eta_4) \\ r & -r & r & -r \end{pmatrix}, \qquad T = \begin{pmatrix} T_1 \\ T_2 \\ T_3 \\ T_4 \end{pmatrix}, \qquad W = \begin{pmatrix} F_X \\ F_Y \\ M \end{pmatrix} \tag{5.4}$$

where η_i is the angle between the x-axis and the ith cable, r is the end-effector and pulley's radius. F_X, F_Y, M are the forces and the torque that the mechanism has to generate. A thin layer of air is always present between the end-effector and the surface, such that the directional and rotational frictions are ignored because of their very low quantities. To apply linear quadratic optimal control, the standard dynamic form of the system in terms of state

Figure 5.1: a. Feriba-3 overall view and b. Statics diagram

space formulation is developed, which is a set of 6 coupled first-order ordinary differential equations expressed as

$$\begin{pmatrix} \dot{q}_1 \\ \dot{q}_2 \\ \dot{q}_3 \\ \dot{q}_4 \\ \dot{q}_5 \\ \dot{q}_6 \end{pmatrix} = \begin{pmatrix} 0 & 0 & 0 & 1 & 0 & 0 \\ 0 & 0 & 0 & 0 & 1 & 0 \\ 0 & 0 & 0 & 0 & 0 & 1 \\ 0 & 0 & 0 & 0 & 0 & 0 \\ 0 & 0 & 0 & 0 & 0 & 0 \\ 0 & 0 & 0 & 0 & 0 & 0 \end{pmatrix} \begin{pmatrix} q_1 \\ q_2 \\ q_3 \\ q_4 \\ q_5 \\ q_6 \end{pmatrix} + \begin{pmatrix} 0 & 0 & 0 & 0 & 0 & 0 \\ 0 & 0 & 0 & 0 & 0 & 0 \\ 0 & 0 & 0 & 0 & 0 & 0 \\ 0 & 0 & 0 & \frac{1}{m} & 0 & 0 \\ 0 & 0 & 0 & 0 & \frac{1}{m} & 0 \\ 0 & 0 & 0 & 0 & 0 & \frac{1}{I} \end{pmatrix} \begin{pmatrix} 0 \\ 0 \\ 0 \\ F_X \\ F_Y \\ M \end{pmatrix} \tag{5.5}$$

where m and I are the end-effector mass and the moment of inertia, respectively. q_1 and q_2 are states of the system corresponding to the linear positions of the end-effector in the X and Y directions. q_4 and q_5 are the states related to the velocity of the end-effector in the X and Y directions. q_3 and q_6 are the states corresponding to angular position and angular velocity of the end-effector, respectively. In our system, the values of r, m and I are equal to $3 \times 10^{-2} m$, $0.1 kg$, and $4.5 \times 10^{-5} kg.m^2$, respectively.

5.3 Synthesis of the Optimal Controller

A very brief explanation of the LQ optimal control is provided in this section (see [118] for more details). By definition,

$$\dot{q}(t) = [\dot{q}_1, \dot{q}_2, \dot{q}_3, \dot{q}_4, \dot{q}_5, \dot{q}_6]^T, \tag{5.6}$$
$$q(t) = [q_1, q_2, q_3, q_4, q_5, q_6]^T,$$

$$A = \begin{pmatrix} 0 & 0 & 0 & 1 & 0 & 0 \\ 0 & 0 & 0 & 0 & 1 & 0 \\ 0 & 0 & 0 & 0 & 0 & 1 \\ 0 & 0 & 0 & 0 & 0 & 0 \\ 0 & 0 & 0 & 0 & 0 & 0 \\ 0 & 0 & 0 & 0 & 0 & 0 \end{pmatrix}, \quad B = \begin{pmatrix} 0 & 0 & 0 & 0 & 0 & 0 \\ 0 & 0 & 0 & 0 & 0 & 0 \\ 0 & 0 & 0 & 0 & 0 & 0 \\ 0 & 0 & 0 & \frac{1}{m} & 0 & 0 \\ 0 & 0 & 0 & 0 & \frac{1}{m} & 0 \\ 0 & 0 & 0 & 0 & 0 & \frac{1}{I} \end{pmatrix} \tag{5.7}$$

$$W(t) = [0, 0, 0, F_X, F_Y, M]^T. \tag{5.8}$$

$$\dot{q}(t) = Aq(t) + BW(t) \tag{5.9}$$
$$y(t) = Cq(t)$$

Therefore, the actual size of the system state variable is six. For brevity, the dependence from time has been removed. The matrix C is an identity matrix. The output vector $y(t)$ is considered to be a full state vector because of the implementation of the experimental tests. In other words, $y(t)$ contains all of the states of the system.

The controller design is based on the LQ optimal control for the modeled system stands on the state-space form presented in Eq. 5.9. Let us assume that the end-effector is going to move based on a trajectory with certain velocity and acceleration. The aim is to determine

$W(t)$ as the control function to minimize the performance index J, which is the integral of a quadratic function of the system output variables $y(t)$ and control function $W(t)$. However, we may encounter some error in motion. The performance index is described as follows:

$$\int_0^\infty [y^T(t)Qy(t) + W^T(t)LW(t)]dt = \int_0^\infty [q^T(t)C^TQq(t) + W^T(t)LW(t)]dt, \tag{5.10}$$

where Q and L are weighting matrices related to the system output and to the control input, respectively. The index considers takes both the tracking error of the end-effector and the control effort. The first term inside the integral in Eq. 5.10 minimizes the entire error values related to the linear and angular positions of the end-effector. The second term reduces the absolute values related to the plant inputs that are the wrenches and are applied as tensions in cables via Eq. 5.2. Consequently, the performance index J is minimized. If the system input is regarded as the result of a linear feedback from the output, the following equation can be written:

$$W(t) = -Ky(t) = -KC_q(t), \tag{5.11}$$

where the optimal value of is obtained by:

$$K = L^{-1}B^TP, \tag{5.12}$$

and is achieved by using Riccarti's equation

$$-A^TP - PA + PBL^{-1}B^TP - C^TQC = 0. \tag{5.13}$$

By including the optimal controller, the equations of the system are written as

$$\dot{q}(t) = (A - BKC)q(t) \tag{5.14}$$
$$y(t) = Cq(t)$$

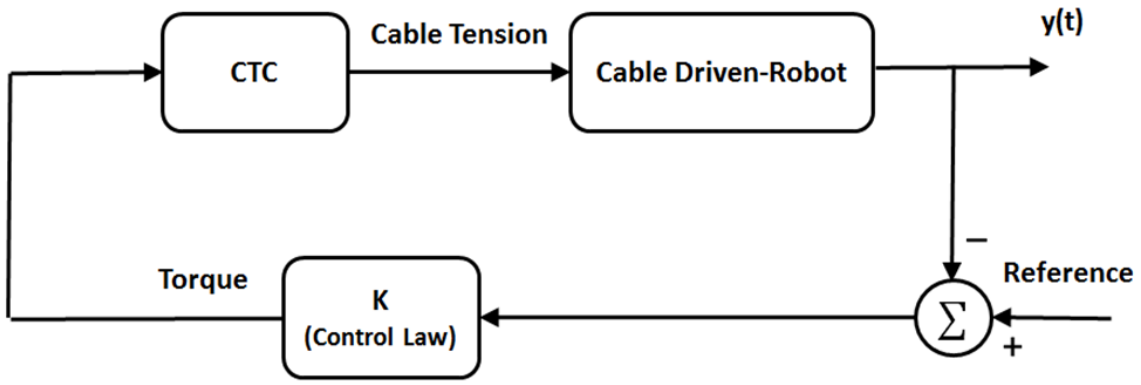

Figure 5.2: Block diagram of the control system

Fig. 5.2 shows the block diagram of the designed controller system. The required wrench quantity is calculated based on the inverse dynamics equations of the system and the controller with respect to the reference. The estimated wrench is inserted to the CTC block that works based on Eq. 5.2. The CTC calculates the appropriate cable tensions. Based on the tension values, the torques that should be produced by the electrical motors are calculated using Eq. 5.3. Both the linear and angular positions as well as the velocity of the end-effector are obtained using the rotary encoders of motors through forward kinematics in a closed loop system.

5.4 Experimental results

In this section, the results of experimental tests are provided and discussed to demonstrate the capabilities of the proposed LQ controller for position and velocity control of the Feriba-3 cable robot. The tuning of the LQ controller depends on the displacement and the velocity along the X and Y directions as well as on the angular rotation of the end-effector. Our aim is to track the reference trajectory with the least error in displacement and velocity. To this end, we considered the optimal control described in the previous section with following weighting matrices:

$$A = \begin{pmatrix} q_x & 0 & 0 & 0 & 0 & 0 \\ 0 & q_y & 0 & 0 & 0 & 0 \\ 0 & 0 & q_\theta & 0 & 0 & 0 \\ 0 & 0 & 0 & q_{vx} & 0 & 0 \\ 0 & 0 & 0 & 0 & q_{vy} & 0 \\ 0 & 0 & 0 & 0 & 0 & q_{v\theta} \end{pmatrix} \tag{5.15}$$

The size of diagonal matrices Q and L are $[6 \times 6]$ and $[3 \times 3]$, respectively. To synthesize the optimal controller, the values of the diagonal elements of the matrices Q and L should be selected properly. Parameters q_x, q_y, q_θ correspond to linear and angular positions, whereas $q_{vx}, q_{vy}, q_{v\theta}$ are related to the linear and angular velocities.

Two different reference trajectories were designed to test the proposed optimal control algorithm. The first trajectory is a combination of linear and circular trajectory in the $X-Y$ plane with rotation motion. The end-effector starts from the center of the plane where $(X,Y) = (0,0)$. Then, a motion in the X-direction based on a $3rd$ order time-function polynomial occurs, which locates the end-effector in the surroundings of a circle where $(X,Y) = (R,0)$. At the next step, a 360-degree counterclockwise circular motion occurs in the $X-Y$ plane, and the end-effector returns to the former position of $(X,Y) = (R,0)$. The last step of the motion involves another X-direction motion based on a $3rd$ order time-function polynomial to move the end-effector back to the $(X,Y) = (0,0)$. In all periods of the $X-Y$ motion, the rotation of the end-effector occurs based on a time sinusoidal reference.

The second reference trajectory includes four linear motions in the $X-Y$ plane and a sinusoidal function of time as the rotational motion. The $X-Y$ linear motions in the X and Y directions are planned in consideration of a trapezoidal velocity profile. The end-effector starts from the center of the plane and, after traveling the designed trajectories, returns to the initial position.

Fig. 5.3.a-c show the reference trajectory and the response of both the closed loop employed LQ optimal controller and the open loop system for the first reference trajectory in terms of the linear and angular motion of the end-effector. An open-loop control system is controlled directly by an input signal without the benefit of feedback. The open-loop control

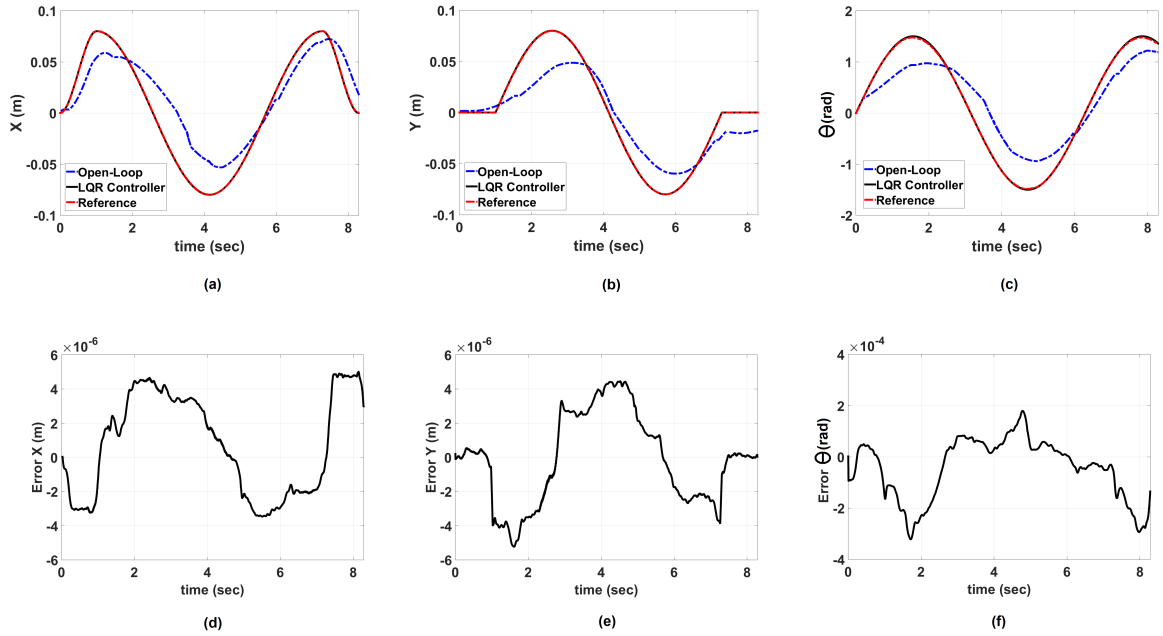

Figure 5.3: Comparison of the open loop and the LQ optimal controller for position of circular reference trajectory (X-Y plane) tracking for a. X-axis, b. Y-axis, and c. sinusoidal rotation θ. The reference tracking error for the LQ optimal controller in terms of d. X-axis, e. Y-axis and f. sinusoidal rotation θ

system clearly tracks the reference with high errors. According to Figs. 5.3.d–f, the LQ optimal controller made the system track the reference efficiently with very low error.

Fig. 5.4.a-c depict the reference trajectory and the results of the response of both the LQ optimal controller and the open loop system for the trapezoidal velocity reference trajectory in terms of the linear and angular motion of the end-effector. Similarly to the former experiment, the open loop application presents unsatisfactory results, whereas employing the LQ optimal controller results in a good level of trajectory tracking in terms of displacement and velocity. The errors of trajectory tracking are very small, as illustrated in Figs. 5.4.d–f.

The cable tensions in four cables through circular and trapezoidal trajectories are shown in Figs. 5.5 and 5.6. The minimum tension in cables was set to 0.5 N. The motors have a maximum torque of 3.5 N. According to these figures, the overall torque applied to control the cable-driven parallel robot for each motor does not exceed the range of 1.8 N, which is much lower than the desired limit (3.5 N) for both circular and trapezoidal trajectories.

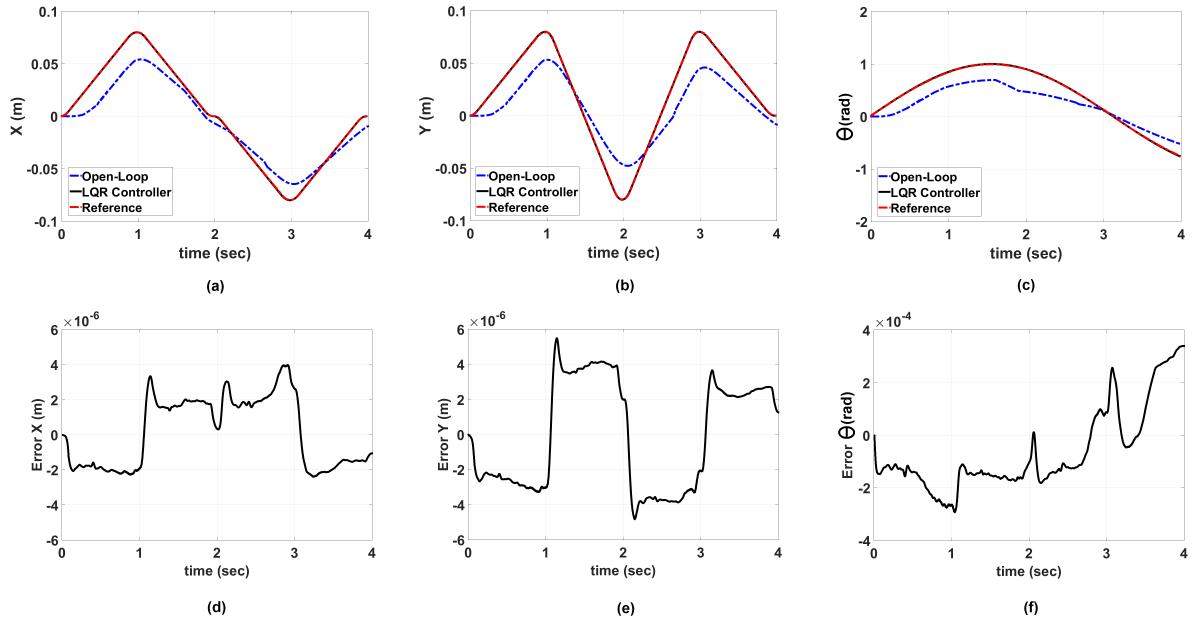

Figure 5.4: Comparison of the open loop and the LQ optimal controller for trapezoidal reference trajectory for a. X-axis, b. Y-axis, and c. sinusoidal rotation θ. The reference tracking error for the LQ optimal controller in terms of d. X-axis, e. Y-axis and f. sinusoidal rotation θ

5.5 Summary

High-level control algorithms can play an important role in performance of cable-driven parallel robots. Linear quadratic (LQ) optimal controllers can provide all the states of the system for the feedback, including velocity and position, in addition to optimal results which is quite desirable in cable-driven systems.

In this work, a linear quadratic (LQ) optimal controller for both position and velocity of a parallel cable-driven robot was designed and experimentally tested. The static and dynamic modeling of the parallel cable-driven robot were described, and the state equations of the system were developed to implement the controller on the system.

The application of the proposed control scheme led to the minimization of the performance index by considering both the tracking error and output variables of the system to minimize the control effort. Riccati's equation was used to obtain the optimal value of the cable tensions. Appropriate weights were associated with the most significant elements of the output vector, which are linear and angular positions and velocities of the end-effector.

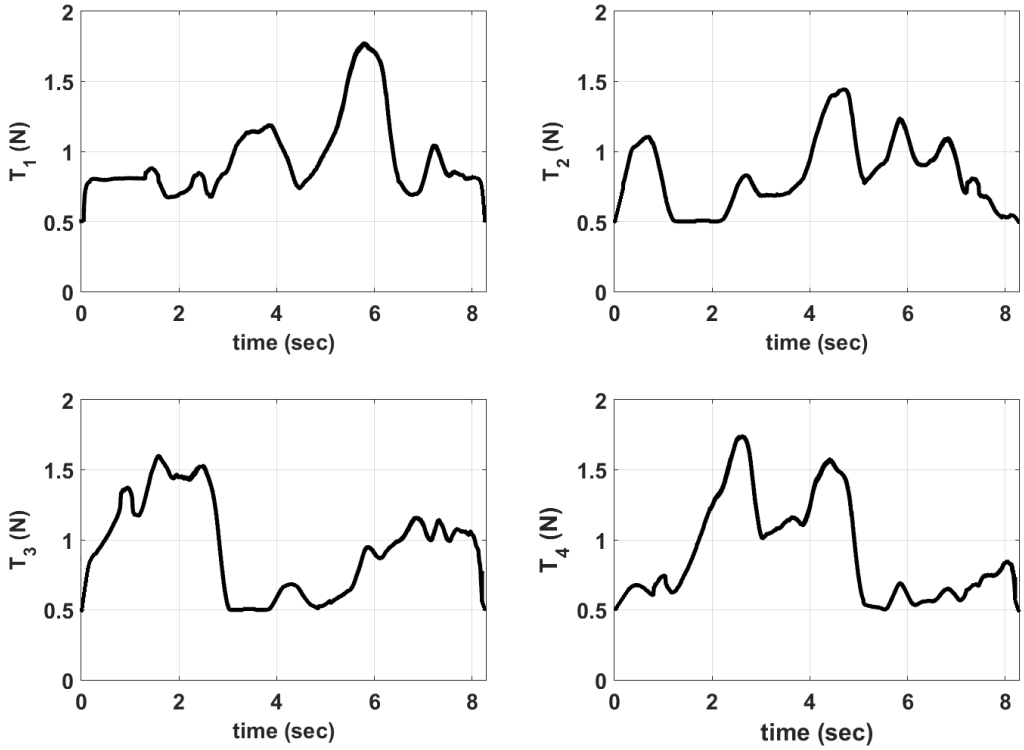

Figure 5.5: Cable tension in four cables for circular reference trajectory (X-Y plane) and sinusoidal rotation

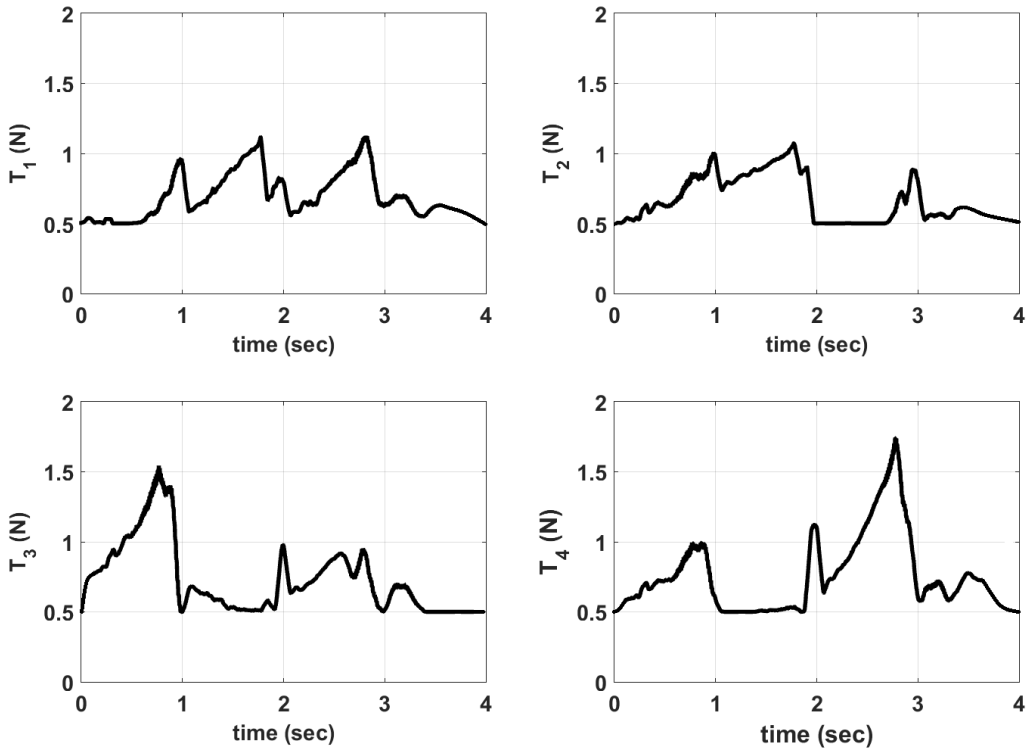

Figure 5.6: Cable tension in four cables for trapezoidal trajectory and sinusoidal rotation

The designed controller was experimentally tested on the circular position and trapezoidal velocity trajectories for both linear and angular displacements. The performance of the controller was compared to the performance of the open loop controller. The results are quite satisfactory, and the synthesized LQ optimal controller proved to be efficient for both linear and angular position tracking within the desired time. Furthermore, the torques applied on the cables were always kept well-below the designed limit.

Chapter 6

Conclusion and Further Work

Cable-driven parallel robots are a type of parallel manipulators in which the end-effector is supported in parallel by cables. Low structural weight, high acceleration, and large workspace are some important advantages of cable-driven devices over their rigid-link counterparts. Adaptive cable-driven parallel robots are defined as those cable-driven systems where in the locations of some pulley blocks is controlled as a function of the end-effector pose to optimize given performance indices within a target workspace.

This research study is dedicated to investigate on trajectory planning and control of adaptive and traditional cable-driven parallel robots to achieve higher performance.

Adaptive cable-driven parallel robots have augmented kinematic redundancy compared to traditional cable-driven systems with equal number of cables. As a result, the inverse kinematics problem of such robots may have more solutions compared to the traditional cable-driven parallel robots. The motivation of this study is to introduce a systematic methodology to use the augmented kinematic redundancy to increase robot performance. Depending on the application, the most efficient solution can be determined based on one or more performance indices.

In this study, the end-effector motion is considered quasi-static and the active stiffness is ignored. Furthermore, cable orientation adaptation is a proper method to improve stiffness index in wider regions of the workspace, because typical settling time of a mechanical system is much higher than that of motor torques; however, this adaptability cannot provide fast

changes in stiffness, which may be necessary to face external noises.

Two important performance indices, dexterity and elastic stiffness were considered simultaneously. The dexterity index defines the kinematic behavior of a robot. The elastic stiffness can affect trajectory tracking, disturbance rejection and vibrations of a system. The best feasible elastic stiffness while keeping ideal dexterity was investigated for three different designs of adaptive-cable driven parallel robots and as a result, the related configuration of cables and pulley blocks were obtained. The same method was applied for the case of a 3-DOF adaptive cable-driven robot with moving pulley blocks on a circle.

A configuration of cables and pulley blocks were proposed to run the system under the ideal dexterity and at the same time approximately isotropic elastic translational stiffness. On the other hand, the best possible dexterity while keeping ideal isotropic stiffness was studied and related equations were presented. The proposed method reduces the feasible configuration of cables and pulley blocks to a unique solution and taking advantages of more redundancy.

In non-adaptive design of cable-driven parallel robots, the elastic stiffness and dexterity indices are unchangeable for a certain position of end-effector due to fixed length and orientation of cables. Only the active stiffness can be changed by modifying the tension in cables.

Another part of this study is dedicated to control the minimum tension and active stiffness. Higher tension in cables results in more stiffness, higher trajectory tracking performance, more precise motion and disturbance rejection. On the other hand, there are always hardware limitations. Therefore, in case of increasing the tension in cables, saturation may occur. Furthermore, energy consumption is an important issue in case of robotic applications.

Important factors influencing on system performance such as active stiffness, total wrench and transverse vibration were studied and Dynamic Minimum Tension Control (DMTC) was proposed. This method works based on changing the minimum tension in cables, according to the stiffness, the system dynamics as a feedforward line, and error value of the system as the feedback. The minimum tension is increased in case of low Wrench, and reduced when Wrench value is high. Also based on the feedback data, minimum tension reduces in case of

high accuracy of motion to save energy consumption; however, minimum tension growth is a good option whenever the error value is high.

Controllers can affect the system performance. This study presents an approach to apply the optimal controller on cable-driven parallel robots. The results of applying a linear quadratic optimal controller on parallel cable-driven robot were presented for both position and velocity control. Riccati's equation was used to obtain the optimal value of the cable tensions. Appropriate weights were associated with the most significant elements of the output vector, which were linear and angular positions and velocities of the end-effector. The designed controller was experimentally tested on the circular position and trapezoidal velocity trajectories for both linear and angular displacements. The establishment of the proposed control scheme led to the minimization of the performance index by considering both the tracking error and output variables of the system to minimize the control effort.

The performance of the controller was compared to the performance of the open-loop system. The results are quite satisfactory, and the synthesized linear quadratic optimal controller proved to be efficient for both linear and angular position tracking within the desired time. Results demonstrate that the application of the proposed controller leads to high accuracy in the trajectory tracking.

One limitation of this study is that the experimental setup included simple test beds, so further testing is needed to verify the DMTC and linear quadratic optimal control in application of complex contexts. Also, active stiffness and highly dynamic motion trajectories can be considered in future studies of adaptive cable-driven parallel robots.

Appendix A

Transverse Vibration Analysis of an Axially Accelerating Cable in Application of Cable-Driven Parallel Robots

Vibration is a significant factor, which can affect on system performance. In this appendix, transverse vibration equation of a cable in motion was solved using four term approximation Galerkin method, and ode45. The vibration of a point at the middle of the cable for three different tension values was estimated. Results were experimentally validated on a system with two DC motors and pulleys with a cable attached them. The amplitude and frequency of vibrations were compared, showing the higher tension in cables results in less amplitude of transversal vibration. This concept can be useful in cable-driven robots, where increasing the minimum tension in cables may lead to achieving better trajectory tracking performance, due to less vibration amplitude. The latter approach was tested on a 1-DOF cable-driven robot, and the results confirmed that higher minimum tension in cables can generate more accurate motion of the end-effector.

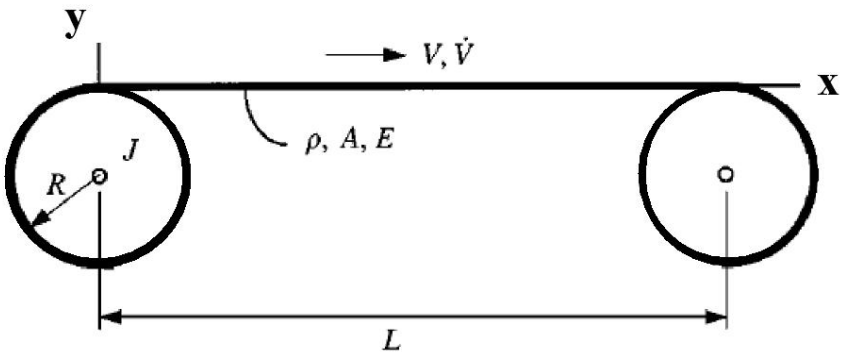

Figure A.1: A system of a cable in motion with transverse vibration

A.1 Transverse Vibration of a Cable in Motion

To model the transversal vibration of a cable in motion, let us consider the system in Figure A.1 which is a combination of two pulleys and a cable attached to them, unrolling from one, and rolling to the other. The cable moves with the velocity of V which can be a function of time, and $\dot{V}$ is the acceleration of the cable. Parameters R, L, A, ρ and E are respectively pulley radius, cable length, cross sectional area, mass per unit of length, and Young's modulus. P(t), F(x,t), and y(x,t) represent tension in cable, external force per unit length of the cable, and the transverse vibration of the cable.

Transverse vibration of a cable in motion can be formulated as [77]:

$$\rho A(y_{tt} + 2Vy_{xt} + V^2 y_{xx} + \dot{V}y_x) = F(x,t) + P(t)y_{xx} + \frac{1}{2}EAy_{xx}\int_0^L y^2 dx. \tag{A.1}$$

Various numerical techniques were applied to solve the differential equations. In this study, we used the Galerkin method, which is widely used in cable vibration analysis. The solution is approximated with the following equation:

$$y(x,t) = \sum_{i=1}^{n} \phi_i(x) q_i(t). \tag{A.2}$$

Where $\phi_i(x)$ can be considered as $sin(i\pi x/L)$ which is the ith eigenfunction of the simply supported stationary string[74], and $q_i(t)$ is a time dependent function of displacement. By substitution of equation (A.2) in (A.1), the residual can be calculated as the following expres-

sion:

$$
\begin{aligned}
R = \sum_{i=1}^{n} \{ & \rho A \ddot{q}_i sin(\frac{i\pi x}{L}) + 2\rho AV \frac{i\pi}{L} \dot{q}_i cos(\frac{i\pi x}{L}) + \\
& \rho A\dot{V} \frac{i\pi}{L} q_i cos(\frac{i\pi x}{L}) + (P - \rho AV^2)(\frac{i\pi}{L})^2 q_i sin(\frac{i\pi x}{L}) + \\
& \frac{1}{2} EA(\frac{i\pi}{L})^2 {q_i}^3 sin(\frac{i\pi x}{L}) \int_0^L sin^2(\frac{i\pi x}{L}) dx \}.
\end{aligned} \tag{A.3}
$$

In the next step, the residual is minimized by multiplying with a weight function, and integration over the domain. The weighting function $W_j(x)$ can be chosen as the stationary string eigenfunction,

$$
\int_0^L R W_j(x) dx = 0, \quad W_j(x) = sin(\frac{j\pi x}{L}), \quad j = 1, 2, 3, ..., n. \tag{A.4}
$$

By the integration over the domain, for a four term approximation, it can be gained:

$$
\begin{pmatrix} 1 & 0 & 0 & 0 \\ 0 & 1 & 0 & 0 \\ 0 & 0 & 1 & 0 \\ 0 & 0 & 0 & 1 \end{pmatrix} \begin{pmatrix} \ddot{q}_1 \\ \ddot{q}_2 \\ \ddot{q}_3 \\ \ddot{q}_4 \end{pmatrix} + \begin{pmatrix} 0 & \frac{-16V}{3L} & 0 & \frac{-32V}{15L} \\ \frac{16V}{3L} & 0 & \frac{-48V}{5L} & 0 \\ 0 & \frac{48V}{5L} & 0 & \frac{-96V}{7L} \\ \frac{32V}{15L} & 0 & \frac{96V}{7L} & 0 \end{pmatrix} \begin{pmatrix} \dot{q}_1 \\ \dot{q}_2 \\ \dot{q}_3 \\ \dot{q}_4 \end{pmatrix} + \begin{pmatrix} \frac{E\pi^2}{4\rho L} & 0 & 0 & 0 \\ 0 & \frac{E\pi^2}{\rho L} & 0 & 0 \\ 0 & 0 & \frac{9E\pi^2}{4\rho L} & 0 \\ 0 & 0 & 0 & \frac{4E\pi^2}{\rho L} \end{pmatrix} \begin{pmatrix} q_1^3 \\ q_2^3 \\ q_3^3 \\ q_4^3 \end{pmatrix}
$$

$$
+ \begin{pmatrix} (\frac{P}{\rho A} - V^2)(\frac{\pi}{L})^2 & \frac{-8\dot{V}}{3L} & 0 & \frac{-16\dot{V}}{15L} \\ \frac{8\dot{V}}{3L} & (\frac{P}{\rho A} - V^2)(\frac{2\pi}{L})^2 & \frac{-24\dot{V}}{5L} & 0 \\ 0 & \frac{24\dot{V}}{5L} & (\frac{P}{\rho A} - V^2)(\frac{3\pi}{L})^2 & \frac{-48\dot{V}}{7L} \\ \frac{16\dot{V}}{15L} & 0 & \frac{48\dot{V}}{7L} & (\frac{P}{\rho A} - V^2)(\frac{4\pi}{L})^2 \end{pmatrix} \begin{pmatrix} q_1 \\ q_2 \\ q_3 \\ q_4 \end{pmatrix} = 0. \tag{A.5}
$$

To solve the equation (A.5), we used ode45 (Matlab) which implements versions of 4th/5th-order Runge-Kutta method [119]. Velocity, acceleration, and tension in cables can be chosen arbitrary which results in different transverse vibration profiles; however, validating the results with experimental setup especially in case of numerical solution is an important issue, which was not implemented in other research studies.

There are always some limitations for the experimental setup. For example, using a controller to make the system follow a special reference can result in some vibrations. We have used a constant value of tension, and a fixed acceleration in the cable, which can be very convenient to implement in case of validating data by a real system. So the equation was solved for three cases of 6, 10, and 14 N as fixed tensions in cable, and a constant motion acceleration of 1.72 m/s^2.

A.2 Experimental Setup and Validation

To validate the numerical results, a system composed of two DC motors with pulleys connected to a cable was built (Figure A.2.a). Two rotational encoders were used to measure the rotation of the motors. This plant was connected to a PC via a PCI Multifunction I/O Sensoray626 board to control the system by Matlab and Simulink RTWT.

A high frequency Pike F032B ASG16 camera with the Phlox high bright LED backlight was used to take the cable vibration frames. To gain an acceptable resolution a telecentric lens, and focal length multiplier were connected to the camera. The system was tuned to take narrow frames from middle of the cable. The frames were received with 9.3 pixel per millimeter and 1500 FPS (Frames Per Second). A black/white filter was implemented on the frames, and vibration of the cable was estimated using an image processing algorithm. A sample image and the filtered one are illustrated in Figure A.2.b.

As it was mentioned, to avoid any kind of noise and vibration, no closed-loop controller was used. In this experiment, we kept a fixed value of the tension F in the cable. To estimate the tension, dynamics of the system was formulated. Negelecting the mass of the cable around the pulley, and considering the similarity of two pulleys, necessary torque of motors can be obtained from following equation based on the direction of motion. A more precise

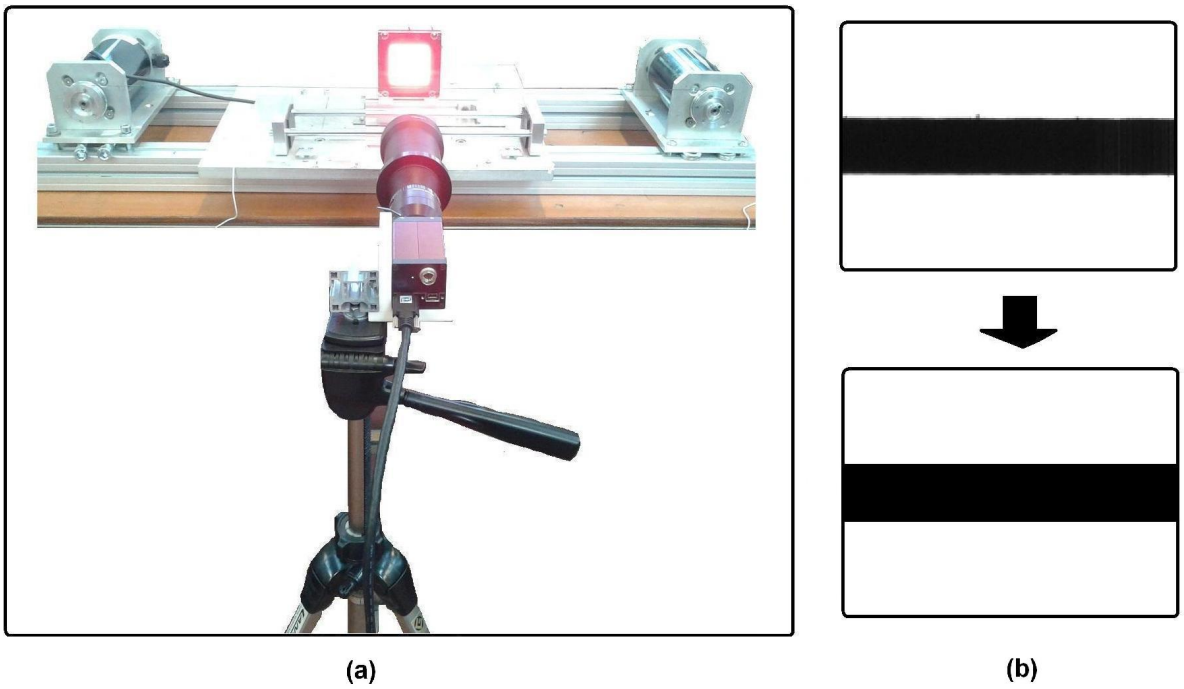

Figure A.2: a. Experimental setup for measuring the transverse vibration of an axially accelerating cable, b. Sample frame from middle of the cable before and after the image processing filter

comparision is illustrated in Table A.1.

$$F = \frac{T \pm I\ddot{\theta}}{r} \tag{A.6}$$

where I is the pulley inertia, T is motor torque and r is pulley radius. A simulink file was used to generate the fixed tension in the cable. To refuse any kind of pre-motion vibration, the system starts with equal torques from both motors for 40 seconds, and after stabilizing the system, the motion starts by increasing torque in one motor. Results are illustrated in Figure A.3 which shows good matching between numerical and experimental data. It is clear that the amplitude of vibration is decreased by increasing tension in the cable, while the frequency of vibration is increasing.

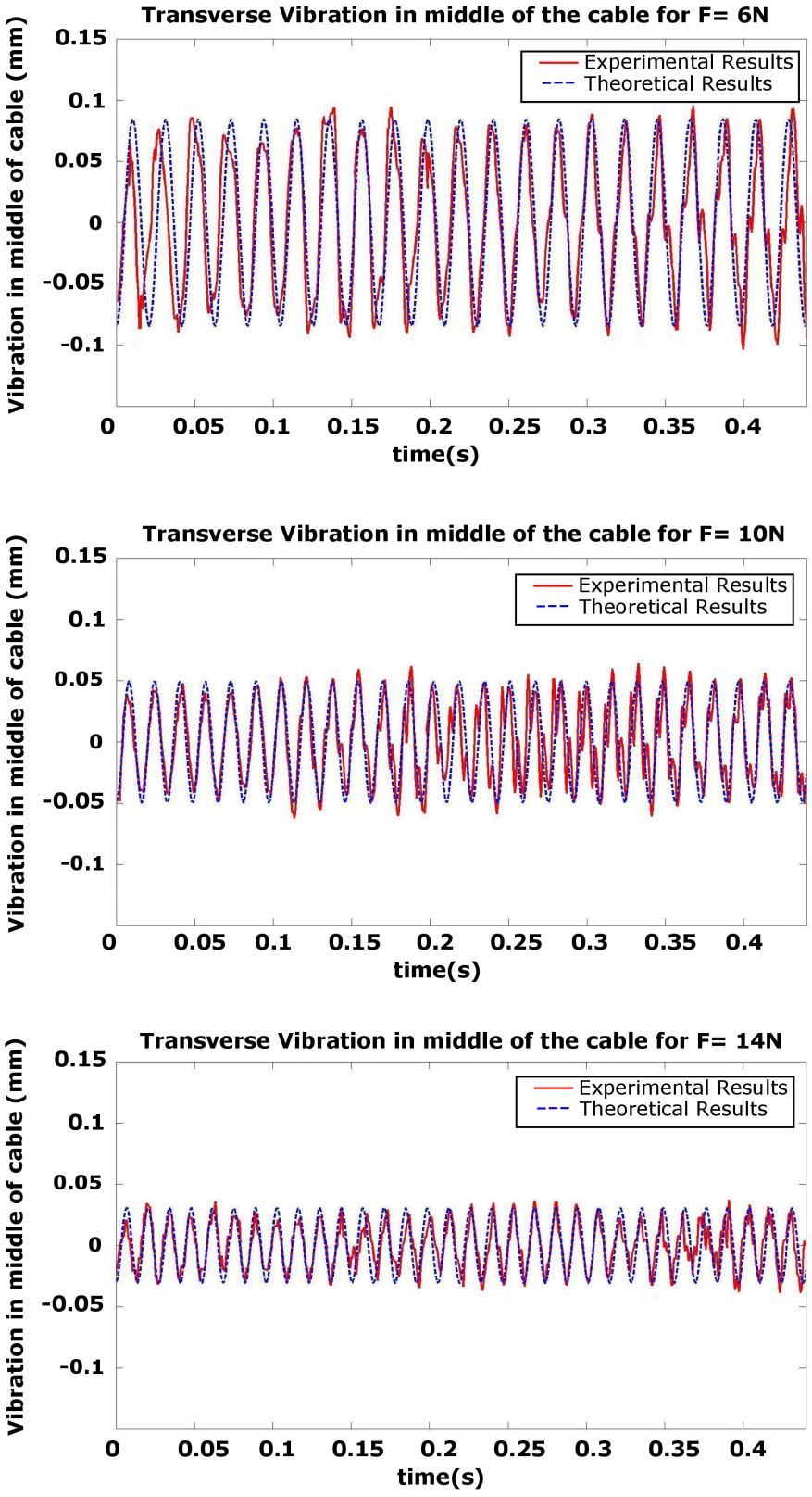

Figure A.3: Experimental and theoretical results of transverse vibration of the cable for the case of 6, 10, and 14 N as tension in the cable

Table A.1: Frequency and transverse variation of the cable in motion with different tensions

Tension (N)	Variance of Transverse Vibration (mm)	Frequency (Hz)
6	3.6e-3	47.7
10	1.3e-3	61.4
14	4.83e-4	72.7

A.3 Application to Cable-Driven Robots

Results show that increasing the minimum tension in cables can lead to dramatic reduction in vibration amplitude. The findings can play an important role in the case of cable-driven robots. Increasing minimum tension in cables, i.e. increasing tension in all cables, will lead to less cable vibration amplitude and better accuracy of motion.

In parallel cable-driven robots, all the cables are connected to the end-effector, and vibrations can be transferred easily, which can result in high tracking errors. Also, cables with higher tension are more stiff, consequently, less deviation happens in presence of external forces and noise, and controller-induced vibrations are less likely to happen.

So, we can increase the minimum tension in cables to have a more stiff, stable and accurate system. One major limitation to this approach is related to saturation of actuators, so a compromise between stiffness and force performance will be chosen.

To validate this approach, we used a 1-DOF cable-driven robot with two DC motors and a slider (end-effector). One linear and two rotational encoders were used to measure the position of the slider, and motors rotation. Using the linear encoder, we gain more precise data about the end-effector position, to check the accuracy of the system. The robot is illustrated in Figure A.4.

A periodic, fifth degree polynomial reference with fixed amplitude of ($35mm$), and various frequencies (0.5, 1 and $2Hz$) was used, and a PID controller was tuned in order to control the system. The motion was tested with three different minimum tensions: $6N$, $10N$ and $14N$. The results are shown in Table A.2. To compare different conditions, the variance of position error and the average tension in cables were used. The former was calculated as the variance of the difference between reference and actual (linear encoder) positions. The latter

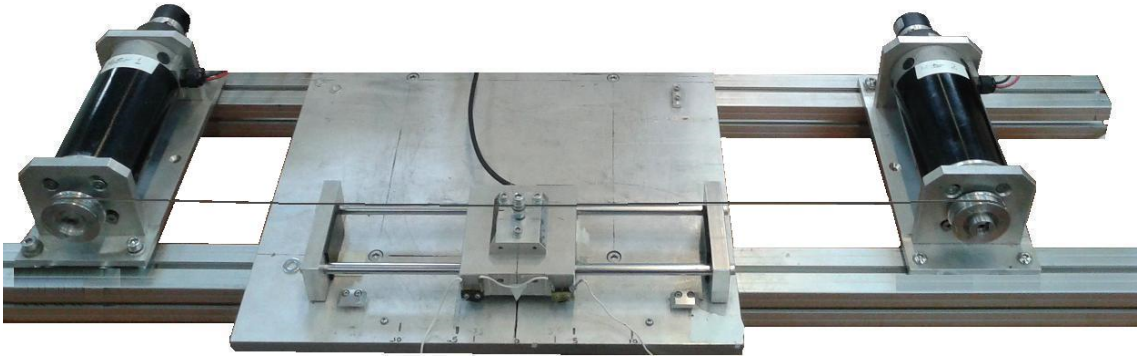

Figure A.4: 1-DOF cable-driven robot, with two DC motors, end-effector and encoders

was calculated as the average of both cable tensions. Measures were repeated during ten periods (i.e., twenty travels of the slider). By increasing the minimum tension in cables, less error variance (better accuracy) was achieved; however, average tension in cables increased.

Table A.2: Comparison of different fixed minimum tension effect on accuracy and average tension of the system

Frequency (Hz)	Minimum Tension (N)	Error Var. (mm)	Ave. Tension in Cables (N)
0.5	6 N	0.145	8.87
	10 N	0.128	12.82
	14 N	0.101	16.80
1	6 N	0.288	8.94
	10 N	0.231	13.01
	14 N	0.212	16.98
2	6 N	0.384	10.71
	10 N	0.357	16.19
	14 N	0.314	20.32

Figure A.5 shows the tension in cables for a motion with frequency of 0.5 Hz in a two-second period of motion. In (a) the minimum tension is always set to be 6 N, however, in (b), (c), they were set to be 10, 14N respectively. So in half of the period, one motor produces a minimum tension; however, the second motor produces motion torque, and in the next half of the period, the roles are changed. It is clear that, by increasing the minimum tension, power

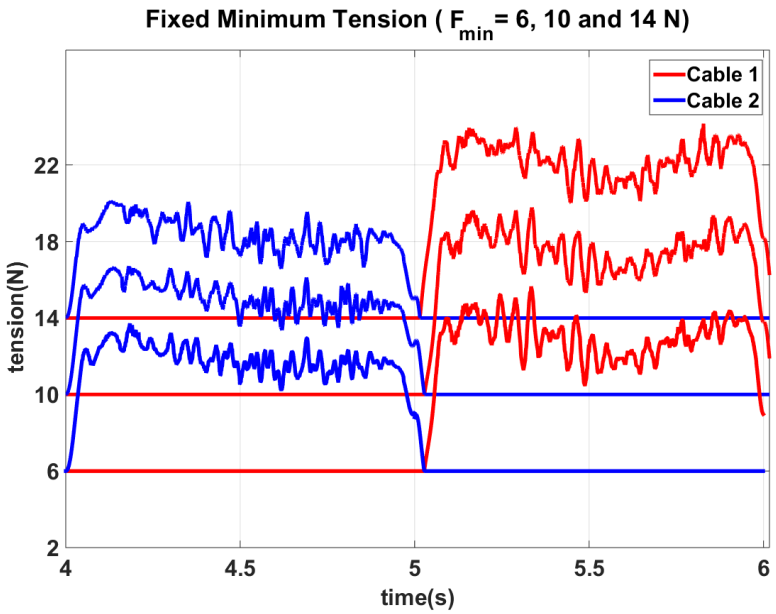

Figure A.5: Tension in cables for a motion with frequency of 0.5 Hz in a two-second period of motion

consumption will grow, which is not desirable.

Bibliography

[1] W. Wang, X. Tang, Z. Shao, J. Yang, and W. Yi, "Design and analysis of a wire-driven parallel mechanism for low-gravity environment simulation," *Advances in Mechanical Engineering*, vol. 6, p. 810606, 2014.

[2] G. Rosati, D. Zanotto, and S. K. Agrawal, "On the design of adaptive cable-driven systems," *Journal of mechanisms and robotics*, vol. 3, no. 2, p. 021004, 2011.

[3] R. Bostelman, J. Albus, N. Dagalakis, A. Jacoff, and J. Gross, "Applications of the nist robocrane," in *Proceedings of the 5th International Symposium on Robotics and Manufacturing*.

[4] R. Bostelman, J. Albus, N. Dagalakis, and A. Jacoff, "Robocrane [r] project: an advanced concept for large scale manufacturing," in *AUVSI-PROCEEDINGS-*, pp. 509–522, Citeseer, 1996.

[5] "Cogiro project." http://www.lirmm.fr/cogiro/. Accessed: 2016-01-20.

[6] S. Kawamura, W. Choe, S. Tanaka, and S. R. Pandian, "Development of an ultrahigh speed robot falcon using wire drive system," in *Robotics and Automation, 1995. Proceedings., 1995 IEEE International Conference on*, vol. 1, pp. 215–220, IEEE, 1995.

[7] S. Kawamura, H. Kino, and C. Won, "High-speed manipulation by using parallel wire-driven robots," *Robotica*, vol. 18, no. 01, pp. 13–21, 2000.

[8] X. Yangwen, L. Qi, Z. Yaqing, and L. Bin, "Model aerodynamic tests with a wire-driven parallel suspension system in low-speed wind tunnel," *Chinese Journal of Aeronautics*, vol. 23, no. 4, pp. 393–400, 2010.

[9] C. Gosselin, R. Poulin, and D. Laurendeau, "A planar parallel 3-dof cable-driven haptic interface," in *12th World Multi-Conference on Systemics, Cybernetics and Informatics, Orlando, FL, USA*, pp. 266–271, 2008.

[10] P. Gallina, G. Rosati, and A. Rossi, "3-dof wire driven planar haptic interface," *Journal of Intelligent and Robotic Systems*, vol. 32, no. 1, pp. 23–36, 2001.

[11] G. Rosati, P. Gallina, and S. Masiero, "Design, implementation and clinical tests of a wire-based robot for neurorehabilitation," *Neural Systems and Rehabilitation Engineering, IEEE Transactions on*, vol. 15, no. 4, pp. 560–569, 2007.

[12] G. Rosati, M. Andreolli, A. Biondi, and P. Gallina, "Performance of cable suspended robots for upper limb rehabilitation," in *Rehabilitation Robotics, 2007. ICORR 2007. IEEE 10th International Conference on*, pp. 385–392, IEEE, 2007.

[13] E. Brackbill, Y. Mao, S. K. Agrawal, M. Annapragada, V. N. Dubey, *et al.*, "Dynamics and control of a 4-dof wearable cable-driven upper arm exoskeleton," in *Robotics and Automation, 2009. ICRA'09. IEEE International Conference on*, pp. 2300–2305, IEEE, 2009.

[14] X. Jin, X. Cui, and S. K. Agrawal, "Design of a cable-driven active leg exoskeleton (c-alex) and gait training experiments with human subjects," in *Robotics and Automation (ICRA), 2015 IEEE International Conference on*, pp. 5578–5583, IEEE, 2015.

[15] X. Jin and S. K. Agrawal, "Exploring laparoscopic surgery training with cable-driven arm exoskeleton (carex-m)," in *Rehabilitation Robotics (ICORR), 2015 IEEE International Conference on*, pp. 490–495, IEEE, 2015.

[16] P. Bosscher, R. L. Williams, and M. Tummino, "A concept for rapidly-deployable cable robot search and rescue systems," in *ASME 2005 International Design Engineering Technical Conferences and Computers and Information in Engineering Conference*, pp. 589–598, American Society of Mechanical Engineers, 2005.

[17] J.-P. Merlet and D. Daney, "A portable, modular parallel wire crane for rescue oper-

ations," in *Robotics and Automation (ICRA), 2010 IEEE International Conference on*, pp. 2834–2839, IEEE, 2010.

[18] R. Nan, "Five hundred meter aperture spherical radio telescope (fast)," *Science in China series G*, vol. 49, no. 2, pp. 129–148, 2006.

[19] A. Pott, H. Mutherich, W. Kraus, V. Schmidt, P. Miermeister, T. Dietz, and A. Verl, "Cable-driven parallel robots for industrial applications: The ipanema system family," in *Robotics (ISR), 2013 44th International Symposium on*, pp. 1–6, IEEE, 2013.

[20] "Cable-driven parallel robots – motion simulation in a new dimension." http://www.ipa.fraunhofer.de/en/cable-driven_parallel_robots.html. Accessed: 2016-01-20.

[21] L. L. Cone, "Skycam-an aerial robotic camera system," *Byte*, vol. 10, no. 10, p. 122, 1985.

[22] "Skycam." https://en.wikipedia.org/wiki/Skycam. Accessed: 2016-01-20.

[23] "Lights, camera, hike!." http://profilemagazine.com/2012/skycam/. Accessed: 2016-01-20.

[24] D. Zanotto, "Analysis and development of cable-driven robotic devices," 2011.

[25] J. S. Sulzer, M. Peshkin, J. L. Patton, *et al.*, "Design of a mobile, inexpensive device for upper extremity rehabilitation at home," in *Rehabilitation Robotics, 2007. ICORR 2007. IEEE 10th International Conference on*, pp. 933–937, IEEE, 2007.

[26] X. Yin and A. P. Bowling, "Dynamic performance limitations due to yielding in cable-driven robotic manipulators," *Journal of Mechanical Design*, vol. 128, no. 1, pp. 311–318, 2006.

[27] A. Trevisani, "Underconstrained planar cable-direct-driven robots: A trajectory planning method ensuring positive and bounded cable tensions," *Mechatronics*, vol. 20, no. 1, pp. 113–127, 2010.

[28] A. Trevisani, P. Gallina, and R. L. Williams II, "Cable-direct-driven robot (cddr) with passive scara support: theory and simulation," *Journal of Intelligent and Robotic Systems*, vol. 46, no. 1, pp. 73–94, 2006.

[29] Y. Mao and S. K. Agrawal, "Wearable cable-driven upper arm exoskeleton-motion with transmitted joint force and moment minimization," in *Robotics and Automation (ICRA), 2010 IEEE International Conference on*, pp. 4334–4339, IEEE, 2010.

[30] S. Kurbanhusen Mustafa, G. Yang, S. Huat Yeo, W. Lin, and M. Chen, "Self-calibration of a biologically inspired 7 dof cable-driven robotic arm," *Mechatronics, IEEE/ASME Transactions on*, vol. 13, no. 1, pp. 66–75, 2008.

[31] J. F. Veneman, R. Ekkelenkamp, R. Kruidhof, F. C. van der Helm, and H. van der Kooij, "A series elastic-and bowden-cable-based actuation system for use as torque actuator in exoskeleton-type robots," *The international journal of robotics research*, vol. 25, no. 3, pp. 261–281, 2006.

[32] J. F. Veneman, R. Kruidhof, E. E. Hekman, R. Ekkelenkamp, E. H. Van Asseldonk, and H. Van Der Kooij, "Design and evaluation of the lopes exoskeleton robot for interactive gait rehabilitation," *Neural Systems and Rehabilitation Engineering, IEEE Transactions on*, vol. 15, no. 3, pp. 379–386, 2007.

[33] S. K. Mustafa and S. K. Agrawal, "Reciprocal screw-based force-closure of an n-dof open chain: Minimum number of cables required to fully constrain it," in *Robotics and Automation (ICRA), 2011 IEEE International Conference on*, pp. 3029–3034, IEEE, 2011.

[34] S. Behzadipour and A. Khajepour, "Industrial robotics theory, modelling and control," 2007.

[35] A. Risoli, G. M. Prisco, F. Salsedo, and M. Bergamasco, "A two degrees-of-freedom planar haptic interface with high kinematic isotropy," in *Robot and Human Interaction, 1999. RO-MAN'99. 8th IEEE International Workshop on*, pp. 297–302, IEEE, 1999.

[36] J. Lenarcic and P. Wenger, *Advances in robot kinematics: analysis and design*. Springer, 2008.

[37] M. Hiller, S. Fang, S. Mielczarek, R. Verhoeven, and D. Franitza, "Design, analysis and realization of tendon-based parallel manipulators," *Mechanism and Machine Theory*, vol. 40, no. 4, pp. 429–445, 2005.

[38] P. Gallina and G. Rosati, "Manipulability of a planar wire driven haptic device," *Mechanism and Machine Theory*, vol. 37, no. 2, pp. 215–228, 2002.

[39] S. Landsberger and P. Shanmugasundram, "Workspace of a parallel link crane," in *Proceedings of IMACS/SICE International Symposium on Robotics, Mechatronics and Manufacturing Systems*, pp. 479–486, 1992.

[40] X. Diao and O. Ma, "Workspace determination of general 6-dof cable manipulators," *Advanced Robotics*, vol. 22, no. 2-3, pp. 261–278, 2008.

[41] Y. Shen, H. Osumi, and T. Arai, "Set of manipulating forces in wire driven systems," in *Intelligent Robots and Systems' 94.'Advanced Robotic Systems and the Real World', IROS'94. Proceedings of the IEEE/RSJ/GI International Conference on*, vol. 3, pp. 1626–1631, IEEE, 1994.

[42] A. Ming and T. Higuchi, "Study on multiple degree-of-freedom positioning mechanism using wires. i: Concept, design and control," *International Journal of the Japan Society for Precision Engineering*, vol. 28, no. 2, pp. 131–138, 1994.

[43] P. Bosscher and I. Ebert-Uphoff, "Wrench-based analysis of cable-driven robots," in *Robotics and Automation, 2004. Proceedings. ICRA'04. 2004 IEEE International Conference on*, vol. 5, pp. 4950–4955, IEEE, 2004.

[44] T. Bruckman *et al.*, "Parallel manipulators, new developments, chap," *Wire robot part I, kinematics, analysis and design*, pp. 109–132, 2008.

[45] A. Fattah and S. K. Agrawal, "On the design of cable-suspended planar parallel robots," *Journal of Mechanical Design*, vol. 127, no. 5, pp. 1021–1028, 2005.

[46] G. Rosati and D. Zanotto, "A novel perspective in the design of cable-driven systems," in *ASME 2008 International Mechanical Engineering Congress and Exposition*, pp. 617–625, American Society of Mechanical Engineers, 2008.

[47] D. Zanotto, G. Rosati, S. Minto, and A. Rossi, "Sophia-3: A semiadaptive cable-driven rehabilitation device with a tilting working plane," *Robotics, IEEE Transactions on*, vol. 30, no. 4, pp. 974–979, 2014.

[48] X. Zhou, C. P. Tang, and V. Krovi, "Analysis framework for cooperating mobile cable robots," in *Robotics and Automation (ICRA), 2012 IEEE International Conference on*, pp. 3128–3133, IEEE, 2012.

[49] X. Zhou, C. P. Tang, and V. Krovi, "Cooperating mobile cable robots: Screw theoretic analysis," in *Redundancy in Robot Manipulators and Multi-Robot Systems*, pp. 109–123, Springer, 2013.

[50] X. Zhou, S.-k. Jun, and V. Krovi, "Wrench reconfigurability via attachment point design in mobile cable robots," in *ASME 2013 International Design Engineering Technical Conferences and Computers and Information in Engineering Conference*, pp. V06AT07A072–V06AT07A072, American Society of Mechanical Engineers, 2013.

[51] X. Zhou, S.-k. Jun, and V. Krovi, "Stiffness modulation exploiting configuration redundancy in mobile cable robots," in *Robotics and Automation (ICRA), 2014 IEEE International Conference on*, pp. 5934–5939, IEEE, 2014.

[52] G. Rosati, P. Gallina, S. Masiero, and A. Rossi, "Design of a new 5 dof wire-based robot for rehabilitation," in *Rehabilitation Robotics, 2005. ICORR 2005. 9th International Conference on*, pp. 430–433, IEEE, 2005.

[53] S. Masiero, M. Armani, G. Rosati, *et al.*, "Upper-limb robot-assisted therapy in rehabilitation of acute stroke patients: focused review and results of new randomized controlled trial," *J Rehabil Res Dev*, vol. 48, no. 4, pp. 355–366, 2011.

[54] D. Q. Nguyen, M. Gouttefarde, O. Company, and F. Pierrot, "On the analysis of large-dimension reconfigurable suspended cable-driven parallel robots," in *Robotics and Automation (ICRA), 2014 IEEE International Conference on*, pp. 5728–5735, IEEE, 2014.

[55] D. Q. Nguyen and M. Gouttefarde, "Study of reconfigurable suspended cable-driven parallel robots for airplane maintenance," in *Intelligent Robots and Systems (IROS 2014), 2014 IEEE/RSJ International Conference on*, pp. 1682–1689, IEEE, 2014.

[56] L. Gagliardini, S. Caro, M. Gouttefarde, P. Wenger, and A. Girin, "A reconfigurable cable-driven parallel robot for sandblasting and painting of large structures," in *Cable-Driven Parallel Robots*, pp. 275–291, Springer, 2015.

[57] L. Gagliardini, S. Caro, M. Gouttefarde, and A. Girin, "A reconfiguration strategy for reconfigurable cable-driven parallel robots," in *Robotics and Automation (ICRA), 2015 IEEE International Conference on*, pp. 1613–1620, IEEE, 2015.

[58] G. Boschetti, G. Rosati, and A. Rossi, "A haptic system for robotic assisted spine surgery," in *Control Applications, 2005. CCA 2005. Proceedings of 2005 IEEE Conference on*, pp. 19–24, IEEE, 2005.

[59] R. Caracciolo, G. Boschetti, N. De Rossi, G. Rosati, and A. Trevisani, "A master-slave robotic system for haptic teleoperation," in *ASME 8th Biennial Conference on Engineering Systems Design and Analysis*, pp. 739–748, American Society of Mechanical Engineers, 2006.

[60] G. Rosati, D. Zanotto, and A. Rossi, "Performance assessment of a 3d cable-driven haptic device," in *ASME 2008 International Mechanical Engineering Congress and Exposition*, pp. 597–606, American Society of Mechanical Engineers, 2008.

[61] C. Fanin, P. Gallina, A. Rossi, U. Zanatta, and S. Masiero, "Nerebot: a wire-based robot for neurorehabilitation," in *The 8th International Conference on Rehabilitation Robotics PROCEEDINGS*, pp. 23–26, 2003.

[62] S. Masiero, A. Celia, G. Rosati, and M. Armani, "Robotic-assisted rehabilitation of the upper limb after acute stroke," *Archives of physical medicine and rehabilitation*, vol. 88, no. 2, pp. 142–149, 2007.

[63] G. Rosati, P. Gallina, A. Rossi, and S. Masiero, "Wire-based robots for upper-limb rehabilitation," *International Journal of Assistive Robotics and Mechatronics*, vol. 7, no. 2, pp. 3–10, 2006.

[64] W. T. Dempster, "Space requirements of the seated operator: geometrical, kinematic, and mechanical aspects of the body, with special reference to the limbs," 1955.

[65] G. Rosati, R. Secoli, D. Zanotto, A. Rossi, and G. Boschetti, "Planar robotic systems for upper-limb post-stroke rehabilitation," in *ASME 2008 International Mechanical Engineering Congress and Exposition*, pp. 115–124, American Society of Mechanical Engineers, 2008.

[66] G. Rosati, D. Zanotto, R. Secoli, and A. Rossi, "Design and control of two planar cable-driven robots for upper-limb neurorehabilitation," in *Rehabilitation Robotics, 2009. ICORR 2009. IEEE International Conference on*, pp. 560–565, IEEE, 2009.

[67] G. Rosati, J. E. Bobrow, and D. J. Reinkensmeyer, "Compliant control of post-stroke rehabilitation robots: using movement-specific models to improve controller performance," in *ASME 2008 International Mechanical Engineering Congress and Exposition*, pp. 167–174, American Society of Mechanical Engineers, 2008.

[68] X. Diao and O. Ma, "Vibration analysis of cable-driven parallel manipulators," *Multibody system dynamics*, vol. 21, no. 4, pp. 347–360, 2009.

[69] S. Behzadipour and A. Khajepour, "Stiffness of cable-based parallel manipulators with application to stability analysis," *Journal of mechanical design*, vol. 128, no. 1, pp. 303–310, 2006.

[70] M. Arsenault, "Stiffness analysis of a planar 2-dof cable-suspended mechanism while considering cable mass," in *Cable-Driven Parallel Robots*, pp. 405–421, Springer, 2013.

[71] D. Surdilovic, J. Radojicic, and J. Krüger, "Geometric stiffness analysis of wire robots: a mechanical approach," in *Cable-Driven Parallel Robots*, pp. 389–404, Springer, 2013.

[72] J.-B. Izard, M. Gouttefarde, C. Baradat, D. Culla, and D. Sallé, "Integration of a parallel cable-driven robot on an existing building façade," in *Cable-Driven Parallel Robots*, pp. 149–164, Springer, 2013.

[73] W. Miranker, "The wave equation in a medium in motion," *IBM Journal of Research and Development*, vol. 4, no. 1, pp. 36–42, 1960.

[74] M. Pakdemirli, A. G. Ulsoy, and A. Ceranoglu, "Transverse vibration of an axially accelerating string," 1994.

[75] G. Zen and S. Müftü, "Friction induced transverse vibrations of an axially accelerating string," *Proc 2003 STLE/ASME Int. Joint Trib. Con*, 2003.

[76] L.-Q. Chen, Y.-Q. Tang, and J. W. Zu, "Nonlinear transverse vibration of axially accelerating strings with exact internal resonances and longitudinally varying tensions," *Nonlinear Dynamics*, vol. 76, no. 2, pp. 1443–1468, 2014.

[77] M. Korayem and A. Alipour, "Dynamic analysis of moving cables with variable tension and variable speed," 2010.

[78] N.-h. Zhang, J.-j. Wang, and C.-j. Cheng, "Complex-mode galerkin approach in transverse vibration of an axially accelerating viscoelastic string," *Applied Mathematics and Mechanics*, vol. 28, pp. 1–9, 2007.

[79] S. Abdolshah and G. Rosati, "First experimental testing of a dynamic minimum tension control (dmtc) for cable driven parallel robots," in *Cable-Driven Parallel Robots*, pp. 239–248, Springer, 2015.

[80] A. Pott, "An improved force distribution algorithm for over-constrained cable-driven parallel robots," in *Computational Kinematics*, pp. 139–146, Springer, 2014.

[81] S. Fang, D. Franitza, M. Torlo, F. Bekes, and M. Hiller, "Motion control of a tendon-based parallel manipulator using optimal tension distribution," *Mechatronics, IEEE/ASME Transactions on*, vol. 9, no. 3, pp. 561–568, 2004.

[82] C. B. Pham, G. Yang, and S. H. Yeo, "Dynamic analysis of cable-driven parallel mechanisms," in *Advanced Intelligent Mechatronics. Proceedings, 2005 IEEE/ASME International Conference on*, pp. 612–617, IEEE, 2005.

[83] S.-R. Oh and S. K. Agrawal, "Cable suspended planar robots with redundant cables: controllers with positive tensions," *Robotics, IEEE Transactions on*, vol. 21, no. 3, pp. 457–465, 2005.

[84] G. Barrette and C. M. Gosselin, "Determination of the dynamic workspace of cable-driven planar parallel mechanisms," *Journal of Mechanical Design*, vol. 127, no. 2, pp. 242–248, 2005.

[85] H. Li, X. Zhang, R. Yao, J. Sun, G. Pan, and W. Zhu, "Optimal force distribution based on slack rope model in the incompletely constrained cable-driven parallel mechanism of fast telescope," in *Cable-driven parallel robots*, pp. 87–102, Springer, 2013.

[86] W. Lim, S. Yeo, G.-M. Yang, S. Mustafa, and Z. Zhang, "Tension optimization for cable-driven parallel manipulators using gradient projection," in *Advanced Intelligent Mechatronics (AIM), 2011 IEEE/ASME International Conference on*, pp. 73–78, IEEE, 2011.

[87] M. Hassan and A. Khajepour, "Optimization of actuator forces in cable-based parallel manipulators using convex analysis," *Robotics, IEEE Transactions on*, vol. 24, no. 3, pp. 736–740, 2008.

[88] C. Gosselin and M. Grenier, "On the determination of the force distribution in overconstrained cable-driven parallel mechanisms," *Meccanica*, vol. 46, no. 1, pp. 3–15, 2011.

[89] J. Snyman and A. Hay, "Analysis and optimization of a planar tendon-driven parallel manipulator," in *On Advances in Robot Kinematics*, pp. 303–312, Springer, 2004.

[90] P. Voglewede, I. Ebert-Uphoff, *et al.*, "Application of the antipodal grasp theorem to cable-driven robots," *Robotics, IEEE Transactions on*, vol. 21, no. 4, pp. 713–718, 2005.

[91] M. A. Khosravi and H. D. Taghirad, "Dynamics analysis and control of cable driven robots considering elasticity in cables," in *CCToMM 2011 Symposium*, 2011.

[92] K. Yu, L.-F. Lee, C. P. Tang, and V. N. Krovi, "Enhanced trajectory tracking control with active lower bounded stiffness control for cable robot," in *Robotics and Automation (ICRA), 2010 IEEE International Conference on*, pp. 669–674, IEEE, 2010.

[93] J. Lamaury and M. Gouttefarde, "Control of a large redundantly actuated cable-suspended parallel robot," in *Robotics and Automation (ICRA), 2013 IEEE International Conference on*, pp. 4659–4664, IEEE, 2013.

[94] H. Kino, T. Yahiro, F. Takemura, and T. Morizono, "Robust pd control using adaptive compensation for completely restrained parallel-wire driven robots: translational systems using the minimum number of wires under zero-gravity condition," *Robotics, IEEE Transactions on*, vol. 23, no. 4, pp. 803–812, 2007.

[95] L. Qi, H. Zhang, and G. Duan, "Task-space position/attitude tracking control of fast fine tuning system," *Frontiers of Mechanical Engineering in China*, vol. 3, no. 4, pp. 392–399, 2008.

[96] M. A. Khosravi and H. D. Taghirad, "Experimental performance of robust pid controller on a planar cable robot," in *Cable-Driven Parallel Robots*, pp. 337–352, Springer, 2013.

[97] B. Zi, B. Duan, J. Du, and H. Bao, "Dynamic modeling and active control of a cable-suspended parallel robot," *Mechatronics*, vol. 18, no. 1, pp. 1–12, 2008.

[98] A. B. Alp and S. K. Agrawal, "Cable suspended robots: feedback controllers with positive inputs," in *American Control Conference, 2002. Proceedings of the 2002*, vol. 1, pp. 815–820, IEEE, 2002.

[99] A. Alikhani and M. Vali, "Modeling and robust control of a new large scale suspended cable-driven robot under input constraint," in *Ubiquitous Robots and Ambient Intelligence (URAI), 2011 8th International Conference on*, pp. 238–243, IEEE, 2011.

[100] E. Laroche, R. Chellal, L. Cuvillon, and J. Gangloff, "A preliminary study for h_\ infty control of parallel cable-driven manipulators," in *Cable-Driven Parallel Robots*, pp. 353–369, Springer, 2013.

[101] M. H. Korayem and H. Tourajizadeh, "Maximum dlcc of spatial cable robot for a predefined trajectory within the workspace using closed loop optimal control approach," *Journal of Intelligent & Robotic Systems*, vol. 63, no. 1, pp. 75–99, 2011.

[102] C. Gosselin, *Kinematic analysis, optimization and programming of parallel robotic manipulators*. 1988.

[103] S. Behzadipour and M. A. Sohi, "Antagonistic stiffness in cable-driven mechanisms," in *IFToMM World Congress, Besançon, France, In*, 2007.

[104] S. Yeo, G. Yang, and W. Lim, "Design and analysis of cable-driven manipulators with variable stiffness," *Mechanism and Machine Theory*, vol. 69, pp. 230–244, 2013.

[105] "Interval analysis." https://en.wikipedia.org/wiki/Interval_arithmetic. Accessed: 2016-01-20.

[106] M. Gouttefarde, D. Daney, and J.-P. Merlet, "Interval-analysis-based determination of the wrench-feasible workspace of parallel cable-driven robots," *Robotics, IEEE Transactions on*, vol. 27, no. 1, pp. 1–13, 2011.

[107] A. Taghvaeipour, J. Angeles, and L. Lessard, "On the elastostatic analysis of mechanical systems," *Mechanism and Machine Theory*, vol. 58, pp. 202–216, 2012.

[108] V. Vashista, X. Jin, and S. K. Agrawal, "Active tethered pelvic assist device (a-tpad) to study force adaptation in human walking," in *Robotics and Automation (ICRA), 2014 IEEE International Conference on*, pp. 718–723, IEEE, 2014.

[109] J. Morrell and J. Salisbury, "Parallel coupled actuators for high performance force control: a micro-macro concept," in *Intelligent Robots and Systems 95. 'Human Robot Interaction and Cooperative Robots', Proceedings. 1995 IEEE/RSJ International Conference on*, vol. 1, pp. 391–398 vol.1, Aug 1995.

[110] J. M. Veciana and S. Cardona, "Residual vibration reduction in mechanical systems: A time-domain approach," *International Journal of Precision Engineering and Manufacturing*, vol. 13, no. 8, pp. 1327–1339, 2012.

[111] T. M. Huh, Y.-J. Park, and K.-J. Cho, "Design and analysis of a stiffness adjustable structure using an endoskeleton," *International Journal of Precision Engineering and Manufacturing*, vol. 13, no. 7, pp. 1255–1258, 2012.

[112] M. Khosravi and H. Taghirad, "Dynamic modeling and control of parallel robots with elastic cables: Singular perturbation approach," *Robotics, IEEE Transactions on*, vol. 30, pp. 694–704, June 2014.

[113] A. Müller, *Redundant actuation of parallel manipulators*. INTECH Open Access Publisher, 2008.

[114] R. Verhoeven, M. Hiller, and S. Tadokoro, "Workspace, stiffness, singularities and classification of tendon-driven stewart platforms," in *Advances in robot kinematics: Analysis and Control*, pp. 105–114, Springer, 1998.

[115] J. Du and S. K. Agrawal, "Dynamic modeling of cable-driven parallel manipulators with distributed mass flexible cables," *Journal of Vibration and Acoustics*, vol. 137, no. 2, p. 021020, 2015.

[116] R. Mittal and I. Nagrath, *Robotics and control*. Tata McGraw-Hill New Delhi, 2003.

[117] "Optimal control." https://en.wikipedia.org/wiki/Optimal_control. Accessed: 2016-01-20.

[118] B. D. Anderson and J. B. Moore, *Optimal control: linear quadratic methods*. Courier Corporation, 2007.

[119] P. Howard, "Solving ode in matlab," *University of Maryland*, 2007.